NTNU – Trondheim
Norwegian University of
Science and Technology

Numerical Simulation of Twin Nozzle Injectors

Dino Milak

Marine Technology
Submission date: June 2015
Supervisor: Eilif Pedersen, IMT

Norwegian University of Science and Technology
Department of Marine Technology

MASTER THESIS IN MARINE MACHINERY

SPRING 2015

FOR

STUD.TECHN. DINO MILAK

NUMERICAL SIMULATION OF TWIN NOZZLE INJECTORS

Work description

The internal combustion engine is still the most important power producer for all kinds of vehicles, especially for marine applications. Due to the growing importance of stringent emission restrictions, engine manufacturers are forced to continuously improve the combustion process in order to reduce engine raw emissions. High-pressure injection systems enable considerable control of the combustion process in terms of reduced fuel consumption and raw emissions. The nozzles in injections systems are one of the decisive features for spray patterns and mixture formation. The optimization of spray and mixture formation processes, through nozzle design, is therefore of great interest to study more in detail.

Twin nozzles which utilizes two closely spaced orifices to substitute conventional single orifice nozzles, is regarded as a promising approach to facilitate improved spray pattern and mixture formation for the in-cylinder combustion process. Better fuel atomization and evaporation can be achieved, with attenuation of soot formation as a consequence. Twin nozzles also have the potential to provide stable spray patterns independent of the fuel quantity delivered through the nozzle.

The aim of this project is to develop a numerical model for a twin nozzle configuration utilizing diesel as fuel source. The outcome of the model will then be compared with a conventional single orifice nozzle. The numerical model is to be developed using the commercial CFD software AVL FIRE. This project is a part of an ongoing research project at the department.

Scope of work:

1. Give a background of spray processes in combustion engines.
2. Perform numerical simulation of L'Orange's twin nozzle.
3. Investigate effects of various rail and in-cylinder pressures.
4. Perform numerical simulation of conventional single orifice nozzle.
5. Present, compare and discuss results

The work scope may prove to be larger than initially anticipated. Subject to approval from the supervisor, topics may be deleted from the list above or reduced in extent without consequences with regard to grading.

In the thesis the candidate shall present his personal contribution to the resolution of problem within the scope of the thesis work. Theories and conclusions should be based on mathematical derivations and/or logic reasoning identifying the various steps in the deduction. The candidate should utilize the existing possibilities for obtaining relevant literature. The thesis should be organized in a rational manner to give a clear exposition of results, assessments, and conclusions. The report shall be written in English and edited as a research report including simulations results, discussion and conclusion including a proposal for further work. The text should be brief and to the point, with a clear language.

The Department of Marine Technology, NTNU, can use the results freely in its research work by referring to the students work.

The thesis should be submitted in three copies within 5 months after the registered start-up of this thesis.

Trondheim January, 2015

Eilif Pedersen
Associate Professor (Supervisor)

Preface

This thesis ends my education in Marine Technology and is a result of the work required for fulfilment of the degree Master of Science at the Norwegian University of Science and Technology (NTNU) in Trondheim.

The thesis has been performed at MARINTEK, a part of SINTEF, in Trondheim.

The work is conducted with associate professor Eilif Pedersen and Ph.D. candiate Maximillian Malin. I would like to express my sincere gratitude to them both for the amount of support and guidance they have provided throughout this study. Especially, Ph.D. candiate Malin who has kept my mind on the given task, pointed me in the right direction and offered his expertise in both late and early hours. Your dedication for my work has truly been an inspiration for me to push forward.

I would like to thank senior research scientist Per Magne Eingang and the other employees at MARINTEK for allowing me to undertake this study at their workplace and for offering their knowledge whenever I have needed it.

Special thanks goes to the injection systems manufacturer L'Orange who has been kind enough to share their twin nozzle prototype with me. A second special thanks goes to AVL for contributing with a software license for their CFD solver FIRE.

Last, but not least, I would like to thank my family and my fellow students in class of 2015, for supporting my through these five years.

Trondheim, *June 10, 2015*

Dino Milak

Abstract

Fuel injectors for marine applications have traditionally utilized nozzles with symmetric equispaced orifice configuration. But in light of the new marine emission legislations the twin nozzle concept has arisen. The twin nozzle differs from the conventional configuration by utilizing two closely spaced orifices to substitute each orifice in the conventional nozzle. Injector manufacturers regard twin nozzle injectors as a promising approach to facilitate stable spray patterns independent of the fuel quantity delivered through the nozzle. If true, injector systems in dual fuel engines can be simplified by reducing the amount of nozzles needed. It is also believed that twin nozzles can improve mixture formation for the combustion process for all diesel applications.

This thesis explores the possibility of using the commercial computational fluid dynamics (CFD) software AVL FIRE to predict the behaviour of L'Orange's twin nozzle during fuel injection. The thesis does not seek to verify and validate the proposed numerical model, but rather perceive an understanding of the overall flow trend in a twin nozzle and how it may outperform a conventional nozzle.

The nozzle is represented by a moving grid where the moving part replicates the needle movement. The needle profile is a ramp function. To take cavitation in account the numerical model is a multiphase model, containing three phases (diesel, vapour and air). The twin nozzle injects the fuel into a constant volume filled with air. The chosen turbulence model is the high Reynolds number $k - \epsilon$ model.

The mass flow and the velocity is found to be greater for the upper injector hole. A vortex in the SAC volume i.e. the lower part of the nozzle seems to be the reason for this. Cavitation is found to have major effect on internal nozzle flow, especially during opening and closing of the needle. Vapour is formed at sharp injector hole inlets and it travels all the way to the outlets, reducing the effective cross sectional area which the fuel can flow through. In-cylinder pressure and rail pressure is found to have an effect on the nozzle behaviour. It is noted that the numerical model has a discrepancy causing too high air density. This only affects the results obtained downstream of the outlet and not the internal nozzle flow.

The twin nozzle is compared to a conventional single orifice nozzle. The proposed numerical model lack certain features making it difficult to explicitly state if the twin nozzle outperforms the conventional nozzle. However, the outlets in the twin nozzle have a smaller vapour fraction than the outlet in the single orifice nozzle. This enhances the effective cross sectional area and might render twin nozzles more effective for injecting larger quantities even if its injector hole dimensions favour pilot injections.

Sammendrag

Innsprøytningssystemer for marine applikasjoner har tradisjonelt benyttet symmetrisk konfigurerte dyser med lik avstand mellom dysehullene. I lys av den nye marine utslippslovgivning har «twin nozzle» konseptet oppstått. «Twin nozzle» dyser benytter to tett plasserte dysehull med mindre diameter som erstatning for hvert av dysehullene i de konvensjonelle dysene. Produsenter av innsprøytningssystemer anser «twin nozzle» konseptet som lovende da det potensielt kan levere gunstige innsprøytningsmønster uavhengig av brennstoffmengden som avgis. Dette kan igjen forenkle innsprøytningssystemet på dual fuel motorer ved å redusere antall nødvendige dyser. Det er også antatt at «twin nozzle» dyser kan forbedre forbrenningsprosessen i dieselmotorer generelt.

Denne avhandlingen utforsker bruken av den kommersielle Computational Fluid Dynamics (CFD) programvaren AVL FIRE til å forutsi oppførselen til L'Orange's «Twin Nozzle». Avhandlingen forsøker ikke å verifisere eller validere den foreslåtte numeriske modellen, men heller danne en overordnet forståelse av det generelle strømningsbildet i «twin nozzle» dyser og hvordan disse potensielt kan overgå konvensjonelle dyser.

For å representere dysenålens bevegelse er også dysens grid bevegelig. Nålen beveger seg etter en fastsatt rampefunksjon. Kavitasjon er tatt i betraktning ved å blant annet innføre flere faser i den numeriske modellen. Disse er diesel, damp og luft. Dysen injiserer drivstoffet i en del av gridet som har konstant volum og er fylt med luft. Den valgte turbulensmodellen er den høye Reynolds-tall $k - \epsilon$ modellen.

For «twin nozzle» dysen er massestrømmen og hastigheten funnet å være større for øvre dysehull enn det nedre. En virvel i SAC volumet, dvs. den nedre del av dysen, synes å være årsaken til dette. Kavitasjon er funnet å ha en større innvirkning på strømningsbilde, særlig under åpning og lukking av dysenålen. Kavitasjonsboblene dannes ved dysehullenes innløp og vandrer så gjennomen hele dysen, noe som reduserer det effektive tverrsnittarealet som drivstoffet kan strømme gjennom. Sylindertrykket og common rail trykket er funnet å ha en effekt på dysens atferd. Det bemerkes at den numeriske modellen har et avvik forårsaket av for høy lufttetthet. Dette påvirker bare resultatene i det konstante volumet der drivstoffet injiseres og ikke dysens interne strømningsbilde.

«Twin nozzle» dysen er sammenlignet med en konvensjonell dyse. Den foreslåtte numeriske modellen har ikke de tilstrekkelige egenskapene for å kunne eksplisitt fastslå hvorvidt en «twin nozzle» dyse er bedre enn en tradisjonell dyse. «Twin Nozzle» dysen er dog mindre preget av kavitasjon enn de tradisjonelle dysene. Dette øker drivstoffets effektive tverrsnittareal, og kan føre til at «twin nozzle» dyser mer effektivt kan injisere større mengder drivstoff, selv om dysehullenes dimensjoner favoriserer pilot injeksjoner.

Contents

List of Figures

List of Tables

Abbreviations

2D	2-Dimensional
3D	3-Dimensional
BiCGstab	Biconjugate Gradient Stabilized Method
CAD	Computer Aided Design
CAD	Crank Angle Degree
CFD	Computational Fluid Dynamics
ECA	Emission Control Areas
ECU	Electric Control Unit
ILU(0)	Incomplete Lower Upper factorization
LNG	Liquefied Natural Gas
N/A	Not Applicable
PDE	Partial Differential Equation
RPM	Revolutions Per Minute
SIMPLE	Semi-Implicit Method for Pressure-Linked Equations
SMD	Sauter Mean Diameter
STEP	Standard for the Exchange of Product Model Date
STL	STereoLithography
TKE	Turbulent Kinetic Energy
VCO	Valve Covered Orifice
VOF	Volume of Fluid

Symbols

$\boldsymbol{C_{CR}}$	Condensation Reduction Factor
$\boldsymbol{C_E}$	Egler Coefficient
$\boldsymbol{D}$	Orifice Diameter
$\boldsymbol{M}$	Interfacial Mass Exchange
$\boldsymbol{N'''}$	Bubble Number Density
$\boldsymbol{N_0'''}$	Initial Bubble Number Density
$\boldsymbol{R}$	Bubble Radius
$\boldsymbol{\Delta\varphi}$	Crank Angle Step
$\boldsymbol{\Delta t}$	Time Step
$\boldsymbol{\Gamma}$	Interfacial Mass Exchange
$\boldsymbol{\alpha}$	Volume Fraction
$\boldsymbol{\lambda}$	Air to Fuel Ratio
$\boldsymbol{\mu}$	Dynamic Viscosity
$\boldsymbol{\phi}$	Spray Cone Angle
$\boldsymbol{\rho}$	Density
$\boldsymbol{\sigma}$	Liquid Surface Tension
$\boldsymbol{d}$	Droplet Diameter
$\boldsymbol{k}$	Turbulent Kinetic Energy
$\boldsymbol{p_{sat}}$	Saturation Pressure
$\boldsymbol{u}$	Jet Velocity
$\boldsymbol{u_{rel}}$	Relative Velocity
$\boldsymbol{y^+}$	Non-Dimensional Wall Distance

Chapter 1

Introduction

This chapter presents how the need for twin nozzles has emerged and why it is beneficial to gain more knowledge about them. The thesis' objective is stated together with how it is intended to solve the challenges, questions, and issues that arise from the objective. Lastly, twin nozzles are explained with an emphasis on orifice configuration. It is assumed that the reader possesses fundamental knowledge about reciprocating internal combustion engines, their cycle of operation and the nomenclature associated with them. Experience in computational fluid dynamics (CFD) is also highly recommended.

1.1 Background

Ever since the steam engine was considered obsolete, diesel engines have been the workhorse in the marine industry. The diesel engine has continuously been developed. Efficiency has improved and exhaust emissions have reduced. But in later years international agreements have worked intensely to reduce marine pollution, and stringent requirements have been set. The diesel engine's ability to meet these requirements has proven to be problematic, especially when utilizing low quality residual fuels. In order to comply with the requirements engine manufacturers have partially shifted their focus towards gas engines. Such engines considerably reduce emissions, enough to comply with the requirements, without the need for any external exhaust gas treatment systems. Furthermore, manufacturers endeavour reduction of emission in diesel engines by optimization of the injection system. A favourable fuel spray pattern can enable prominent improvements in the combustion process in terms of reduced emissions and fuel consumption.

As of 2015, ship operators are required to burn fuel with less than 0.1% sulphur content if sailing within the designated areas called emission control areas (ECA). Alternatively they can burn high sulphur fuel if using exhaust treatments systems that can reach an equivalent level of emission reduction. The global sulphur cap is due to be lowered to 0.5% in 2020 or 2025 depending on the outcome of review scheduled in 2018. In addition to this the NOx emissions for a ship constructed on or after 1 January 2016 must not exceed Tier III level when sailing within ECA[1].

As compliance to all these stringent emission requirements can be achieved with gas fueled engines, it is expected that such engines will gain popularity among ship operators. The shipping industry is still adopting liquefied natural gas (LNG) as a

[1] All emission requirements are according to IMO [18].

fuel source, hence are bunkering locations scarce. To overcome this ship operators tend to favour dual fuel engines which can run in either diesel mode or gas mode. Gas availability along the ship route is then not a restrictive feature and route flexibility is not impaired.

A dual fuel engine in gas mode operates according to the Otto principle. The gas is injected into the intake manifold and drawn into the cylinder as the intake valves open during the induction stroke. The mixture in the combustion chamber is lean, meaning that there is more air present than what is needed for a complete stoichiometric combustion. This allows for increased efficiency and a cooler combustion where less NOx is produced [40]. Instead of a spark plug, which is normally used in Otto engines, the lean mixture in the combustion chamber is ignited by a small amount of diesel fuel. The injection of this fuel is often referred to as a pilot injection. This injection initiates a powerful ignition which is needed to prevent misfiring and knocking when running with a lean mixture [40]. When in diesel mode, the engine operates according to the normal diesel concept. Figure 1.1 illustrates the three first strokes of an operational cycle for a dual fuel engine in gas mode.

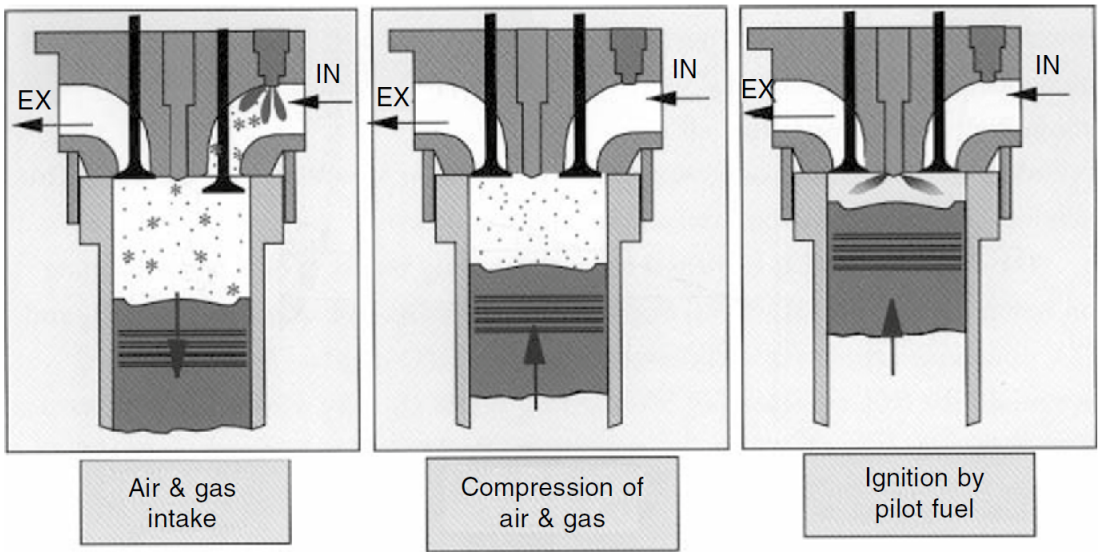

Figure 1.1: Dual fuel engine in gas mode [40]

Traditionally three different injectors are used to facilitate the necessary fuel in a dual fuel engine:

Gas injector
: Located in the intake manifold and allows gas to be mixed with air before the mixture is pulled into the cylinder during the intake stroke. The injector with its belonging spray pattern can be seen in the leftmost picture in Figure 1.1.

Small quantity diesel injector

Specifically designed to inject the small quantity of fuel needed, to ignite the air-fuel mixture during pilot injections. These injectors are, together with the gas injectors, active during gas mode. The injector with its belonging spray pattern can be seen in the rightmost picture in Figure 1.1 where it is located in the cylinder head.

Large quantity diesel injector

During diesel mode the small quantity injectors can not supply the engine with sufficient fuel, thus is there a need for a third type of injector, namely the large quantity injectors. They are located in the cylinder head and they deliver fuel during the compression stroke in diesel mode.

The orifices in the nozzles of small quantity injectors are too small to deliver sufficient fuel during diesel operation. If presumably enough fuel could be pushed out through the small orifices during the limited injection duration, the spray pattern would unlikely be optimal. To overcome this engine manufacturers normally utilize diesel injectors with larger orifices in diesel mode. This solution enforces the use of two independent diesel injector systems or injectors with multiple needles[2] and nozzles. This induces elevated capital and operational expenditures as installation and maintenance costs increase. The injectors also occupy space in the cylinder head which may affect valve size and combustion chamber geometry. Injector manufacturers have looked upon how to omit the use of a second diesel injector. They regard twin nozzle injectors as a promising approach due to their potential ability to facilitate stable spray patterns independent of the fuel quantity delivered through the nozzle. If true, the small and large quantity diesel injector can be merged and replaced by one injector that serves both purposes. It is also believed that twin nozzles can improve mixture formation for the combustion process for all diesel applications. NOx and soot formation is supposedly reduced through better fuel atomization and evaporation.

The dual fuel engines in question are low pressure dual fuel engines and must not be mistaken for high pressure dual fuel engines which sometimes also are referred to as Gas-Diesel engines. While low pressure engines inject gas into the intake manifold, high pressure engines inject gas straight into the cylinder during the compression stroke. The large and small quantity injectors in Gas-Diesel engines can possibly be replaced by twin nozzles as well, but the gas injector can not. Gas is compressible and it is often injected with totally different pressures than diesel, something which renders a necessity for separate injectors or at least separate needles for the two fuel types.

[2]Injector needles are described in Section 3.1

1.2 Motivation

The motivation for this thesis is the need to better understand twin nozzles, and the mechanisms that potentially can contribute to improved fuel sprays. The understanding is to be achieved through numerical simulations. Numerical simulations of combustion processes and fuel injections are becoming more and more important as computational power becomes more inexpensive. In contrast to prohibitively expensive and time consuming experiments, numerical simulations are cheap and results can often be achieved faster. The thesis does not seek to verify and validate the proposed numerical model, but rather perceive an understanding of the overall flow trend in a twin nozzle and how it may outperform a conventional nozzle

1.3 Twin Nozzle

There exist several types of nozzles today, and the most extensively used is the multi-hole nozzle. It consists of a number of orifices, bored in the tip of the nozzle. The number of orifices and their diameter depends on several factors, some of them being engine size, fuel consumption and combustion bowl geometry. Normally there are between 4 to 18 orifices with a diameter ranging from 35 to 200 µm [13].

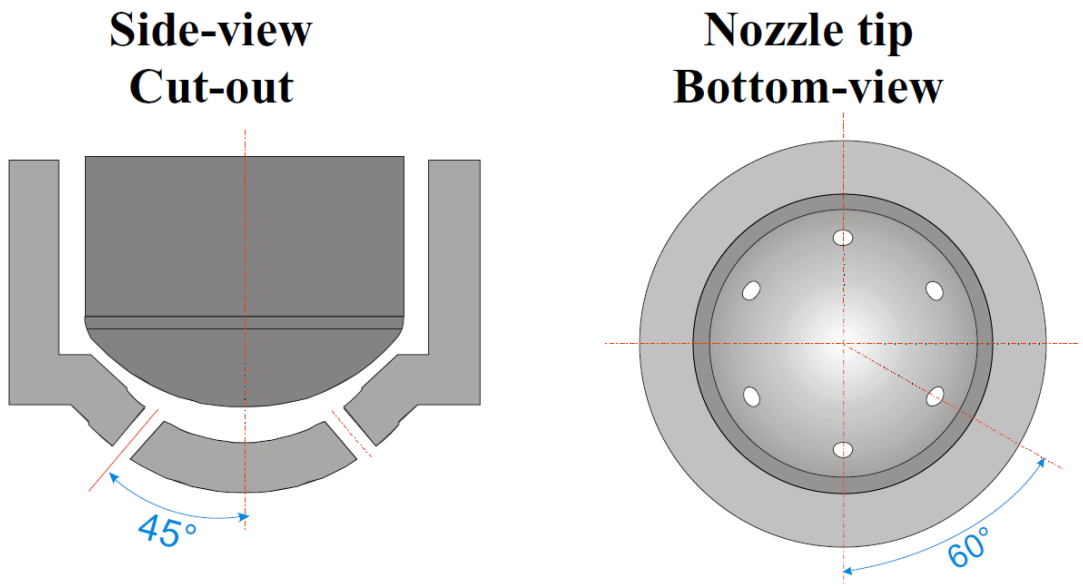

Figure 1.2: Conventional multi-hole nozzle [24]

Figure 1.2 illustrates a conventional symmetric equispaced orifice configuration. The twin nozzle concept that has arisen in light of the new emission legislation differs from the conventional configuration by utilizing two closely spaced orifices to substitute each orifice in the conventional nozzle. New technologies such as electrical discharge machining has emerged over the recent years and enables manufacturers to drill smaller orifices more precisely [41] which makes the twin nozzles possible to manufacture.

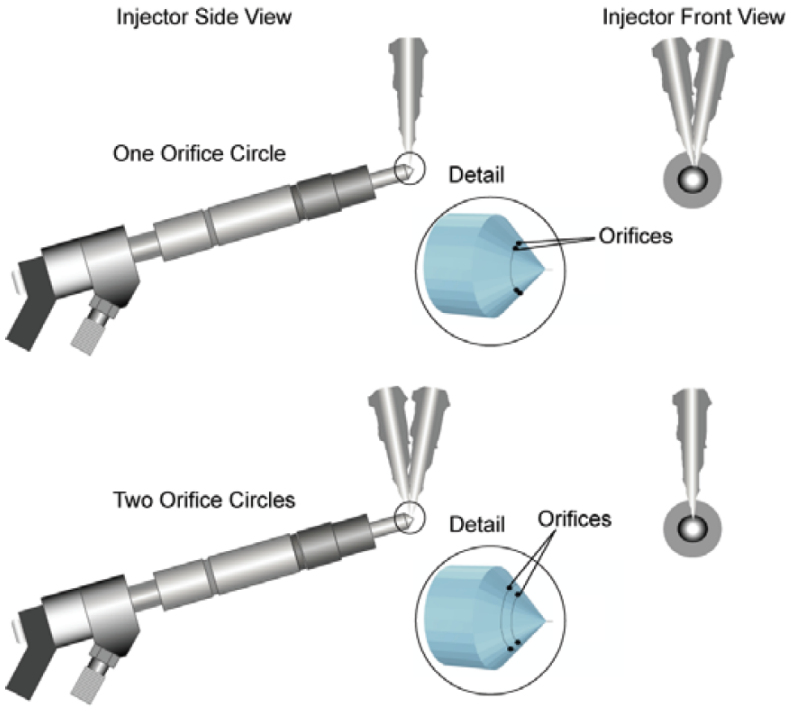

Figure 1.3: Twin nozzle configurations [28]

As Figure 1.3 depicts, orifices are grouped together in a twin configuration. This can be done by one or two orifice circles. If only one circle is utilized the orifices are grouped next to each other along the same circle. If two circles are chosen each orifice in a grouped twin pair is located on adjacent orifice circles. The side view and the front view in Figure 1.3 illustrates the differences in spray pattern between the utilization of one and two orifice circles. If the conventional multi-hole nozzle in Figure 1.2 where to be converted to a twin nozzle, the orifice number would double and the diameter of each orifice would decrease. The nozzle can remain symmetrical, but the equispaced configuration among all the orifices is lost. Only the closely spaced orifice pairs can be equispaced in a twin nozzle.

In addition to the number of orifice circles, there are several other features that make the twin nozzles more complicated than conventional nozzles. The nozzle in Figure 1.4 displays these features. The nozzle has two orifice circles and each orifice pair can diverge, converge or be parallel to each other. The present study will solely focus on a diverging nozzle design with two orifice circles, provided by the injection system manufacturer L'Orange. The angle between the orifice pairs

is not given due to a non-disclosure agreement with L'Orange.

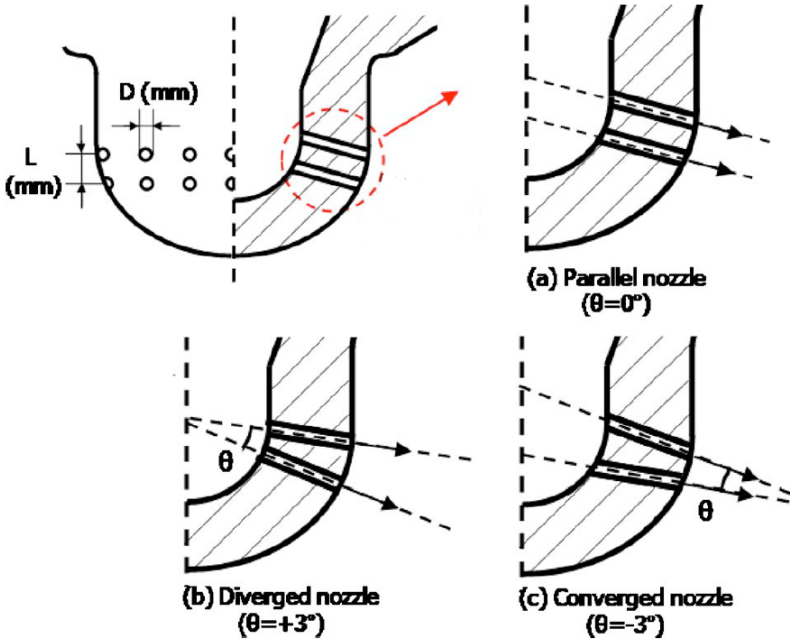

Figure 1.4: Orifice variation [36]

Chapter 2

Fuel Spray

Twin nozzle injectors are to be utilized in diesel engines, dual fuel engines and possibly other engines with diesel-like conditions. Unlike in port fueled engines, and even in direct injected spark engines, diesel spray plays an important role in determining combustion characteristic and formation of pollutants. When diesel is injected into a high pressure and high temperature combustion chamber it should, ideally, atomize into microscopic droplets, vaporize and yield an easy combustible mixture without formation of NOx or soot. The diesel spray and its features is the chief concern of this chapter. The theory presented is, if not stated otherwise, according to Baumgarten [8].

2.1 Spray Breakup

When high pressure diesel leaves the nozzle orifice a jet is formed. This jet subsequently disintegrates and the break up is governed by the fluid's velocity together with the properties of the fluid and the surrounding gas. According to Reitz and Braco [31] there are four different distinguishable regimes of break-ups; the Rayleigh regime, the first and second wind-induced regime and the atomization regime. A break-up is identified by the break-up length and the size of the droplets that are produced during the jet disintegration. The break-up length is the length of the intact jet core which is the distance between the nozzle and the first droplet formation. Ohnesorge [26] characterized the behaviour of the jet by using the Weber number(2.1) and Reynolds number(2.2):

$$We = \frac{u^2 D \rho_l}{\sigma} \tag{2.1}$$

$$Re = \frac{u D \rho_l}{\mu_l} \tag{2.2}$$

Where u is the jet velocity, D the orifice diameter, ρ the density of the liquid, μ the dynamic viscosity of the liquid and σ the surface tension of the liquid. Ohnesorge introduced the dimensionless Ohnesorge number by dividing the square of the Weber number with the Reynolds number and thereby eliminating the jet velocity,

$$Z = \frac{\sqrt{We}}{Re} = \frac{\mu_l}{\sqrt{\sigma \rho_l D}}. \tag{2.3}$$

The following figure shows the Ohnesorge diagram, where the Ohnesorge number is given as a function of the Reynolds number. It shows how the boundaries between the different regions are dependent on the Reynolds and Ohnesorge numbers:

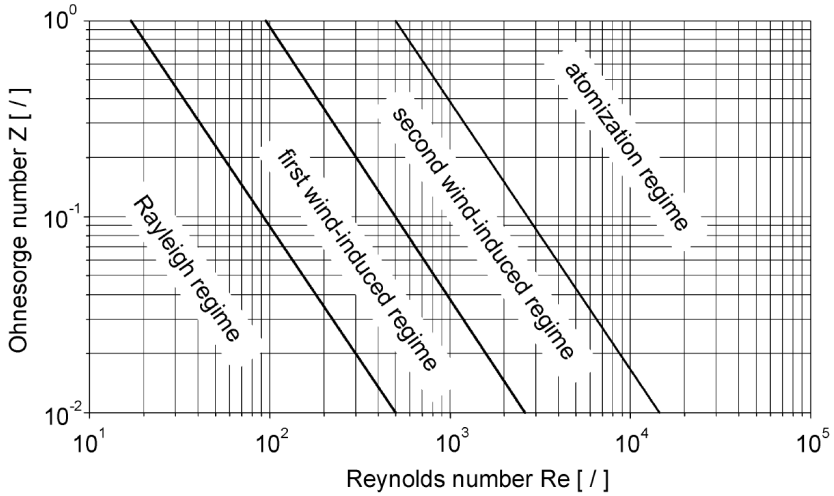

Figure 2.1: Break-up regimes [8]

Eventually it was acknowledged that the properties of the gas which the jet enters also affect the description of the break-up regimes. Reitz [30] then introduced an third dimension to Ohnesorge's diagram, thereby extending it to also include the gas to liquid density ratio:

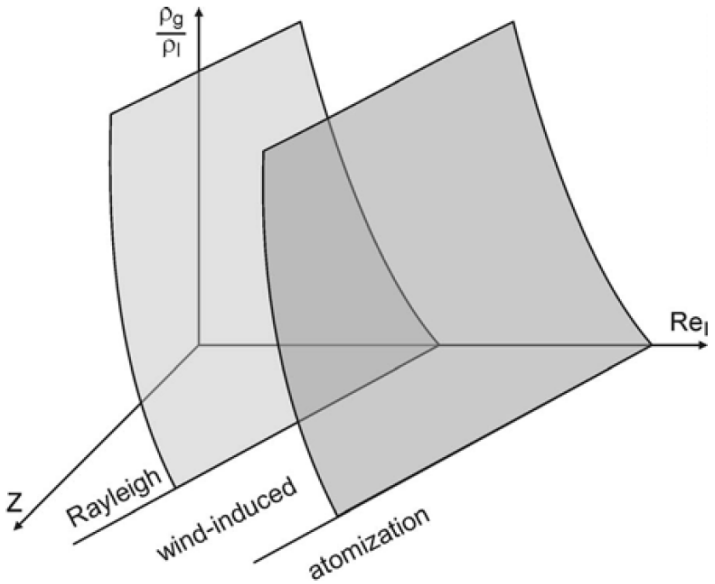

Figure 2.2: Break-up regimes including the effect of gas density [8]

A convenient method to characterize the jet break-up is to consider the break-up length as a function of the jet velocity only. This is an reasonable approximation as

the jet velocity is normally the only variable that fluctuates extensively in Equation 2.1 and 2.2, regardless of the injection application.

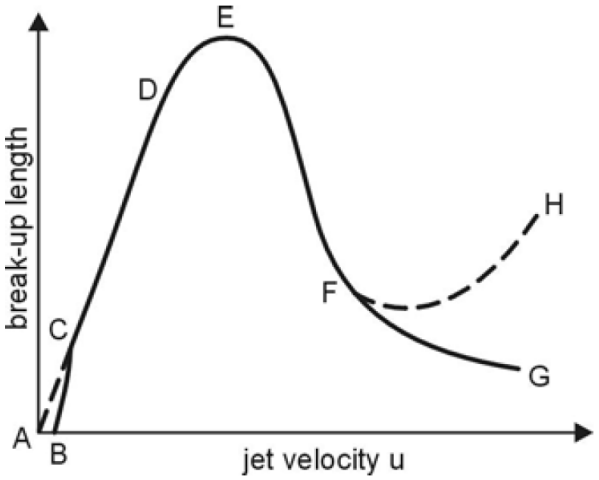

Figure 2.3: Break-up length as function of jet velocity [31]

When the jet velocity is very low, seen as ABC in Figure 2.3, the flow has no distinctive jet and therefore no break-up length. It is then a dripping flow, much like the flow seen when a water-tap is not properly shut. As the jet velocity increases, beyond the dripping flow regime, a jet is formed and the break-up length increases linearly with the jet velocity. When the jet breaks somewhere between C and D it is in the Rayleigh regime. The droplets which break off have a greater diameter than the nozzle orifice diameter. In the first wind-induced break-up, EF, further increase in jet velocity will decrease the break-up length. The droplet size decreases to the same range as the orifice size. The jet velocity is now sufficiently high so that aerodynamic forces do affect the spray (see Sec. 2.2). As jet velocity increases the flow inside the nozzle becomes turbulent and the flow then enters the second wind-induced break-up regime. The droplets which are pinched off from the jet are smaller than the nozzle diameter. The jet no longer disintegrates as whole, but it gradually breaks up from the surface and continuing inwards through its core until it is completely broken up. As a result two different break-up lengths are used to describe the flow. The intact surface length, FG, describes where the surface break-up commences while the core length, FH, describes where the jet break-up ends. The intact surface length decreases with increasing jet velocity, while the core length may increase even though Figure 2.3 does not depict it. The atomization regime is reached if the jet velocity goes beyond point G or H in the above figure and the intact surface length approaches zero. Distinctive for the atomization regime is the conical spray developed by the flow. The spray starts to diverge as soon as the flow leaves the nozzle. There may be an intact core or a dense core present several nozzle diameters downstream of the nozzle. The atomization regime is the relevant regime for fuel injection in engines. It also the regime which is hardest to theoretically describe as the spray is highly dependent on the flow inside the nozzle which is complex and often of a chaotic nature. The appearance of the flows in the different break-up regimes is reflected in Figure 2.4.

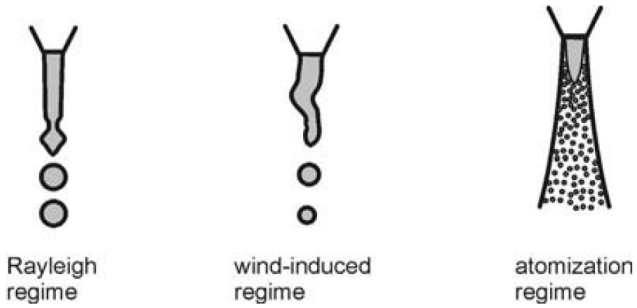

Figure 2.4: Description of jet break-up regimes [8]

2.2 Droplet Breakup

A travelling jet will experience aerodynamic forces which are forces present due to pressure difference and friction induced by the relative velocity, u_{rel} between the jet and the surrounding gas. When the aerodynamic forces are great enough the droplets formed during the jet disintegration will break-up and form new smaller droplets. These new smaller droplets are again subjected to further aerodynamic forces which may cause a new droplet break-up. The surface tension within the droplets strives to keep the droplet spherical and thereby counteracts the droplet break-up. Surface tension will increase as droplet size decrease, thus will a higher relative velocity, u_{rel}, be necessary to break up droplets any further. This leads to an uneven and unstable droplet disintegration. The behaviour can be described by the gas phase Weber number which represents the ratio between aerodynamic and surface tension forces,

$$We_g = \frac{\rho_g u_{rel}^2 d}{\sigma}. \tag{2.4}$$

Where ρ_g is the gas density, d the the droplet diameter before breakup and σ the surface tension between the liquid and the gas.

Through experiments conducted in the past, researchers have established a relationship between different Weber numbers and droplet break-ups. Figure 2.5 illustrates Wierzba's [38] findings on how droplets break-up behave at different regimes. Vibrational break-up occurs at around $We_g \approx 12$ and catastrophic break up at $We_g > 1000$. However, it must be pointed out that measurement of droplet break-up is difficult, especially for high Weber numbers where droplets are small and fast travelling. Transition Weber numbers for the different regimes vary somewhat in the published literature. In an engine spray all of the break-ups in Figure 2.5 will occur, but the stripping and catastrophic break-up is predominant as most of the disintegration process takes place near the nozzle at high Weber numbers. Further downstream Weber numbers are lower as the droplets are slowed down due to drag forces. Droplets will eventually evaporate rather than break-up.

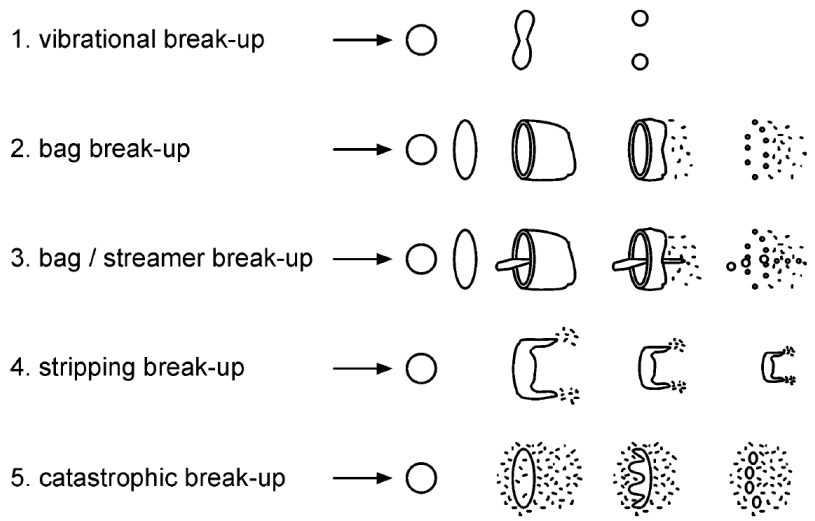

Figure 2.5: Description of drop break-up regimes [38]

2.3 Spray Characterisation

When a jet and the following droplets undergo their respective break-ups in engine-like conditions a spray will emerge. The spray is characterized by parameters such as the penetration length, cone angle, Sauter Mean Diameter (SMD) and the already mentioned break-up length (Sec. 2.1). A single orifice high pressure spray will resemble the following schematic description:

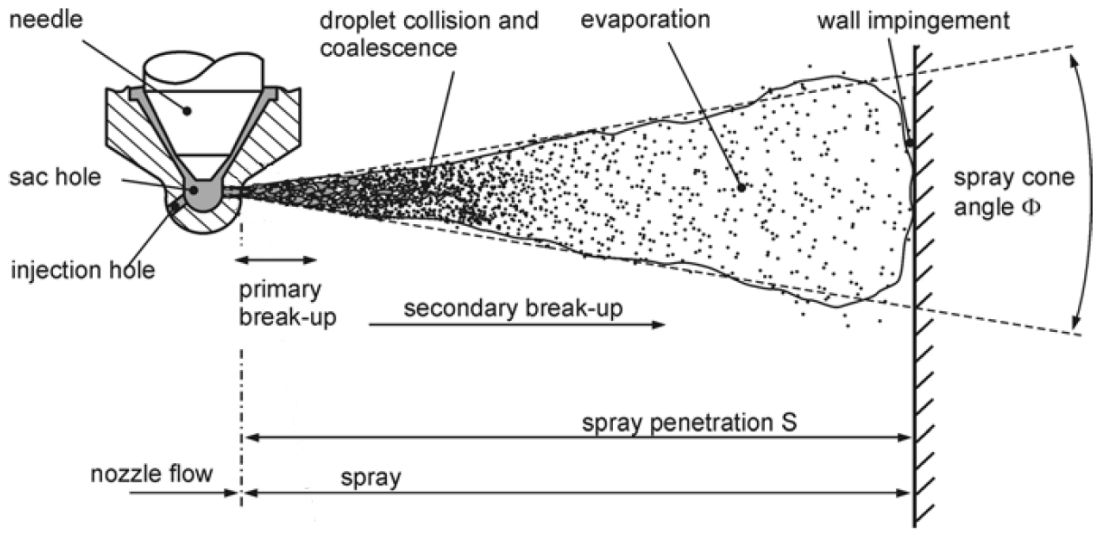

Figure 2.6: Schematic description of a high pressure fuel spray [8]

Immediately after the fuel leaves the nozzle it will undergo an atomization as discussed in Sec. 2.1. This first break-up is called the primary break-up and it

results in a dense spray near the nozzle. The following break-up, where aerodynamic forces disintegrate already existing droplets into new smaller droplets as discussed in the previous section, is called the secondary break-up. During this break-up the spray dilutes due to the entrainment of air. The spray is generally denser along the axis of the spray as the outer regions contain less liquid mass and more fuel vapour. The probability of droplet collision is biggest in this dense region. A collision can change the size and the velocity of the travelling droplets. The can collide and break into smaller droplets or merge into a bigger droplet, where the latter is called coalescence. During a fuel injection the fuel droplets at the spray tip will experience higher drag forces than the droplets following in the wake. The drag forces decelerate the spray tip droplets allowing the droplets in the wake to overtake. The spray propagates in such a way that only the droplets with the highest kinetic energy are located in the spray tip at any given time. The outer region of the spray consists of droplets which were pushed aside by droplets with higher kinetic energy.

2.3.1 Penetration Length

Penetration length is the distance between the nozzle and the droplets that have travelled farthest downstream of the nozzle exit. This parameter is one of the most important in regard of spray characterisation within a combustion chamber. The penetration length must neither be too short, nor too long. Adequate penetration is necessary in order for the fuel to mix with air inside the combustion chamber. When the air is sufficiently utilized the correct air to fuel ratio, λ, can be achieved more efficiently. This allows for cleaner and faster combustion within the cylinder. If the fuel over-penetrates it will hit the combustion bowl wall or/and the piston crown and create undesired wall interactions [19]. Such over-penetration is called wall impinging and is associated with enhancement of soot formation and fuel wastage.

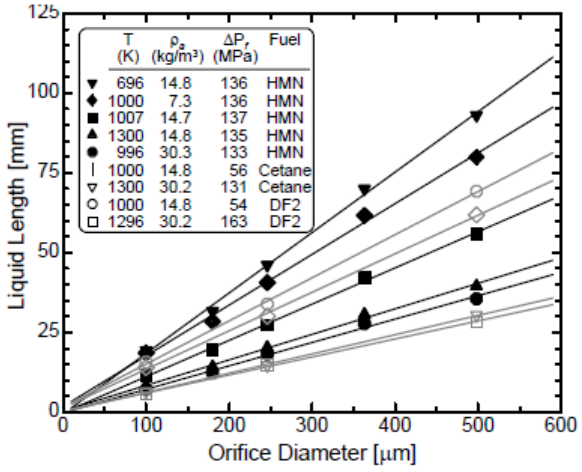

Figure 2.7: Penetration length versus orifice diameter [34]

Siebers [34] experimentally studied the effects of spray tip penetration for various parameters. Figure 2.7 shows the effects of penetration length for a series of orifice diameters. The legend in the upper right corner of the figure describes in-cylinder gas temperature (T) and density (ρ_g), pressure drop over the orifice (Δp_f) and the used fuel type. There is an obvious trend implying longer penetration for larger diameter orifices. Larger orifice diameter delays the start of the secondary break-up regime, thus increasing the penetration length [21]. Siebers [34] also found, as Figure 2.8 shows, that penetration length is very sensitive to in-cylinder pressure and somewhat less sensitive to in-cylinder gas temperature. Higher pressure in the cylinder yields a higher gas density which shortens the penetration length. As the cylinder temperature increases more of the liquid spray evaporates and the penetration length decreases.

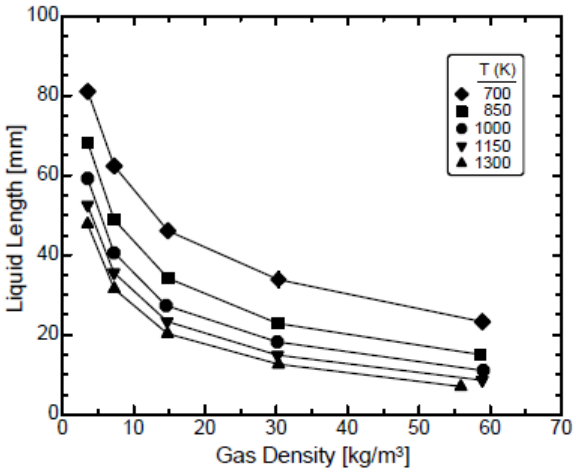

Figure 2.8: Penetration length versus in-cylinder gas density [34]

Siebers [34] also investigated the effects of the injected fuel temperature for two different fuels as shown in the following figure:

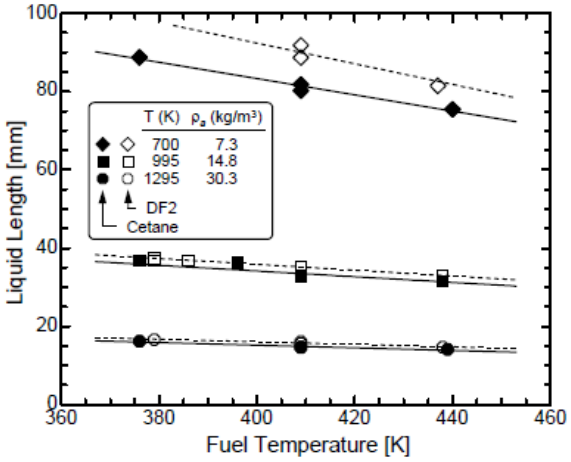

Figure 2.9: Penetration length versus injected fuel temperature [34]

Penetration length decreases linearly with increasing fuel temperature. A higher fuel temperature gives a reduction in the energy required to vaporize the fuel. Thus will the injected spray evaporate earlier and reduce the time the liquid can travel. The effect of fuel temperature is more pronounced for lower in-cylinder pressures. At higher pressures the effect seems rather insignificant.

Abdelghaffar et al. [1] experimentally studied the effect of injection pressure on penetration length using nozzles with both three and five orifices. Their findings are depicted in Figure 2.10. In general a longer penetration length can be noticed for higher injection pressures. The authors report that higher injection pressures quicker produce a developed spray. As soon as the spray is fully developed the penetration length will fluctuate around an average value. Increasing the number of nozzle orifices reduces penetration length somewhat due to greater pressure drop during injection.

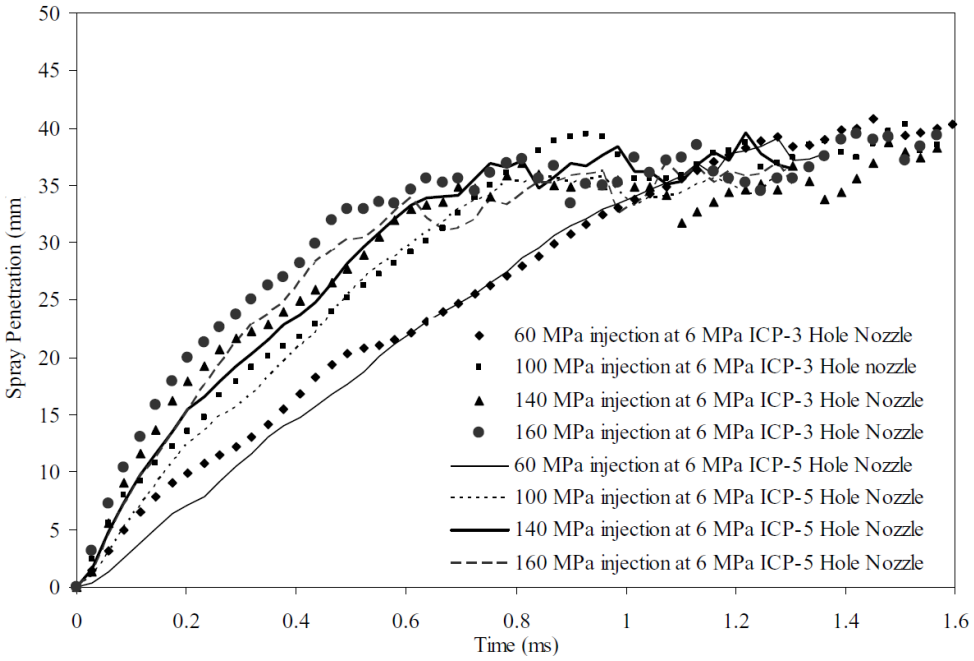

Figure 2.10: Penetration length versus time for various injection pressures [1]

For a given engine, fuel injection manufacturers have to adjust the orifice diameter and injection pressure to suit the piston bowl and the in-cylinder pressures produced by the engine to ensure an adequate penetration length with no wall impingement. When using a twin nozzle the angle between the nozzle orifices (shown as θ in Figure 1.4) is an additional factor that has to be accounted for. Suh and Lee [36] reports that a diverging nozzle orifice shortens the penetration, while converging nozzle orifices extends the penetration length compared to parallel nozzle orifices. Penetration length is by now well understood, but engines running on full load (long injection duration) or engines with early injection (low in-cylinder pressure at time of injection) can suffer from wall impingement [8]. Also cold start condition can contribute to wall impingement as less fuel vaporizes under cold conditions, thus extending the penetration length.

2.3.2 Spray Cone Angle

The spray cone angle (shown as ϕ in Figure 2.6) is the angle that is formed by the periphery of the spray cone. As for the penetration length the optimal spray cone angle is angle that fills the combustion bowl without wall impingement. This yields the best air entrainment and therefore the best conditions for locally obtaining the correct air fuel ratio in order for the mixture to ignite. Cone angle is as penetration length very sensitive to in-cylinder pressure. As the in-cylinder pressure increases the penetration length decreases and thereby elevating the cone angle due to more of the injected fuel being pushed out to the outer boundary of the spray. Bracco[5] shows in Figure 2.11 how the cone angle behaves with varying gas to liquid density ratios. The black and white squares, triangles and circles depict different types of orifices and orifice diameters. The cone angle behaviour is almost inverse to the trend shown in Figure 2.8 which depicts penetration length versus in-cylinder gas density. Bracco [5] investigated this for a nozzle length to nozzle diameter, L_n/d_n, ratio of four. The cone angle trend is similar for other aspect ratios, but with different slope angles. High aspect ratios will in general produce lower slope angles, while low aspects ratios produce higher slope angles [16]. Subsequently will an increase in the aspect ratio give a reduced cone angle and vice versa.

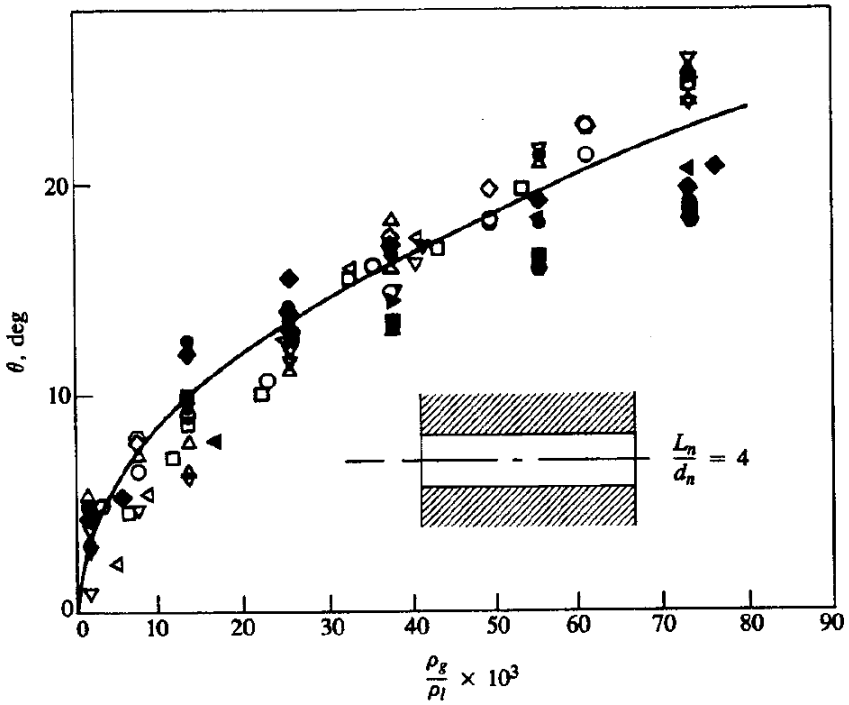

Figure 2.11: Cone angle versus gas to liquid density ratio [5].

Schugger & Renz [33] conducted experiments which showed that nozzle hole geometry plays an important role on the cone angle. An increase in the nozzle K-factor[1] together with rounded inlet edges contributes to a reduction in cone angle.

[1]K-factor is described in Section 3.3

Hiroyasu & Arai [17] studied the effect of injection pressure and kinematic viscosity on the spray cone angle. Their results are shown in Figure 2.12:

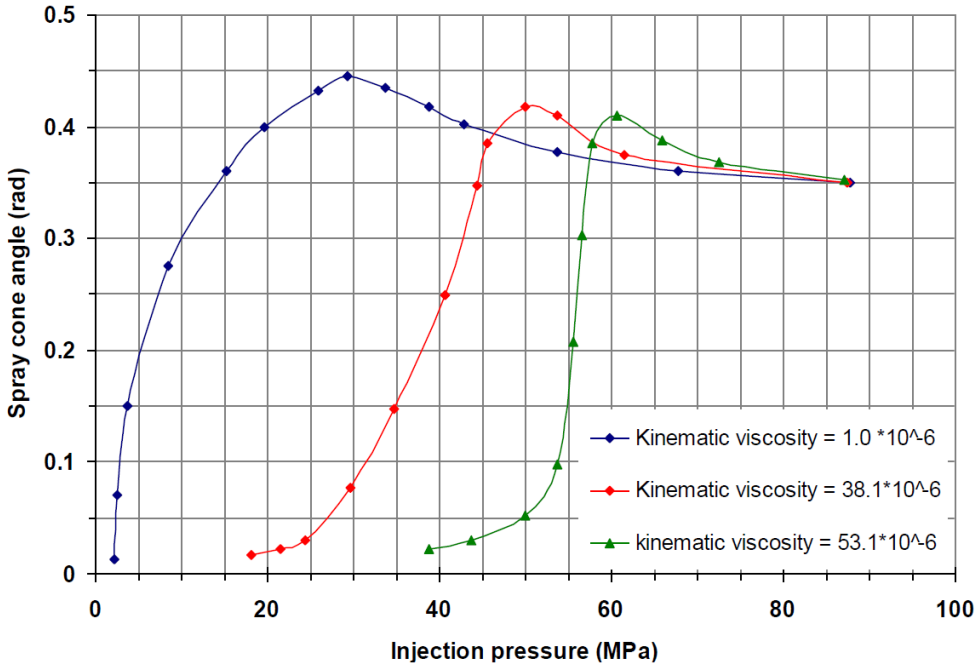

Figure 2.12: Cone angle versus injection pressure [19]

The authors report that the cone angle increases to a maximal value and thereafter decreases to a constant value as the injection pressure is increased and the spray is fully atomized. The cone angle levels off at the same constant angel regardless of the kinematic viscosity of the fuel. This constant level will of course vary for different nozzles due to differences in the parameters described earlier in this subsection. Modern injection applications maintain a high enough pressure to produce the cone angle characteristic for a fully atomized spray.

2.3.3 Sauter Mean Diameter

The Sauter mean diameter (SMD) is used to characterize the average droplet size in a spray. The SMD is the diameter of a droplet that has the same ratio of volume to surface area as the entire spray. The entire spray in this context is regarded as the ratio of the sum of all droplet volumes to the sum of all droplet surfaces. Baumgarten[8] defines the SMD when surface area and volume are not known as,

$$SMD = \sum_{i=1}^{n} d_i^3 / \sum_{i=1}^{n} d_i^2, \tag{2.5}$$

where d is the droplet diameter, n the total number of droplets and i the droplet index.

The relation between the diameter of a sphere and its surface area is the diameter raised to the power of two. Thus, will a smaller SMD produce more surface area per volume unit. The droplet surface area of a spray with many small droplets will be greater than if a spray consisted of fewer, but larger droplets. The SMD is therefore extensively used to characterize the success of a spray break-up. The more surface area, the faster will the fuel evaporate, mix with air and ignite. Qualities that provide for more efficient combustion.

Parameters influencing the SMD have been extensively studied. Arai et al. [2] investigated the effect of injection pressure and nozzle geometry on spray SMD. Their results shows that the SMD decreases as injection pressure increases. The added pressure induces more energy to the spray which generates a finer spray and faster penetration. Figure 2.13a shows that the L_n/d_n ratio influences the SMD at low pressure, while Figure 2.13b shows that a small orifice diameter is always beneficial for decreasing the SMD due to initial smaller droplets.

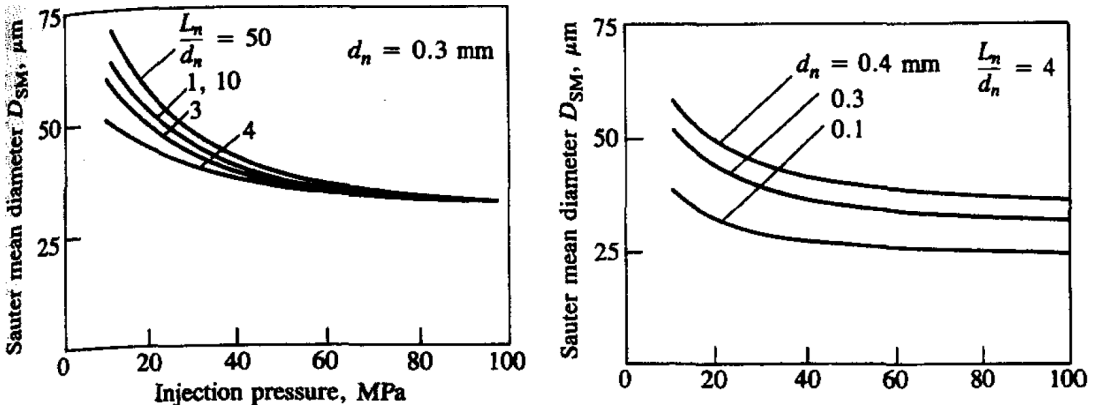

(a) Constant d_n

(b) Constant L_n/d_n ratio

Figure 2.13: Effects of nozzle geometry and injection pressure on SMD [2]

Su et al. [35] report that nozzles with rounded inlet edges produced a larger SMD. However, the difference in SMD for rounded and sharp inlet edges diminishes as the injection pressure is increased. Baumgarten [8] outlines that the SMD increases with higher in-cylinder pressure due to more frequent occurrence of coalescence.

It must be pointed out that the SMD says nothing about the droplet distribution. Two sprays with identical SMD can have completely different droplet distributions. It also very hard to measure the droplet diameter. It can only be done in the diluted region some distance from the nozzle or in the outer edge of the spray. This results in a degree of uncertainty when describing the SMD of a full spray.

2.4 Primary Break-up Mechanisms

In Section 2.1 it was mentioned that the primary break-up occurs in the atomization regime at high Weber numbers near the nozzle, and that the break-up is strongly dependent on the nature of the flow inside the nozzle. This section will try to illuminate, according to Baumgarten [8], possible mechanisms inside the nozzle that can affect the primary break-up.

It is believed that due to turbulence created inside the nozzle a spectrum of tiny surface waves are present on the jet surface as it leaves the nozzle (Figure 2.14a). The jet is experiencing aerodynamic forces induced by the relative velocity between the jet and the surrounding gas. Some of the waves on the jet surface are intensified by the aerodynamic forces so they become unstable, break free from the jet and form the primary droplets. However, this mechanism is of secondary importance as it is a time consuming process that can only affect the surface of the jet and not the inner core. It is a well known fact that the entire jet, both the surface and the inner core, disintegrates rapidly after leaving the nozzle, when in the atomization regime.

Another possible break-up mechanism is the abrupt change of the velocity profile at the instant the fuel leaves the nozzle (Figure 2.14c). Due to the presence of walls in the nozzle hole the no-slip condition slows down the fuel. As the fuel enters the combustion chamber and the no-slip condition no longer applies the fuel in the outer region accelerates until the velocity profile turns into a block profile. This acceleration may cause instabilities and contribute to the break-up of the jet. However, such velocity profiles can only be present if the turbulent flow inside the nozzle is fully developed and this requires large L_n/d_n ratios which are rather uncommon.

The third possible primary break-up mechanism, which is regarded as one of the more important, is the turbulence induced break-up (Figure 2.14b). The turbulence induced in the nozzle can generate vortices strong enough to overcome the fuels liquid tension and leave the jet to form primary droplets.

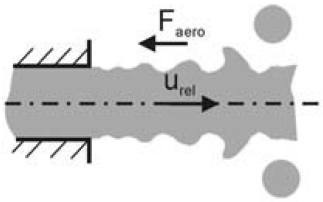

(a) Growth of surface waves

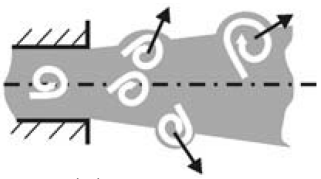

(b) Turbulence

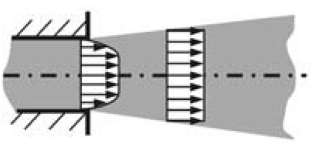

(c) Change in velocity profile

Figure 2.14: Primary break-up mechanisms [8]

2.4.1 Cavitation

Turbulence together with cavitation are the most important break-up mechanisms in a high pressure fuel jet. A general description of cavitation is the occurrence of vapour bubbles in a fluid and their intense implosion due to low local pressure. The pressure decrease is caused by the geometry which the fluid flows through. Such geometries can be the confining regions of nozzle holes. The small cross sectional area increase the fluid velocity resulting in a decrease of the pressure. A flow governed by the Bernoulli equation can be used to explain the fact that an increase in flow velocity yields a decrease pressure. Low pressure can also occur if the flow undergoes a sudden directional change. Nozzles usually have a strong curvature where the fluid undergoes a strong directional change as it is forced into the nozzle orifice. These two geometry characteristics lower the local pressure below the vapour pressure allowing the fuel to evaporate and form vapour bubbles. In general all fluids have some amount of dissolved gas in them. The gas is located in macroscopic bubbles called nuclei and cavitation is initiated from them [6]. These nuclei are present in the fluid or in imperfections and small gasp in the wall. When the pressure falls, more gas tends to come out of the solution and form even more nuclei. The amount of gas that comes out of the solution is governed by Henry's law, which states that at a given temperature the amount of dissolved gas is directly proportional to the partial pressure of the gas in the solution [6]. The nuclei serve as a starting point for bigger vapour bubbles to grow as the pressure falls below the vapour pressure. As the vapour bubbles move with the flow from a low pressure to a high pressure zone they implode. The implosion is so intense that the local speed of sound in the fluid is exceeded and a shock wave is generated. This can lead to damage of nearby surfaces which is referred to as cavitation erosion. The bubble implosion is often accompanied by noise, vibrations and disruption of the flow.

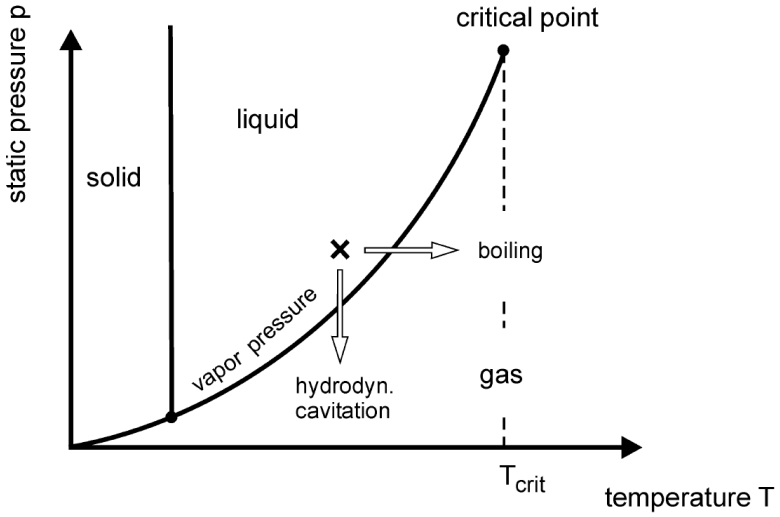

Figure 2.15: Phase diagram [8].

Another way for a fluid to arrive at a transition from liquid to vapour is commonly referred to as boiling, as illustrated in Figure 2.15. The transition into vapour is then not due to lower local pressure, but an increase of the local temperature. The distinction between these phenomena is often not very sharp, because both pressure and temperature effects can be present at the same time. The temperature of the nozzle walls are elevated during the compression stroke, thus will the fuel experience both a pressure drop and temperature increase when entering the nozzle. This increases the probability of a transition into the gas phase and thus also cavitation.

The bubble implosions intensify the jet-break up and increase the turbulence level. Experimental results have shown that cavitation increases the cone angle and decreases the penetration length [8]. The lowest local pressure in the nozzle is located in recirculation zone just downstream of the inlet edge, see Figure 2.16.

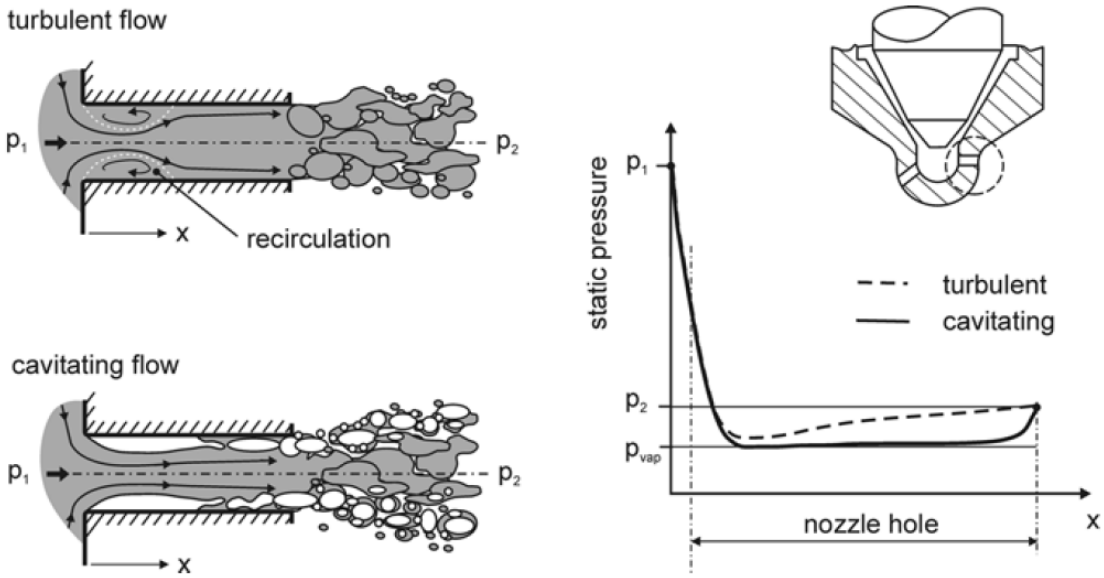

Figure 2.16: Cavitating and non-cavitating nozzle flow [8]

If the pressure in the recirculation zone reaches the vapour pressure it will fill with vapour. Due to the shear force induced by the difference in velocity between the recirculation zone and the main flow the vapour will move along the nozzle wall towards the nozzle exit. The vapour bubbles usually leave the nozzle and collapse inside the combustion chamber, but they may also start to collapse inside the nozzle. Figure 2.16 depicts how a high pressure nozzle flow will behave with and without the presence of cavitation.

The nozzle geometry plays a crucial part in regard of cavitation formation. Schugger & Renz [33] found that nozzles with sharp inlet edges produce more cavitation, larger cone angles and a finer spray than nozzles with rounded inlet edges. The rounded edges allow for a smaller directional change and a smother decrease in pressure as the flow enters the nozzle hole.

The smallest cross sectional area the flow has to go through is normally the nozzle holes. However, the instant the needle lifts and closes the smallest cross sectional area is located at the needle seat. The vapour bubbles that are produced can either collapse before entering the injection holes which results in a turbulence increase or enter the hole, collapse and alter the flow conditions in the holes.

There is a disagreement on whether the presence of cavitation in injection systems enhances engine performance and emissions or not. On one hand cavitation intensifies turbulence and improves spray integration. Its presence also provides for nozzle cleaning by removing any fuel deposits and other stuck impurities that may obstruct the flow. On the other hand cavitation reduced the effective cross sectional area of the injector holes that may impair performance during full load when large fuel masses are injected. If vapour bubbles collapse before they enter the combustion chamber the nozzle may suffer from cavitation erosion. In the long run this can severely damage the nozzle, change its spray characteristics and even render it useless [3].

Chapter 3

Common Rail and Nozzle Types

The purpose of this chapter is to give a brief description of common rail injection systems, the application twin nozzles are intended for. Further on, a brief description of different nozzles type will be given together with a description of the particular nozzle investigated in the present study. For a more thorough review of common rail systems and injector systems in general the reader is referred to Mollenhauer and Tschoke [25].

3.1 Common Rail Injection Systems

Common rail systems are the main application for diesel cars and the system's implementation and can be expected to be seen in virtually every suitable marine engine as well. The task of a injection system is to generate pressure, precisely meter the fuel according to engine speed and load, route it to the nozzle and inject it at the correct time with the desired rate. Until recently, injection systems were camshaft driven and the delivered pressure was a function of engine speed and load. The highest injection pressures could only be delivered at the highest engine speeds. Unlike these mechanically driven systems the common rail system generates pressure by a high pressure pump which is not dependent on the engine speed. The pump constantly feeds pressurized fuel to an accumulator volume or rail. The injectors, one for each cylinder, are connected to this rail, as seen in Figure 3.1. Hence the name common rail.

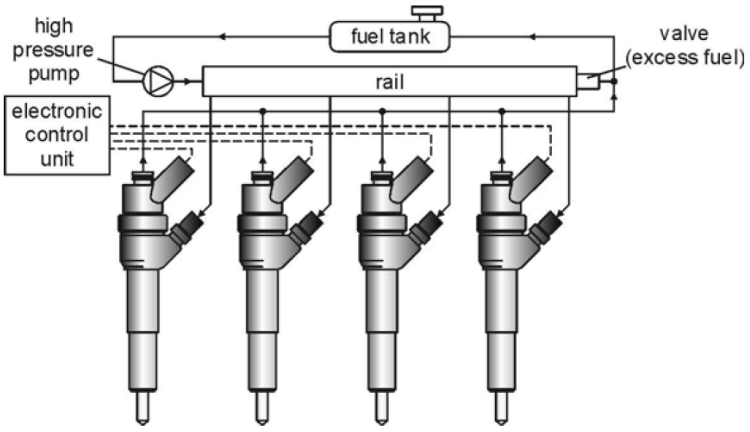

Figure 3.1: Common rail injection system [8]

The rail's main purpose is to serve as accumulator and dampen the pressure fluctuation when fuel is discharged and supplied to it. The common rail systems always maintain a high pressure regardless of engine speed. Its flexibility allows it to perform multiple injections with adaptable duration and timing according to the demands of the actual engine speed and load. In the recent years it has become more common to perform a pre-injection, main injection and post-injection for every engine cycle. Pre-injections reduce noise and NOx emissions while post-injections increases exhaust temperature and enhance soot oxidation. Common rail systems are today capable of generating pressures between 200 and 2000 bars [23].

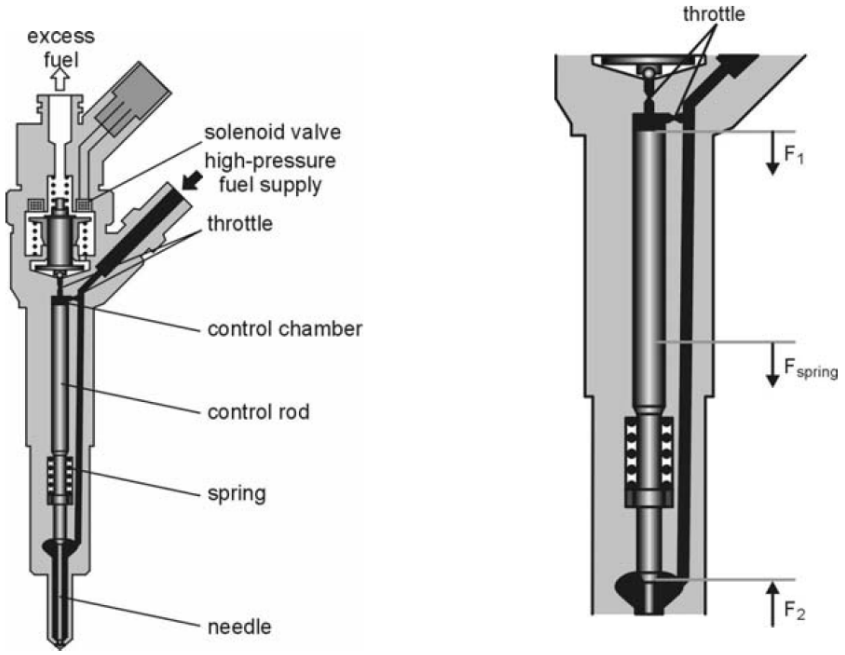

Figure 3.2: Common rail injector [8]

Figure 3.2 shows a typical common rail injector controlled by a solenoid valve. Piezoelectric valves are also extensively used. The injector in the above figure is closed as the needle blocks the injector holes. The force F_1, where pressure from the rail is applied on the control rod, and the spring force F_{spring}, is greater than F_2. When the valve is actuated with a current from the electric control unit (ECU) it will open and fuel will flow from the control chamber through the outlet throttle and towards the top of the injector (as excess fuel). Since the inlet throttle connecting the control chamber with the fuel supply is much smaller than the outlet throttle, the pressure in the control chamber will decrease and so will F_1. As a result the control rod and the needle will rise and expose the injector holes. When the ECU initiates the closing process it terminates the actuating current which closes the valve and allows the pressure to increase in the control chamber. Subsequently will the control rod close the needle. The opening and closing speed of the needle is determined by the size ratio of the throttles which direct fuel in and out of the control chamber.

3.2 Nozzle Types

In direct injected diesel engines mainly two nozzle types are used, the valve covered orifice nozzle (VCO) and the sac hole nozzle (see Figure 3.3). Their main difference lies in how the nozzles block out the fuel flow. The VCO nozzle blocks the flow by covering the injection holes with the needle. The sac hole nozzle blocks the flow by resting the needle on the needle seat without covering the injection holes. The method used is decisive for the sac hole volume. The sac hole nozzle has an larger volume under the needle. It is desirable to keep this volume at a minimal since any fuel present in the volume can enter the combustion chamber after the end of injection. When it enters, it will evaporate at a late stage and increase the engine's soot emission. With its small sac hole volume, the VCO is superior from this viewpoint. However, it is a disadvantage to have a needle covering the injector holes. The movement of the needle will affect the mass flow through the injector holes which may deteriorate the spray characteristics. In addition, the needle in the sac hole nozzle has to only seal one opening while the VCO nozzle needle must seal every injection hole. In case of long term erosion it is more likely that the VCO needle will fail to seal properly.

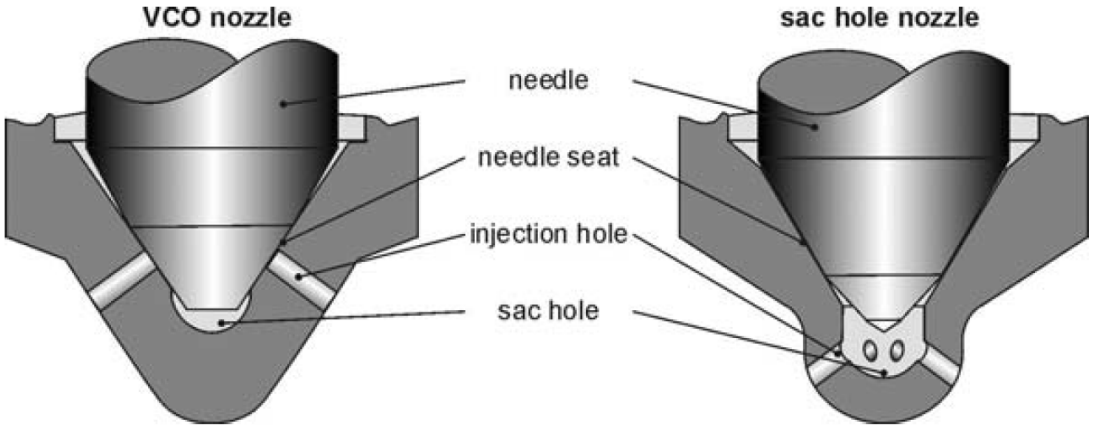

Figure 3.3: VCO and SAC nozzle [8]

3.3 Nozzle Hole Geometries

The inlets of the injection holes are normally rounded. This is as discussed in Section 2.4.1 a measure to suppress cavitation. Along with the rounding, injection holes are often made conical so the inlet has a larger diameter than the outlet. By gradually reducing the cross sectional area of the injector holes cavitation is suppressed even further. The k-factor[8] defines the degree of conicalness as

$$k = \frac{D_{inlet} - D_{outlet}}{10} \tag{3.1}$$

where the diameter is to be given in μm.

Figure 3.4 shows different injection holes geometries used today. The cylindrical injection hole has a constant diameter and a rounded inlet. The k-nozzle has a k-factor in addition to a rounded inlet. The ks-nozzle differs from the k-nozzle by having an uneven degree of rounding at the inlet. In Figure 3.4 the top edge of the ks-nozzle has more rounding than the lower edge. This is beneficial when the injector hole flow is asymmetric. If most of the mass flow enters at the top edge this is the area which will reach the lowest pressure, thus is more rounding required here to suppress cavitation.

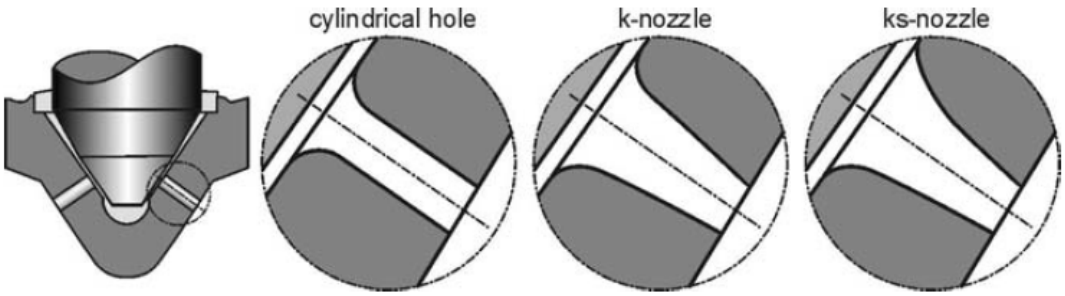

Figure 3.4: Injection hole geometries [8].

By the use of k- and ks-nozzles it is possible to reduce the extent of cavitation significantly, but it is nearly impossible to manufacture completely cavitation free injectors for engine applications. Due to the small dimensions, large flow velocities, and very dense spray at the nozzle outlet, no prior experimental investigation has been published on the structure and size of the cavitation bubbles in the primary spray break-up. Any description of their behaviour solely relies on mathematical models [8].

3.4 L'Orange's Twin Nozzle

The present study simulates a twin nozzle from the injector manufacturer L'Orange. The company specializes in injection technology for heavy duty engines. L'Orange is currently investigating how and if twin nozzle are beneficial for producing a more efficient fuel spray, and if the potential benefits makes the nozzle design commercially viable. They have been kind enough to provide a model of their twin nozzle prototype, see Figure 3.5 and 3.6.

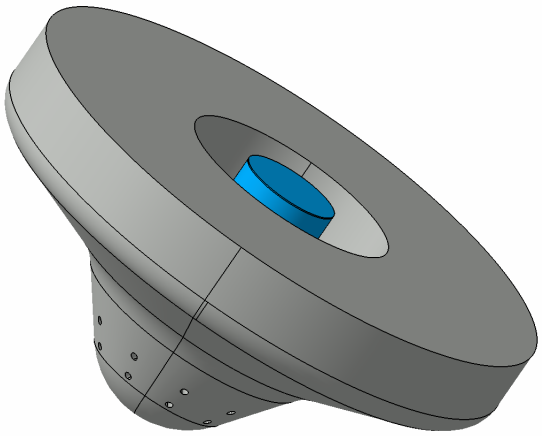

Figure 3.5: L'Orange's twin nozzle

The nozzle is a sac hole nozzle with 20 orifices divided between two orifice circles. The design is intended to be used on high pressure common rail applications. Figure 3.6 shows a section cut of the nozzle where the needle is shaded blue and the internal cavity where fuel would flow is shaded yellow. The depicted nozzle has an open needle. The 10 orifice pairs are equispaced with 36 degrees between each of them.

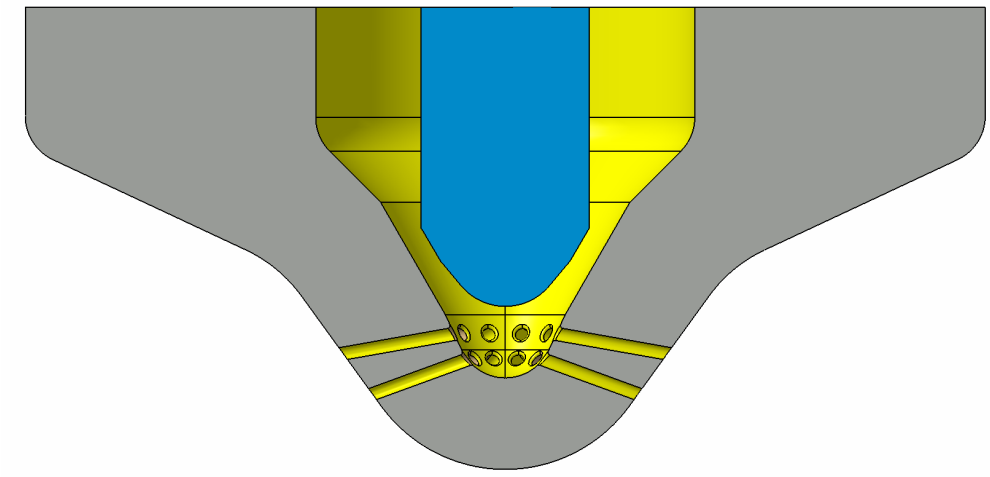

Figure 3.6: L'Orange's twin nozzle - Section cut

Figure 3.7 shows a sketch where some of the main dimensions are depicted[1]. All lengths are given in millimetres. The upper injector hole is slightly longer than the lower. Their respective injector hole length to nozzle diameter ratio, L_n/d_n, is 8.75 and 7.85. All orifices have a constant diameter of 0.27mm.

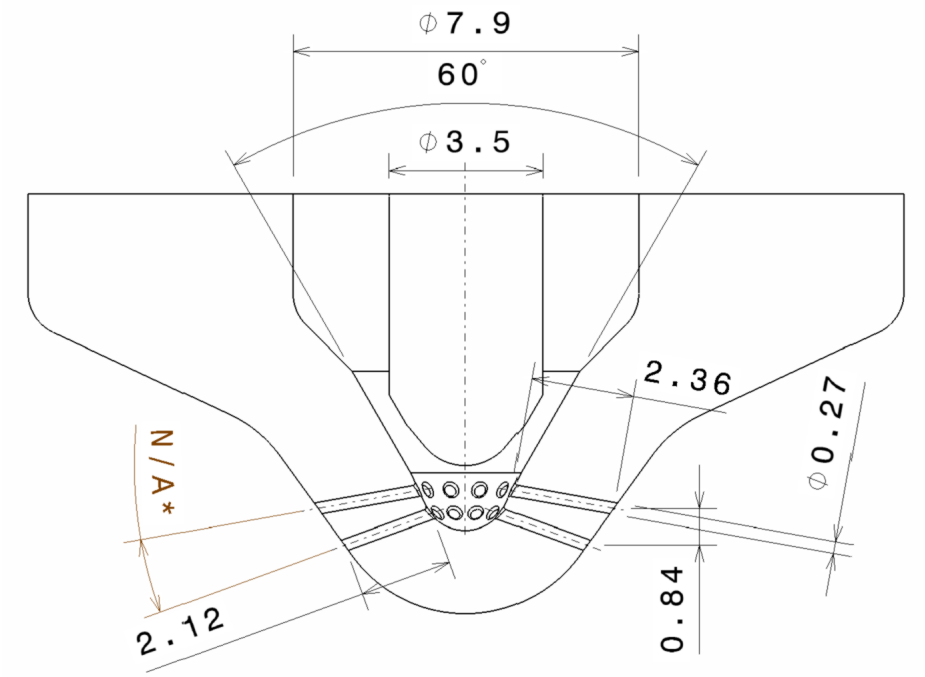

Figure 3.7: L'Orange's twin nozzle - Dimension sketch

All the injector holes inlets are rounded, Figure 3.8. The rounding is, as in the ks-nozzles, significantly more pronounced towards the upper inlet edges.

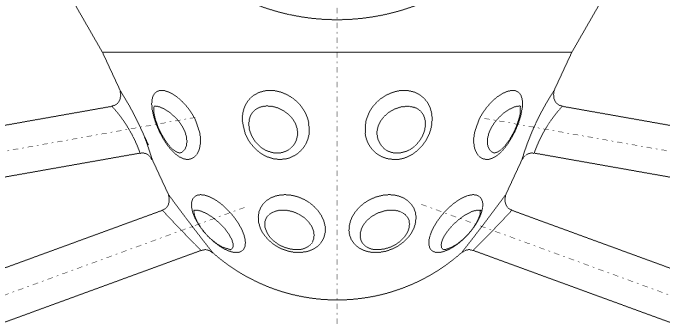

Figure 3.8: L'Orange's twin nozzle - Zoomed in view

[1]The angle between the orifice pairs is censored due to a non-disclosure agreement.

Chapter 4

CFD

Computational Fluid Dynamics (CFD) is a numerical tool mainly used for describing fluid flows and heat transfer. With CFD one can study phenomenons of very small time scales that may be invisible to the naked eye. Phenomenons that otherwise would be too time consuming and prohibitively expensive to analyse experimentally.

Regardless of the phenomenon to be studied all CFD procedures contain three main parts; pre-processing, a solver and post-processor. The pre-processing stage defines all the required input for the solver. The domain, grid, fluid properties and boundary conditions are determined. The solver produces numerical solutions, to a system of algebraic equations, by an iterative method. These equations are approximated by discretisation of the grid where the governing partial differential equations (PDE) of the fluid flow are converted to algebraic equations. The most used numerical solution techniques are the finite volume, finite difference and the spectral methods, where the finite volume is the most well established. The last stage which is the post-processing visualizes the data through plots, contours, streamlines etc.

The present study explores the possibility of using AVL's commercial CFD software FIRE (version 2013, build 13246) to predict the behaviour of twin nozzles mainly terms of internal nozzle flow. The fundamental governing equations of fluid dynamics are well known, and so are the numerical algorithms behind CFD codes that can solve these equations. Deduction of equations, such as the Navier-Stokes equation and explanation of numerical algorithms and other well know fluid dynamics related subjects, such as turbulence, will therefore not be emphasized. For this, the reader is encouraged to read [37] and [10]. However, CFD modelling techniques unique to FIRE will be explained. It must be stressed that internal flow analysis of a prototype nozzle allows for little or no verification and/or validation, neither numerical nor experimental. Published scientific information regarding internal flow of twin nozzles is very scarce (at least to the authors' notice). The little information that is published[28, 36, 39, 22, 15, 14, 20, 29, 42] is mainly devoted to experimental investigation of twin nozzle's pollutant formation, spray penetration, cone angles and SMD. The details given about the nozzle geometry is often not enough to reproduce the model numerically. It is pointless to compare two different nozzle geometries for validation purposes as small variations can yield big flow differences. Thus does this thesis not seek to verify and validate the proposed numerical model, but rather investigate the overall flow trend in a twin nozzle. Even though no verification and validation with existing data will be performed, general guidelines for best practice in CFD are followed.

4.1 Grid Generation

One of the first steps of the pre-processing procedure is to create a grid. The grid is a representation of the geometry of the problem. The PDEs governing the fluid flow are discretized and solved inside each cell. Grid generation for a high Reynold number flow is a sensitive and detailed task. The solution is sensitive to high pressure gradients and these are often observed in the vicinity of wall and close to corners. It is therefore important to create a grid with fine cells in these areas. Regions with smaller pressure gradients can have a coarser cell structure without affecting the solution. The grid has a direct impact on the computational time, the accuracy of the solution and the rate of convergence. A favourable grid arrangement keeps the total cell count low, but high enough to capture all relevant flow features. Grid quality is normally measured by the smoothness, skewness and aspect ratio of the cells [4].

The domain in the present study is based on a 3D model that was provided by L'Orange. Using the commercial Computer Aided Design (CAD) software Catia a negative of the model in Figure 3.5 was created. Meaning that all cavities are turned in to solids and all solids are erased. The result of this transformation is depicted in Figure 4.1. The geometry shows the volume where the fluid in the nozzle can flow. There is a cavity through the middle due to the presence of the needle.

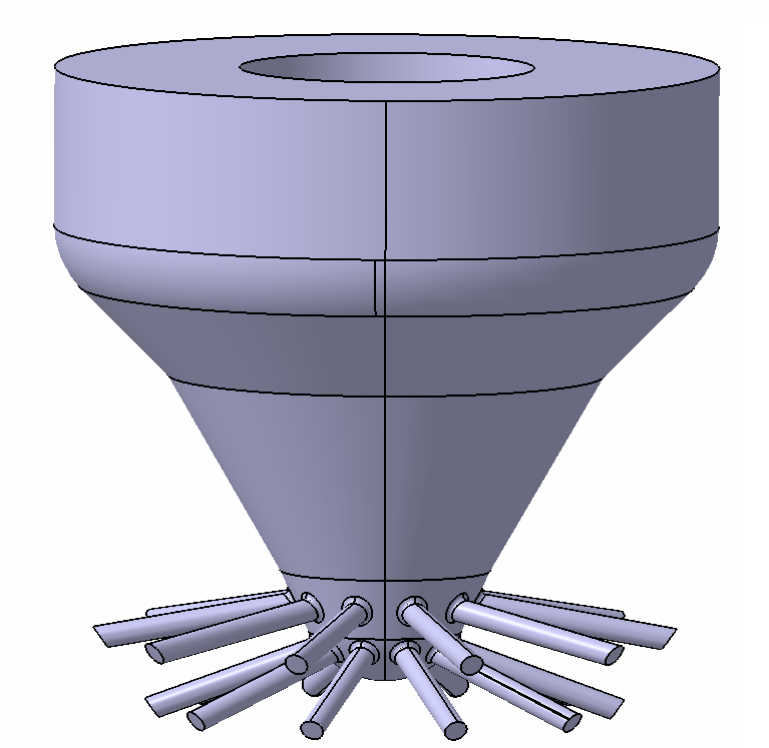

Figure 4.1: Negative of twin nozzle.

The 10 orifice pairs are equispaced with 36 degrees between each of them. Due to symmetry it is sufficient to simulate only 18 degrees of the 360 degree nozzle.

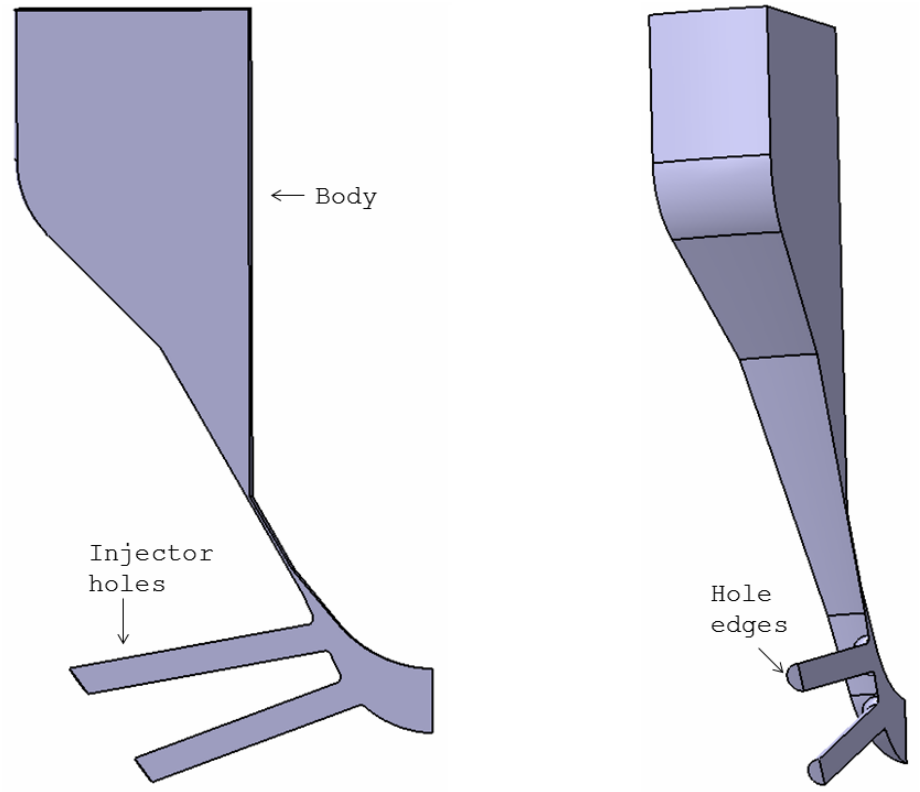

Figure 4.2: 18 degree nozzle section

Figure 4.2 shows such 18 degree section where the needle is closed. The 3D model provided was formatted as a STEP (Standard for the Exchange of Product model date) file. A format which is extensively used to share 3D models between users regardless of which CAD software is being used. To import the above geometry to FIRE the output file was saved in a supported mesh format, in this case a STL (STereoLithography) format. FIRE detects the imported STL geometry as a surface grid. The grid was created according to the methodology used in AVL's manual [11]. In short, the procedure is as follows:

1. Detect the edges of the body.
2. Create a 2D structured grid between the edges.
3. Rotate the 2D grid 18 degrees to form a volume mesh.
4. Detect the nozzle hole edges, create a structured 2D grid between the edges and extrude the grid to form a volume mesh of the injector holes.
5. Map and connect the injector holes to the body.
6. Refine the grid.

In addition to the grid of the nozzle, a spray box is needed. This is a discharge volume for the spray where the outlet pressure conditions can be defined. This volume was made, in Catia, as a simple cylindrical geometry and then exported to FIRE. In FIRE the edges of the top of the cylindrical geometry were detected, a 2D grid constructed between the edges and the 2D grid was then extruded to form a volume mesh. The discharge volume was then mapped and connected to the nozzle grid (the discharge volume is from now on referred to as the spray box).

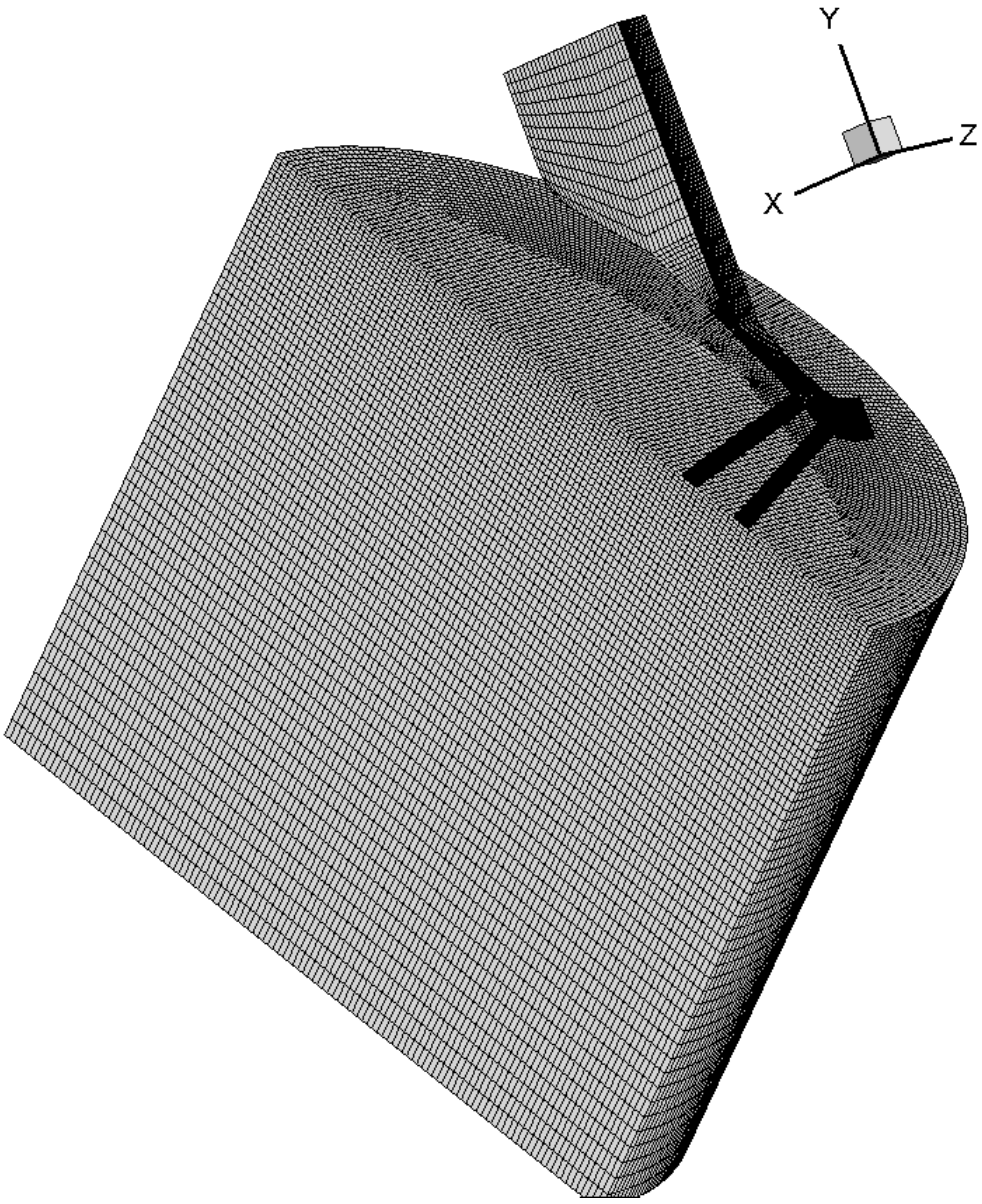

Figure 4.3: Grid

Figure 4.3 shows the finished gird which is a block-structured grid, containing four blocks. The grid structure in each block is different. The spray box is one block, the upper injector hole a second, the lower injector hole a third and the nozzle body a fourth. The spray box dimension are shown in figure 4.4.

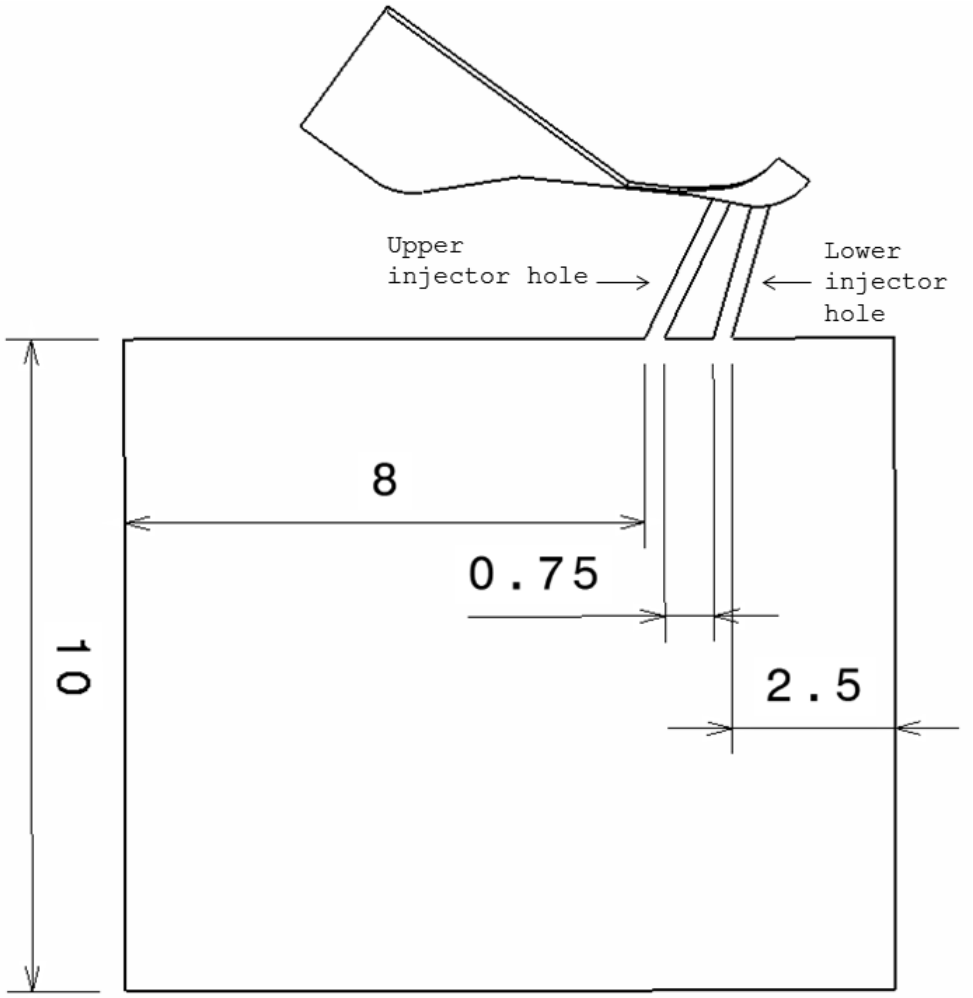

Figure 4.4: Spray box dimensions [mm]

The spray box is constructed as large as a reasonable total cell count allows. This is to ensure that all far field effects are eliminated. A too confining discharge volume can also impose flow restriction for the spray as it enters the volume. Disruption of the spray can also render an incorrect internal nozzle flow. The grid does not account for the rounded inlet edges of the injection holes. Rounding proved to be difficult to perform for a structured grid with AVL FIRE's internal meshing application. Hence are the inlet edges in the grid sharp for both the upper and lower injector hole. The grid is constructed according to AVL's manual for injectors [11] and the manual suggest nothing in regard of the y^+ mesh value [37] other then using a specified wall treatment, so no measures have been done beyond this to obtain specific y^+ values.

The total cell count of the grid exceeds the cell count used in AVL's manual [11]. The cell density is in the same range, but the spray box dimensions are far larger and require more cells. This is done on the expense of computational time, but as no convergence test has been performed this increases the probability of capturing all flow features and the absence of far field effects. The cells are distributed as shown in Table 4.1.

Block	Cells
Spraybox	493698
Body	54794
Lower injector hole	6754
Upper injector hole	5940
Total	493698

Table 4.1: Cell distribution.

The injector holes and the lower part of the body (the sac volume) has the highest cell density. Figure 4.5 shows how the grid is refined so that the cell layers are smaller closer to the injector hole inlet edges. The flow direction in the injector holes is essentially one dimensional and this allows for thinner and more stretched cells. Refinement can also be seen in Figure 4.3 where the cell layers in the spray box are smaller near the injector hole outlets. The cell layers in and around the injector holes where the velocity is high can not be too thin as a unpractical high time step would be needed to keep the Courant number [10] below unity.

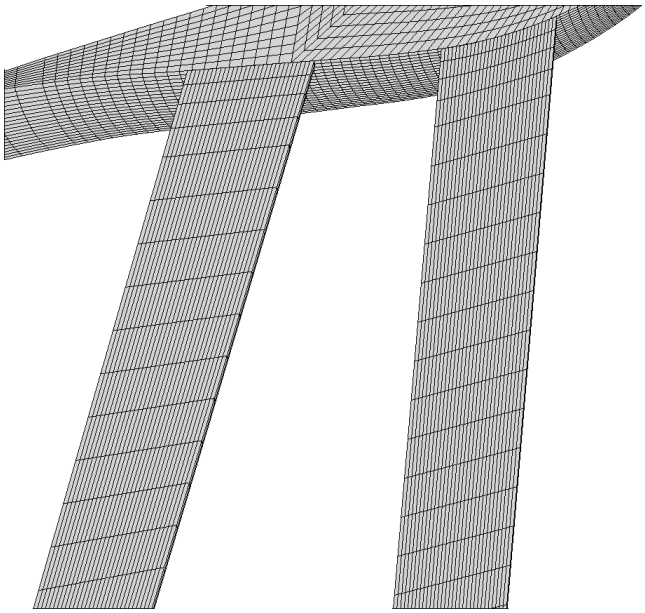

Figure 4.5: Refinement.

4.1.1 Grid Movement

The transient nature of the flow is affected by the needle movement. This effect is accounted for by moving the grid during the simulation to replicate the needle movement.

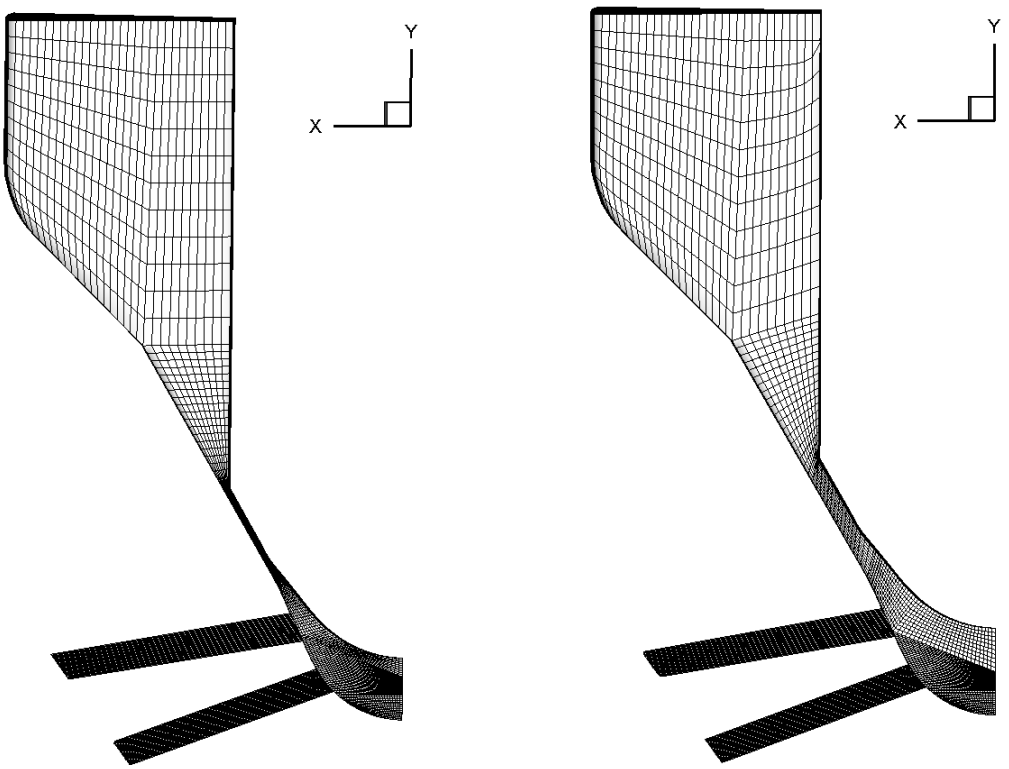

(a) Needle closed.

(b) Needle open.

Figure 4.6: Needle movment.

Each simulation starts with the needle in a closed position (Figure 4.6a) and as the simulation progresses the nozzle becomes fully open (Figure 4.6b). Towards the end of the simulations the needle closes again. The disadvantage of CFD is that the grid has to be continuous. Hence is a very confining grid the only way to close the needle. The needle in Figure 4.6a is therefore not truly closed, and some fluid will flow through the confining area towards the sac volume. To define the movement three different gird selections are required. These are (see Figure 4.7):

- Face selection (red) to specify the moving part of the geometry.
- Cell selection (green) used as buffer for the grid movement. These cells are stretched or compressed during the movement.
- Cell selection (pink) to specify the non-moving part of the geometry.

The face selection is defined to move along the y-axis like a needle. The cells within the buffer selection follow the face selection and change shape accordingly. A non-moving selection is defined to prevent distortion of the geometry as the grid moves. The movement is determined by a needle lift curve[1].

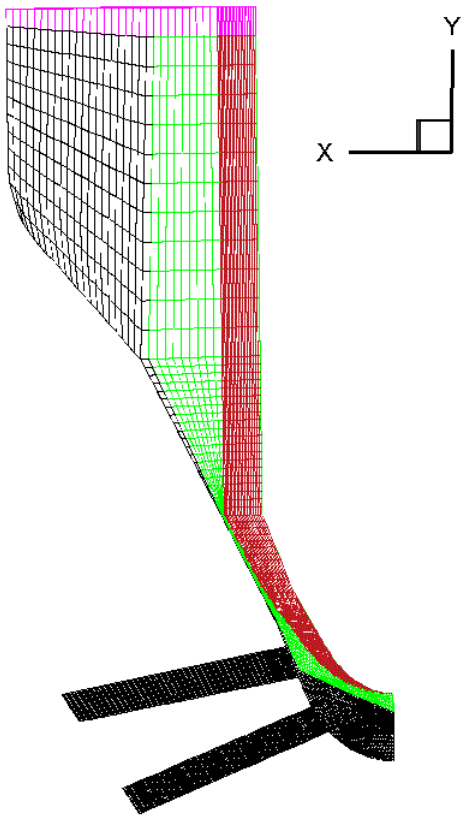

Figure 4.7: Selections for grid movement

The cell structure in the upper part of the body has to be coarse in order for the grid to move. This is especially true for the cell layer next to the non-move selection. If the cells are too fine they may intersect during the movement and produce cells with negative volumes. FIRE can not handle cells with negative volumes.

[1]Presented in Section 5

4.2 Numerical set-up

All simulations have been conducted using AVL FIRE, which utilizes the finite volume solution technique. Furthermore, are all simulations multiphase, containing three phases. One for the fuel, a second for the air in the spray box and a third phase for vapour formed due to cavitation. The temperature in the computational domain is kept ambient. This is common when investigating fuel spray behaviour. The fuel is then not allowed to combust or vapourize allowing measurements of the atomization process.

4.2.1 Boundary Conditions

In order to solve and discretizes the PDEs that govern the fluid flow proper boundary conditions must be set. The grid in the present study is divided into four boundaries; inlet, outlet, wall and symmetry. The location of the inlet (red selection) and outlet (green selection) boundaries are shown in Figure 4.8.

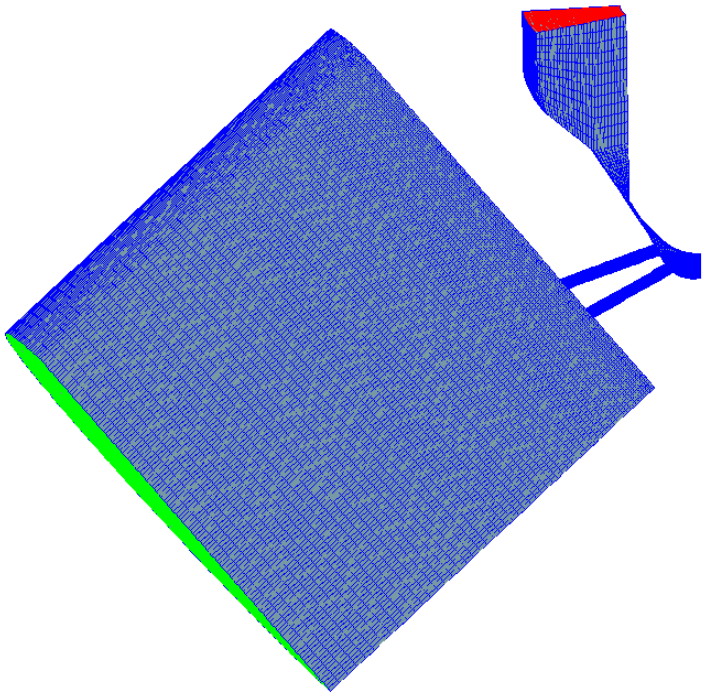

Figure 4.8: Inlet and outlet boundaries.

Both boundaries are defined by static pressure which is equal for all phases. The boundaries have fixed volume fractions and are shown in Table 4.2. The sum of volume fractions for each boundary must be equal to unity. The inlet has a fixed ambient temperature of 293.15 K and fixed turbulent kinetic energy and length scale for all phases. When using the $k-\epsilon$ model the turbulent kinetic energy and turbulent length scale must be set. According to AVL [11] $0.1\text{m}^2/\text{s}^2$ is suitable for

the former and 0.001m for the latter. The temperature and turbulence properties at the outlet boundary are not fixed.

Boundary	Phase	Volume fraction
Inlet	Fuel	0.999998
	Vapour	1e-6
	Air	1e-6
Outlet	Fuel	1e-6
	Vapour	1e-6
	Air	0.999998

Table 4.2: Volume fractions.

To reduce the computational effort the grid only represents an 18 degree section of the nozzle and the majority of the faces can be defined as symmetry boundaries. This condition implies that there will only be a flow parallel to the boundary and not across. This is done numerically by setting all the velocity components normal to the boundary equal to zero. The symmetry boundary is shown in Figure 4.9. Faces not shown in neither Figure 4.8, nor Figure 4.9, are defined as wall boundaries where the no-slip condition is fulfilled.

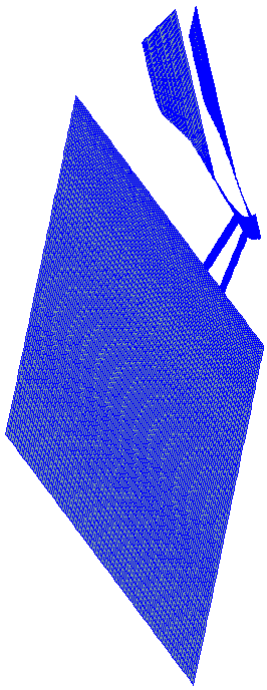

Figure 4.9: Symmetry boundary.

4.2.2 Initial Conditions

The initial conditions are unlike the boundary conditions, only enforced at the beginning of the simulation. The spray box is initially assigned the same fixed volume fractions as the outlet boundary in Table 4.2, while the rest of the grid share the same volume factions as the inlet boundary. Furthermore, are the initial conditions for the whole grid and all phases defined to have the same fixed turbulence and temperature as the inlet boundary. The initial pressure defined for the spray box together with the outlet boundary condition replicates the in-cylinder pressure. The initial pressure assigned for the inlet boundary condition and the rest of the grid replicates the common rail pressure.

4.2.3 Multiphase

Multiphase flow is a necessity in order to simulate cavitation successfully. The present study utilizes two different multiphase models, the homogeneous model and the multifluid model. The homogeneous model calculates a volume fraction for each phase, but only a single momentum equation for the phases in momentum equilibrium. The multifluid model solves all conservation equations for each of the phases, rendering it more accurate. The Volume of Fluid (VOF) model which even more accurate, is also available within the FIRE solver but is not used due to its high resolution requirements that are hard to fulfill. The properties of the different phases are shown in Table 4.3[2].

Phase	Diesel	Diesel vapour	Air
Density [kg/m^3]	830	7	N/A
Dynamic viscosity [Ns/m^2]	0.00214	1e-5	1.84e-5

Table 4.3: Fluid properties

The applied cavitation model is based on the multifluid model. Cavitation is predicted by calculation of the mass exchange between the continuous phase (diesel) and dispersed phase (vapour),

$$\Gamma_d = \rho_v N''' 4\pi R^2 \dot{R} = -\Gamma_v. \tag{4.1}$$

Γ_d and Γ_v represents the interfacial mass exchange between the two phases, ρ_v the vapour density, N''' the bubble number density and R the bubble radius. Bubble number density refers to the total number of bubbles per unit volume. The derivative, $\dot{R}$, is obtained from the Rayleigh equation which is a differential equation governing the dynamics of a spherical bubble:

[2]FIRE's treatment of the air density is discussed in Section 5.5

$$R\ddot{R} + \frac{3}{2}\dot{R}^2 = \frac{\Delta p}{\rho_d} \tag{4.2}$$

$\dot{R}$ and $\ddot{R}$ are the first and second derivatives of the bubble radius with respect to time. ρ_d is the diesel fuel density. By neglecting the inertial term and linearizing the Rayleigh equation the mass exchange can be rewritten as:

$$\Gamma_d = \frac{1}{C_{CR}} \operatorname{sign}(\Delta p) 3.95 \frac{\rho_v}{\sqrt{\rho_d}} N'''^{1/3} \alpha_v^{2/3} |\Delta p|^{1/2} = -\Gamma_v. \tag{4.3}$$

Where α_d is the volume fraction of diesel fuel and the effective pressure difference is:

$$\Delta p = p_{sat} - (p - C_E \frac{2}{3} \rho_d k_d). \tag{4.4}$$

The Egler coefficient, C_E, depends on the local turbulence level and varies within the range 1~1.4. k_d is the turbulent kinetic energy of the diesel phase. p_{sat} is the saturation pressure of the diesel fuel and p is the calculated local pressure. The condensation reduction factor, C_{CR}, in Equation 4.3 is an empirical coefficient used to adjust the condensation rate during cavitation. The factor accounts for weaknesses present due to simplifications in the derivation of the model. The bubble number density is calculated according to the following function:

$$N''' = \begin{cases} N_0''' & \alpha_v \leq 0.5 \\ 2(N_0''' - 1)(1 - \alpha_v) + 1 & \alpha_v > 0.5 \end{cases} \tag{4.5}$$

The initial bubbles are analogous to the nuclei, discussed in Section 2.4.1. The above function models coalescence effects. An increase in vapour fraction yields an increase of bubbles presence, making them more prone to collide. Hence is N''' linearly diminishing for $\alpha_v > 0.5$. The initial bubble number density (N_0''') depends on the characteristics of the continuous liquid phase. The number density is constrained by the maximum bubble diameter:

$$D_{b,max} = \left(\frac{6\alpha_v}{\pi N'''} \right)^{1/3}. \tag{4.6}$$

In the present study the following values have been used according to AVL's manual [11]:

C_E[-]	C_{CR}[-]	P_{sat}[Pa]	N_0'''[1/m^3]	$D_{b,max}$[m]
1.2	1	982	10^{12}	0.01

Table 4.4: Cavitation model

In addition to the mass, momentum exchange between the phases is also calculated. Table 4.5 shows the models utilized between the different phases:

	Continuous phase	Dispersed phase
Multifluid	Diesel	Vapour
Multifluid	Air	Diesel
Homogeneous	Air	Vapour

Table 4.5: Momentum exchange models

The multifluid model ensures that $M_c = -M_d$ where M_c and M_d denotes the momentum exchange of the continuous and dispersed phase. The multifluid model includes drag and turbulent dispersion forces between the phases. The two enforced multifluid models for momentum exchange differ by having different correlations for the drag coefficient. The model between the diesel and vapour phase have a correlation adapted for cavitation.

The phases in the homogeneous model can exchange energy among them but only when they are considered to have undistinguishable momentum fields. The mixture of the two phases is then treated as whole and the governing equations for single phase flows are used to analyse the mixture. For a more thorough review of the equations that constitute the multiphase model the reader is referred to AVL's multiphase manual [12].

4.2.4 Solver Control

AVL FIRE has a range of standard solvers. In the present study the SIMPLE (Semi-Implicit Method for Pressure-Linked Equations) solver is used for the transient incompressible flow problem. Calculation of boundary values and derivatives are done by the Least Square Fit and Extrapolation Method respectively. The differencing schemes are all Upwind except for the continuity term which is Central Differencing. The Upwind scheme is in first order while the Central differencing is in second order. The Crank Nicholson scheme is used for time integration. The linear solver for all symmetrical terms is conjugate gradient with an incomplete Cholesky factorisation as preconditioner and the biconjugate gradient stabilized method (BiCGstab) with an incomplete LU factorization (ILU(0)) as preconditioner for non-symmetrical terms.

The $k - \epsilon$ is chosen as turbulence model. It is the most widely used turbulence model and has been tested on a variety of flows. The model is numerical robust, and despite numerous shortcoming discovered over the past few decades, it is generally accepted that it provides realistic predictions of major flow features in most situations. It is particularly recommended for multiphase interactions where the inherent uncertainties outweigh those in the turbulence model. The standard wall function treatment is used. The turbulence models implemented in FIRE are of the 'high Reynolds number' type which means they are not applicable in the near wall region. The standard wall function is thus a scalable wall functions that can omit the laminar sub-layer regions and focus exclusively on the turbulent region. Also, an internal flow problem has a fully turbulent velocity profile without any flow separation, the need to resolve the boundary layer with respect to y^+ values is then less restrictive.

No time step accuracy test has been performed. The overall cell density and cell structure are kept as in AVL's manual [11]. The time steps used are therefore according to the manual. The transient simulation propagates with a time unit in terms of crank angles degrees (CAD). The time step (Δt) between each crank angle step ($\Delta\varphi$) is specified by setting an engine speed in revolutions per minute(RPM). The total injection duration is 150 CAD which is the equivalent of 835 µs. This time span allows the conditions inside the nozzle to stabilize before the needle closes. Opening and closing of the needle takes place at the first and last 30 CAD of the simulation. Since the grid is moving, different time steps are needed throughout the simulation. Table 4.6 provides a crank angle step and time step overview. To obtain sufficiently small time steps engine speed was held constant at 30 000RPM. To initialize the simulation a very fine time step is required. The time step then gradually coarsens before it is reduced towards the ends as the needle approaches closed position.

CAD [°]	$\Delta\varphi$ [°]	Δt [µs]
0-1	0.005	0.028
1-7	0.01	0.056
7-145	0.05	0.28
145-150	0.01	0.056

Table 4.6: Time step overview

The simulations where run in parallel on a workstation with 4 eight-core processors running at a clock speed of 3.1 GHz. All cores where taken in to use by domain composition, where the grid is split into 32 sub-domains. In average, each simulation needed 36 clock hours and 1152 core hours.

Chapter 5

Results and Discussion

Numerical simulations of L'Orange's twin nozzle with various rail pressures and in-cylinder pressures have been performed. For comparison also a single orifice nozzle was simulated. Essential hydrodynamic quantities, such as phase volume fraction, velocity, pressure, mass flow and turbulent kinetic energy have been predicted at areas of interest. Post-processing was carried out in the software Tecplot and the results extracted from FIRE were parsed with Matlab. The various case configurations with their belonging case names are shown in Table 5.1.

	A	R1	R2	S1	S2	SA
Rail pressure [bar]	1200	1800	600	1200	1200	1200
In-cylinder pressure [bar]	90	90	90	120	60	90

Table 5.1: Case configurations

Case A is chosen as a benchmark case and serves as a reference when compared against the other cases. Only one parameter for the non-benchmark cases are changed compared to the benchmark case. For case R1 and R2 the rail pressure is changed, for case S1 and S2 the spray box pressure is changed. The pressure configurations are all realistic and do occur in turbo charged engines intended for marines applications. The grid is kept constant for all cases, expect for SA, which is the single orifice nozzle.

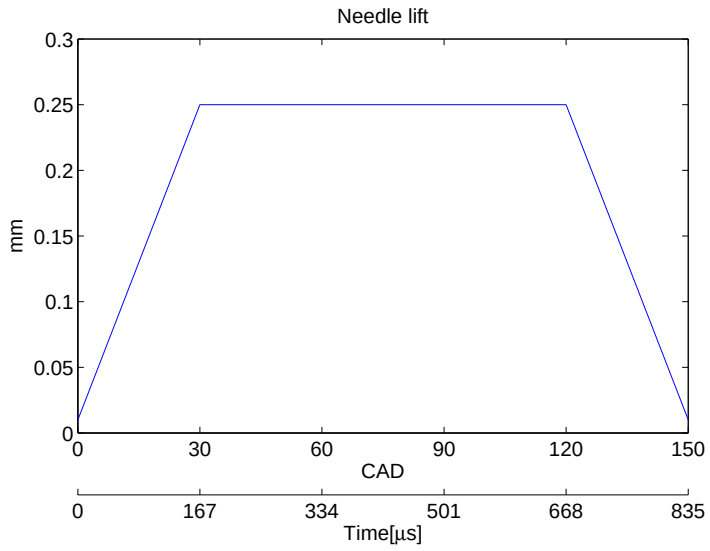

Figure 5.1: Needle lift

The needle lift shown in Figure 5.1 is used for all cases. The needle opens 0.25 mm in the first 30 CAD, stays in the open position, and closes during the last 30 CAD. To avoid numerical errors the needle displacement has to commence and end slightly above zero. The bottom axis shows the equivalent time lapse, but in micro seconds.

For areas of particular interest single layer cell selections have been made. Within each cell selection hydrodynamic quantities are computed for each time step by averaging the cell values weighted with respect to the cell volumes. In Figure 5.2 the chosen cell selections are marked with red lines. The inlets and outlet of both injector holes are chosen, in addition to two slices in the spray box 2.5mm and 5mm from the outlets. The combination of these selections allows for examination of how the internal nozzle flow differs from upper to lower injector hole and how the spray propagates into the spray box.

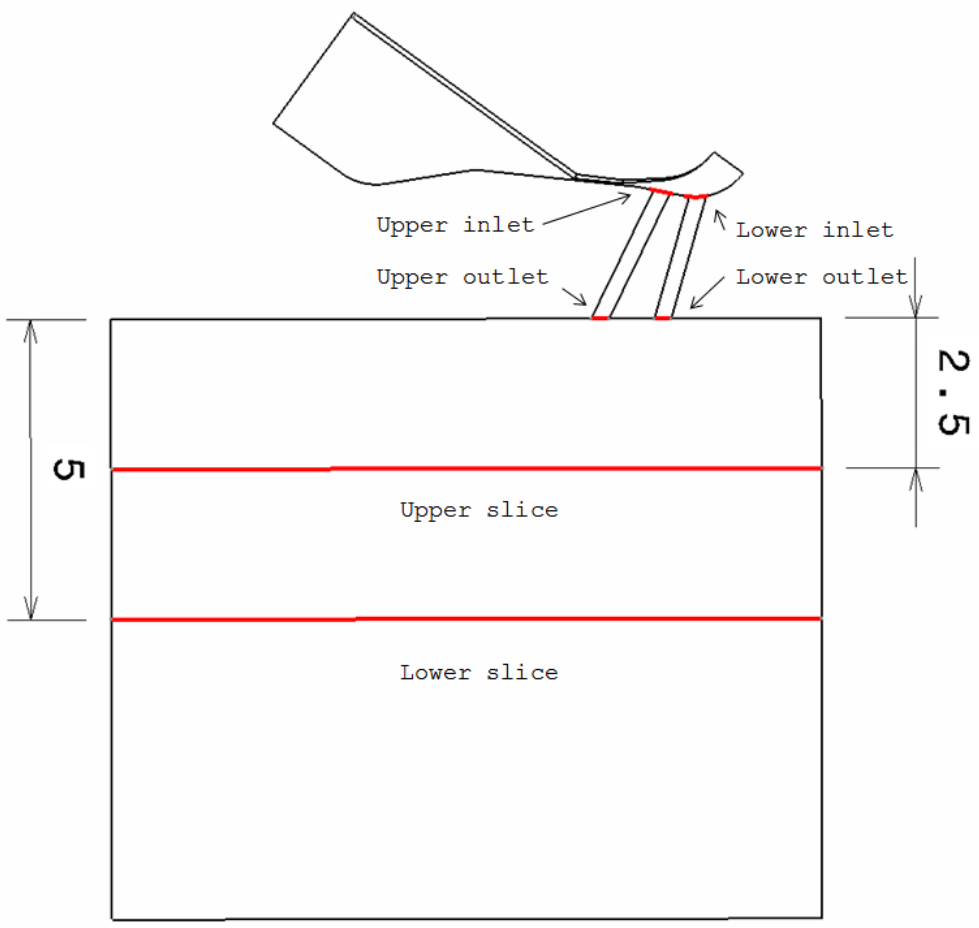

Figure 5.2: Cell selections

5.1 Benchmark Case 3D

The next following pages show 3D visualizations of the benchmark case. Figure 5.4 depicts the volume fraction of the fuel phase. The spray box is initially wit air filled and the nozzle with fuel. The spray commences by two jets, both with a dense high volume fraction core. As the simulation progresses the independent jets merge, even though the injector holes are diverging. Figure 5.4b illustrates how the denser inner cores deflect to each their respective side forming a thicker leading plume. The spray is at this stage somewhat unsymmetrical, but as the needle reaches full lift and nozzle flow condition stabilizes the spray gains its symmetry. The leading plume which has penetrated furthest downstream of the outlets have areas with higher volume fraction. These are present due to the fact that the very first fuel that enters the spray box, at a very small needle lift, doesn't have sufficient kinetic energy to energize a full spray and/or droplet break-up. At full needle lift, the break-up length for the jets exiting from both outlets are a multiple of the nozzle diameter, coinciding with the theory presented in Chapter 2. The last 30 CAD where the needle closes is not depicted. The visual differences are minor and the only noticeable change is a reduction of the dense core at the outlets. An abrupt difference would have been present if the simulation included time steps beyond closed needle position. But as this is of no interest for the present study and due to the fact that the needle is not truly closed, the simulation durations do not extend to include these time steps.

Figure 5.5 shows the pressure distribution in the region with the largest pressure differences. The pressure in the upper part of the nozzle and in the spray box are close to constant throughout the injection, and are therefore not included in the figure. Once again is the focus at the opening of the needle and the needle in fully open position. The lack of ability to close the needle entirely, affects the pressure distribution. The two semicircles in each of the sub-figures are the cross-sections of the injector holes immediately after the inlets. Sub-figure 5.5a serves as illustration. The pressure in the SAC volume and in the injector holes is initially somewhere between the spray box pressure and the rail pressure. When the fuel enters the SAC volume the pressure increases. The injector holes are simply too confining for all the fuel to escape through them. The pressure build-up is counteracted by the needle movement as it expands the SAC volume. The thinner region between the top of the nozzle and the SAC volume depicts the flow at the needle seat. The pressure build-up here is the slowest due to high velocity magnitude and because the region has the highest relative volume increase during the needle movement. In Figure 5.5f the pressure distribution is fully developed and will not change visually as long as the needle is fully open. When fully developed, the SAC volume and the needle seat in particular, have a slightly lower pressure field than the rail pressure. The cross-sections of the inlets show that during the needle opening the pressure in the upper part of the inlets drop. In fact, these are the only areas where the pressure drop below zero. The negative pressure is not only negative relative to the reference pressure of 1 atm, but given

as truly negative. Negative pressure gives no physical sense, but it is used by the cavitation model to predict cavitation.

The vapour phase which predicts the occurrence of cavitation is depicted in Figure 5.6. The leftmost sub-figures show vapour present on the boundary, while the rightmost sub-figures show section cuts of the injector holes to enable a view of the vapour inside the nozzle. The occurrence of vapour presents itself already around 3-4 CAD due to cavitation on the needle seat (discussed in Section 5.2.2). Figure 5.6 depicts the vapour fraction between 15-40 CAD. Its formation at injector hole inlets, with the absence of needle seat affects, commences at 15 CAD and stabilizes around 40 CAD. The formation of vapour is initialized in the upper part of both injector inlets where the pressure distribution shows negative pressure. Vapour protrudes the lower injector hole earlier than the upper. Even though vapour is not present at the boundary the right most sub-figures show that a vapour jet with a dense core travels all the way to outlet. As soon as the vapour bubbles enter the spray box they collapse. At 40 CAD the vapour quantity and distribution are quite similar for both nozzles. The vapour distribution in the present study resembles the distribution presented for single orifice nozzles in [27, 7].

Furthermore, streamlines are plotted to visualize the flow trajectory in the nozzle. Figure 5.3 shows fully developed streamlines, at 40 CAD, where the SAC volume has a recirculation area. The fuel in the SAC volume travels in a circular trajectories prior to entering lower injector hole. The single orifice VCO nozzle studied in [32] exhibits a similar flow movement in its SAC volume.

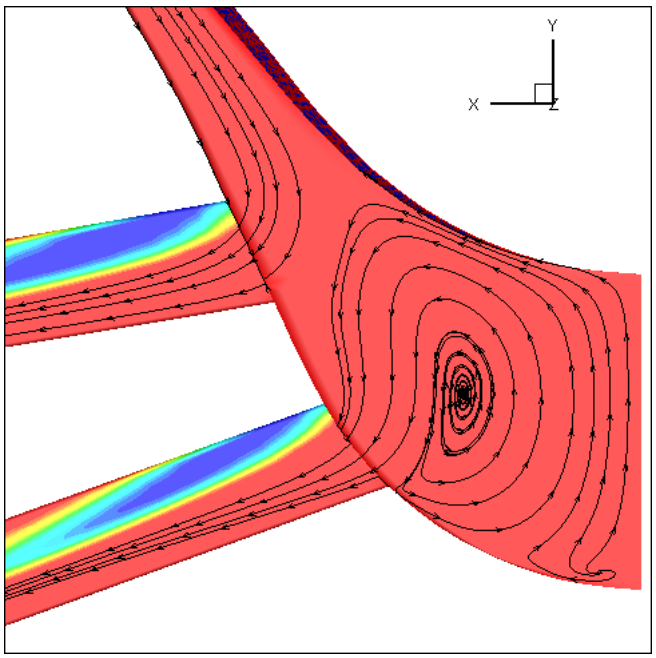

Figure 5.3: Streamlines - Fuel phase

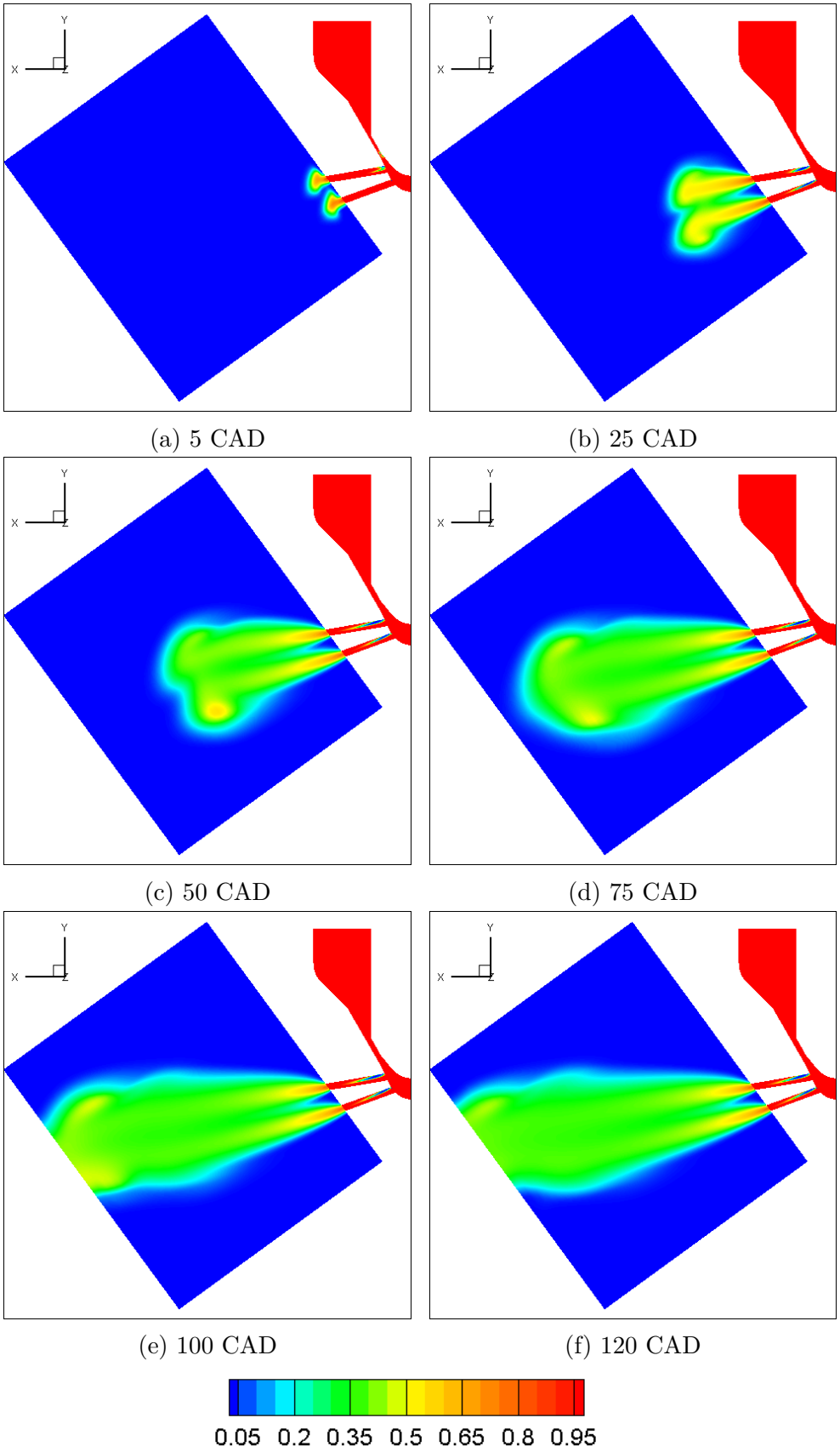

(a) 5 CAD (b) 25 CAD

(c) 50 CAD (d) 75 CAD

(e) 100 CAD (f) 120 CAD

Figure 5.4: Volume fraction fuel phase

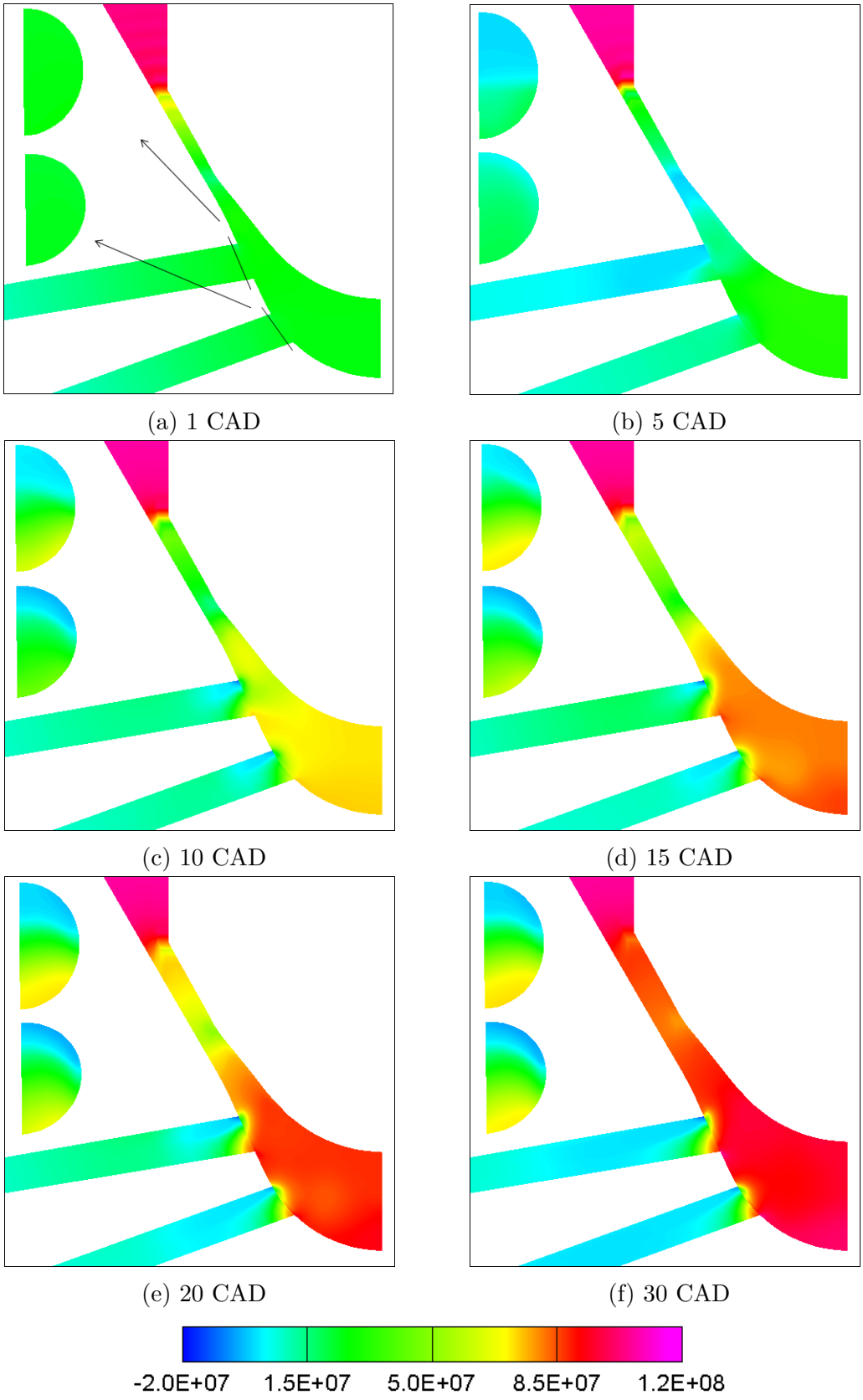

Figure 5.5: Pressure distribution

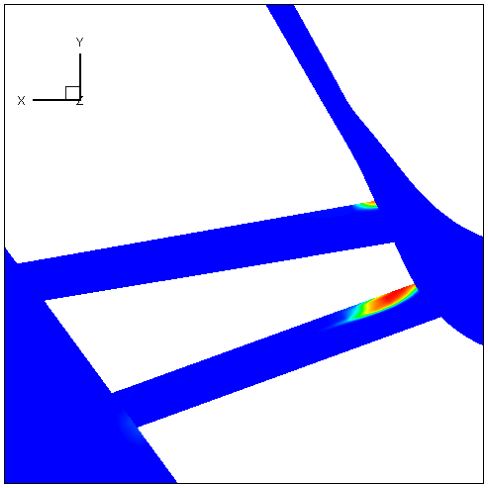

(a) 15 CAD

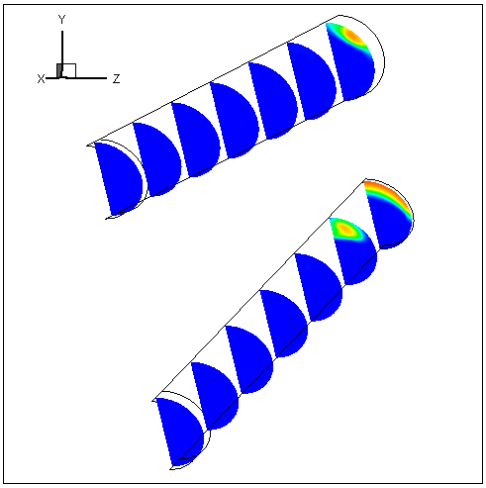

(b) 15 CAD

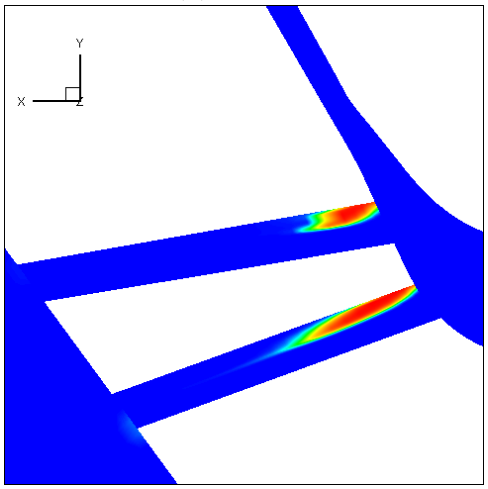

(c) 20 CAD

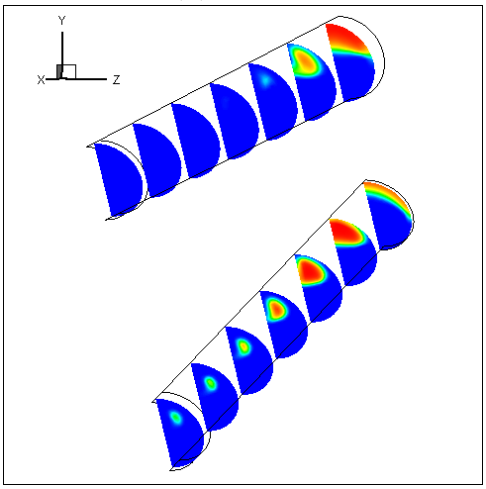

(d) 20 CAD

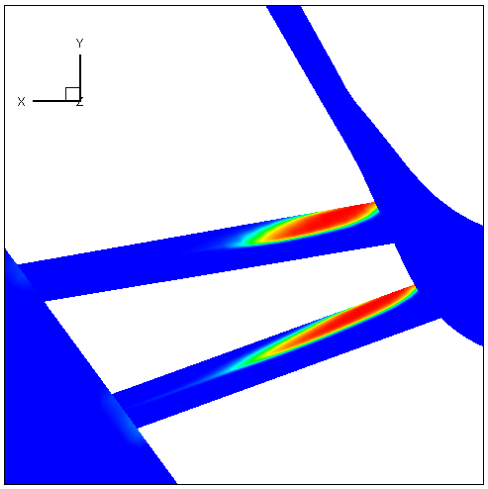

(e) 25 CAD

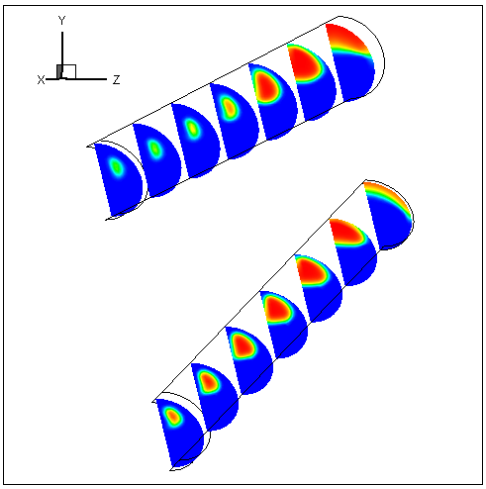

(f) 25 CAD

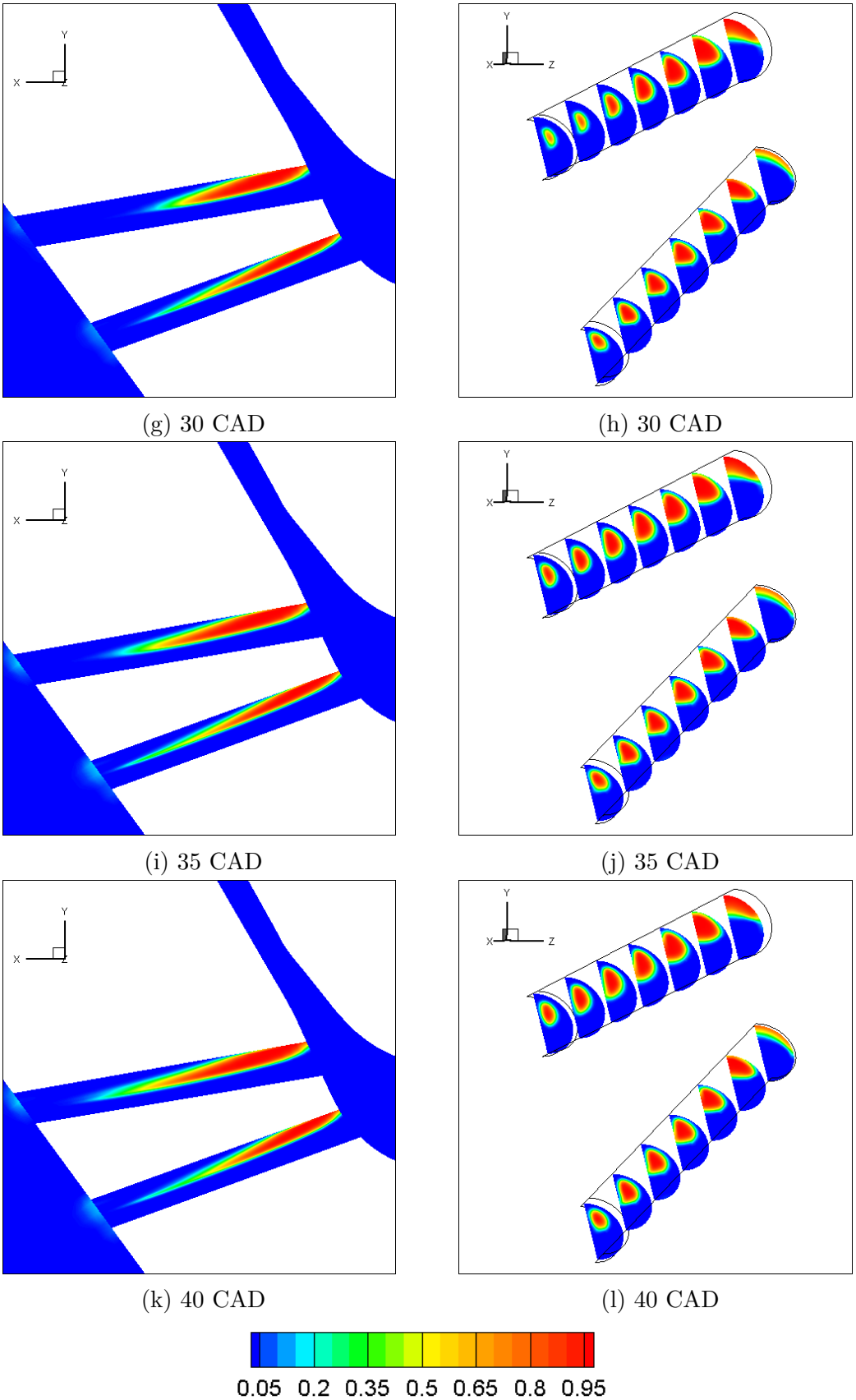

(g) 30 CAD (h) 30 CAD

(i) 35 CAD (j) 35 CAD

(k) 40 CAD (l) 40 CAD

Figure 5.6: Volume fraction vapour phase

5.2 Benchmark Case 2D

Hydrodynamic quantities, from the selections shown in Figure 5.2, are presented as 2D results through various plots where the x-axis is the time lapse in CAD.

5.2.1 Mass Flow

Figure 5.7 depicts the mass of the fuel phase, in milligrams, which passes through the outlets per second:

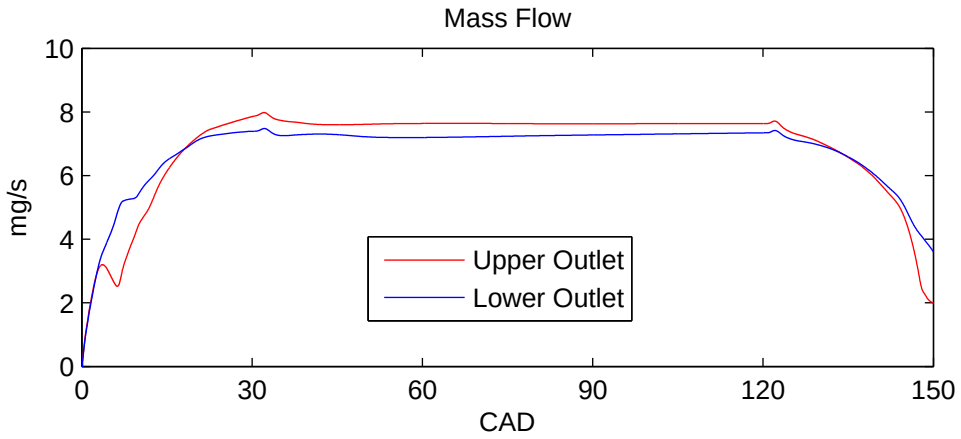

Figure 5.7: Mass flow - Outlets

The lower outlet has the highest mass flow during the first and last 20 CAD, while the upper outlet supersedes it in-between. This can be related to the vortex shown in Figure 5.3. The vortex dissipates kinetic energy during the circular flow movement. Hence will the mass flow through the lower injector hole be reduced. The lower part of the SAC volume will according to the pressure distribution depicted in Figure 5.5 experience an earlier pressure build up. This enables more fuel to be pushed out through the lower injector hole during the needle opening. The mass flow for the inlets is equal to figure above only with a time shift as it takes a couple of CAD for the fuel to travel from the inlets to the outlets.

	0-30 CAD	30-120 CAD	120-150 CAD	Total
Upper outlet [mg]	0.91	3.82	1.01	5.74
Lower outlet [mg]	0.97	3.64	1.03	5.64
Total [mg]	1.88	7.46	2.04	11.38

Table 5.2: Quantity injected - Twin nozzle

Table 5.2 shows the injected quantity through the two outlets for the opening of the needle, the needle in fully opened position and the closing of the needle. The lower outlet injects more during the opening and the closing, though the differences are marginal. In total, the upper outlet injects most due to its larger contribution when the needle is fully open.

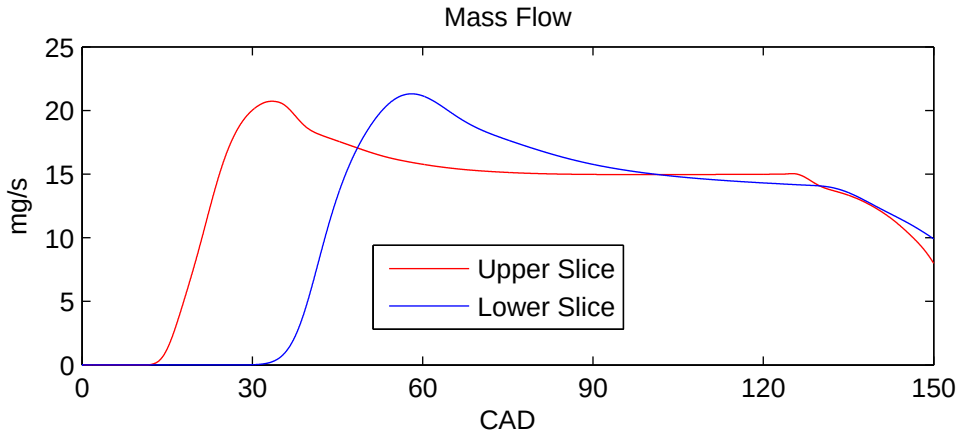

Figure 5.8: Massflow - Slices

The fuel mass flow through the upper and lower slice (see Figure 5.2) are depicted in Figure 5.8. Due to the wider leading plume of the spray, the mass flow will peak as it hits the slice cell selections. As the plume passes the slices, the mass flow drops and levels off to a level equivalent to the mass flow of the upper and lower outlet combined. There is a slight discrepancy for the lower slice as it does not level off properly, but continuous to decrease until the closing of the needle. A possible explanation may be the vortices in the air induced when the fuel is injected into the spray box. These vortices are shown in Figure 5.9 where the contour levels depict the fraction of air. The spray in the outer region is dispersed and of low volume fractions. The vortices may force fuel from this region to travel back towards the outlets and through the lower slice selection in the opposite direction, lowering the total mass flow through the selection.

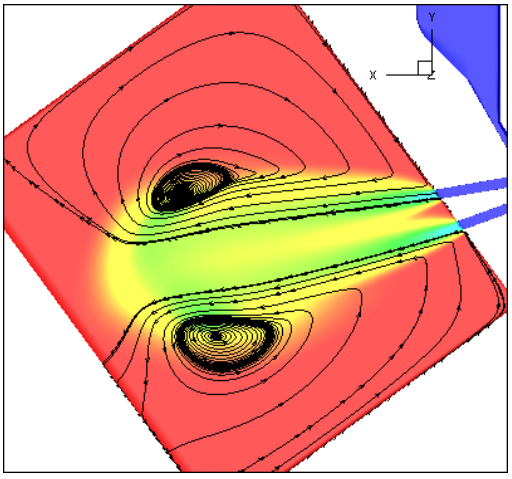

Figure 5.9: Streamlines - Air phase

5.2.2 Vapour Volume Fraction

The mass flow of the fuel phase is strongly dependent on the presence of cavitation i.e. the presence of vapour.

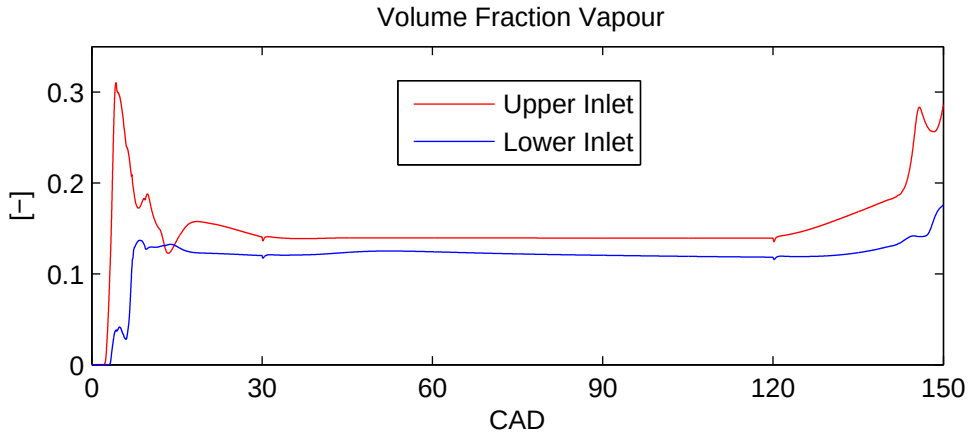

Figure 5.10: Vapour fraction - Inlets

Figure 5.10 shows the vapour fraction at the injector hole inlets. The upper inlets experiences high volume fraction of vapour in the first half of the needle opening and during the closing. This coincides with the reduced mass flow in the same time period for the upper outlet. The presence of vapour restricts the injector holes allowing less fuel to pass. The volume fraction for the upper inlet is generally higher, and this is also seen in Figure 5.6. But, Figure 5.6 also shows that this only true exactly at inlet and that the distribution and quantity of vapour evens out further downstream in the injector holes. This can to some degree be confirmed by looking at Figure 5.11 which shows the vapour fraction at the outlets, where the quantity among the two outlets are much more alike. As Figure 5.6 shows it takes time for the cavitation to develop all the way from inlet the outlet. The initial peaks in Figure 5.10 are therefore not noticeable at the outlets in Figure 5.11.

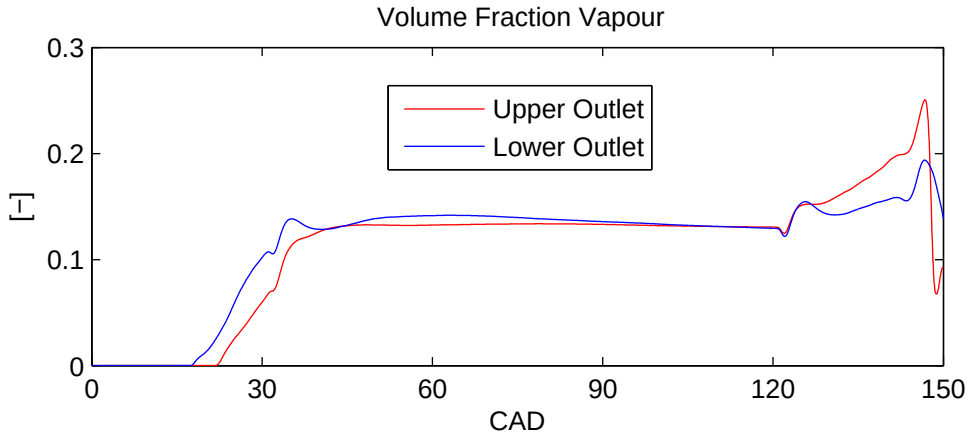

Figure 5.11: Vapour fraction - Outlets

As mentioned, the upper inlet experiences a stronger peak in volume fraction of vapour during opening and closing of the needle. This is due to cavitation on the needle seat. The vapour formed here travels downstream to the upper injector inlet and increases the vapour fraction. None of the vapour from the needle seat makes it the lower injector hole.

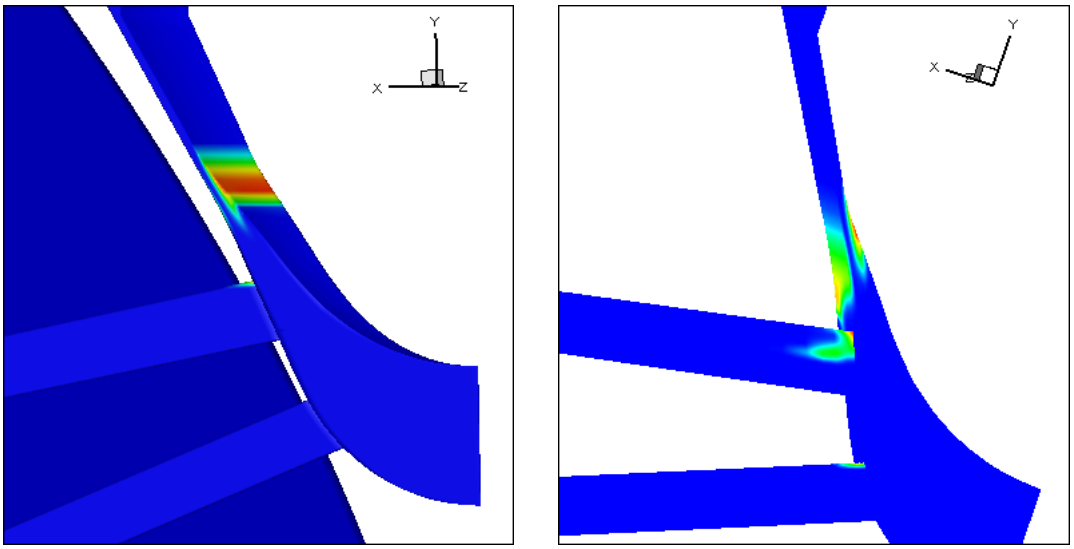

(a) 4 CAD (b) 5 CAD

Figure 5.12: Needle seat cavitation

There is no presence of vapour at the upper and lower slice.

5.2.3 Velocity

The mean velocity magnitude through the injector hole inlets is shown in Figure 5.13. The magnitude is the velocity of all phases normalized with respect to the x-, y-, and x-velocities. During the needle opening and closing the velocity magnitude fluctuates as vapour is formed and the velocity in the different directions changes. When the needle is fully open the vapour formation and the pressure stabilizes, inducing a nearly constant velocity magnitude. The velocity is lower for the lower inlet due to the vortex discussed in section 5.2.1.

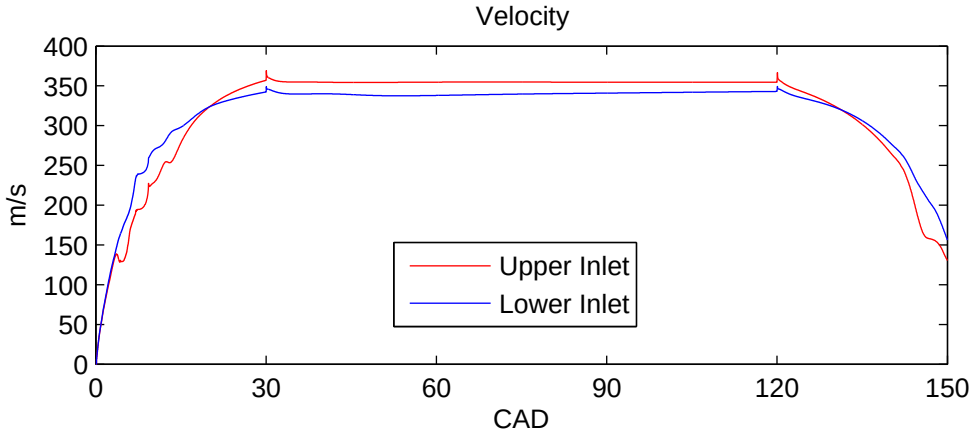

Figure 5.13: Velocity magnitude - Inlets

The mean velocity magnitude at the outlets has a similar trend as the mass flow depicted in Figure 5.7. There are some differences as the velocity magnitude includes the velocity for all phases, while the mass flow only includes the fuel phase. Figure 5.14 portrays how the velocity difference between the injector holes at the inlets diminishes, as the flow travels downstream towards the outlets.

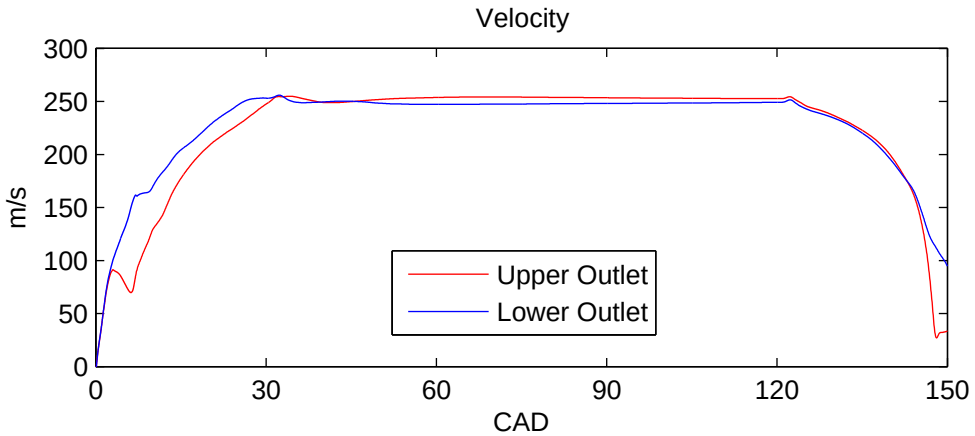

Figure 5.14: Velocity magnitude - Outlets

The big velocity difference between the inlets and the outlets can be described by the use of Figure 5.15 which shows a visualization of the velocity magnitude. The inlets have a high speed velocity profile that covers the entire cross section of the injector hole. The outlets' high speed profile only covers about half of the cross section. This is due to the vapour travelling slower than the fuel. Furthermore, the vapour phase has a conical shape where its diameter at the outlets is smaller than at the inlets. Hence will the fluid phase's effective cross sectional area increase towards the outlet and the fuel phase will decelerate.

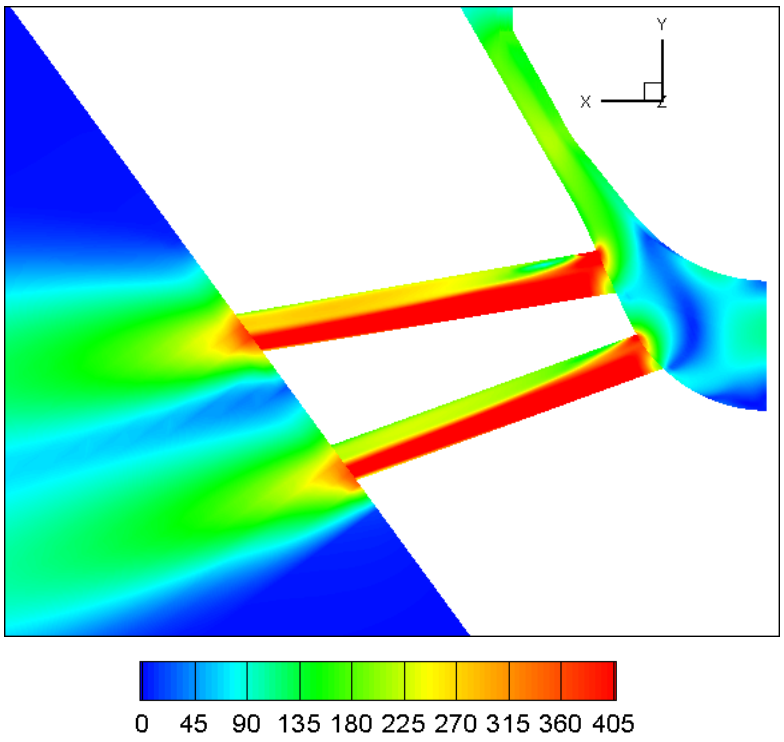

Figure 5.15: Velocity magnitude

Since the velocity magnitude includes the velocity of all phases the upper and lower slice are not presented, as measurements here are obscured by the movement of air inside the spray box during injection.

5.2.4 Pressure

Both the pressure for the inlets in Figure 5.16 and the outlets in Figure 5.17 fluctuates heavily as the simulation initializes. The upper inlet has in general higher pressure then the lower even though the volume fraction of vapour (which presumes low pressure) in the upper inlet is higher. This is contradictory, but can be explained by Figure 5.5f. The part of the upper inlet which is not affected by cavitation has higher pressure than the equivalent region in the lower inlet.

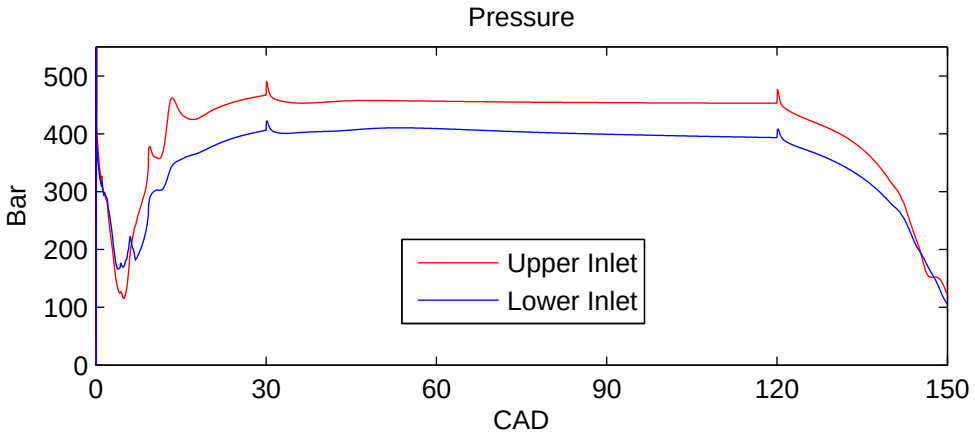

Figure 5.16: Pressure - Inlets

The pressure between the inlet and the outlets is at its minimum just above 10 bar. In the immediate vicinity of the outlets the pressure in the injector holes elevates due to the spray box pressure (90 bar). The pressure distribution through the outlet is, as for the inlet, not evenly distributed. The injector holes are diverging and they are therefore not attached to the spray box in a perpendicular manner. The angle between the top of the spray box and the upper injector is greater than for the lower. This seems to affect the upper outlet by allowing more of the higher pressure in the spray box to protrude the outlet.

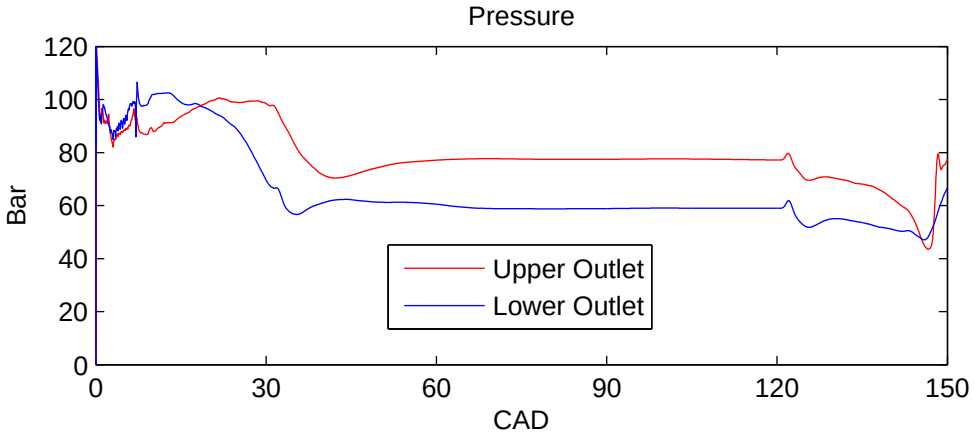

Figure 5.17: Pressure - Outlets

5.2.5 Turbulent Kinetic Energy

Turbulence induced spray break-up is as discussed in Section 2.4 regarded as one of the more important primary break-up mechanisms. The intensity of turbulence is directly related to the turbulent kinetic energy (TKE) [37]. Its quantity can thereby serve as an indicator on the turbulence intensity in the flow. KTE is physically measured as the root mean square value of the velocity fluctuations in all three dimensions.

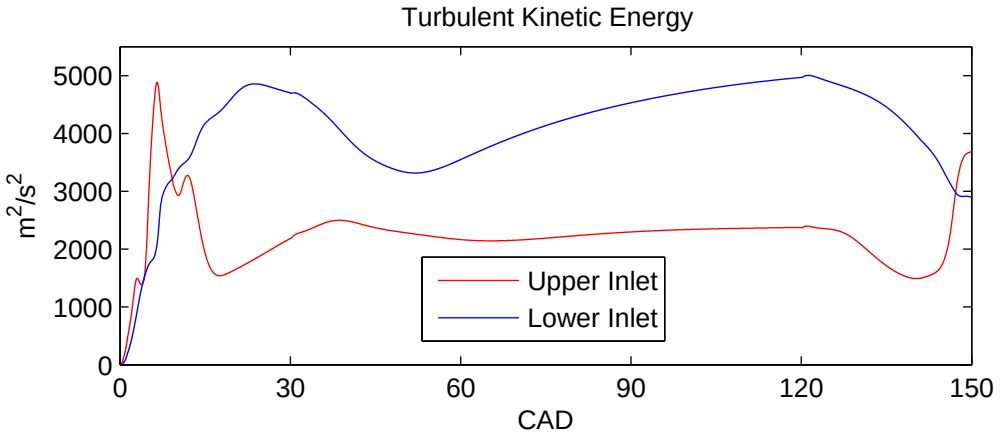

Figure 5.18: TKE - Inlets

Figure 5.18 shows the turbulent kinetic energy of the fuel phase at the inlets. The KTE for the lower inlet is significantly higher than for the lower. This is most certainly due to the velocity fluctuations imposed by the vortex in the SAC volume. The upper inlet is closer to the needle seat where the relative volume change for the grid is larger during to the needle motion. This induces larger velocity fluctuations, making the KTE spike for the upper inlet during the start and end of the needle movement.

KTE at the outlets and spray box slices is depicted in Figure 5.19. TKE dissipates and diminishes as it travels through the injector holes and the spray box.

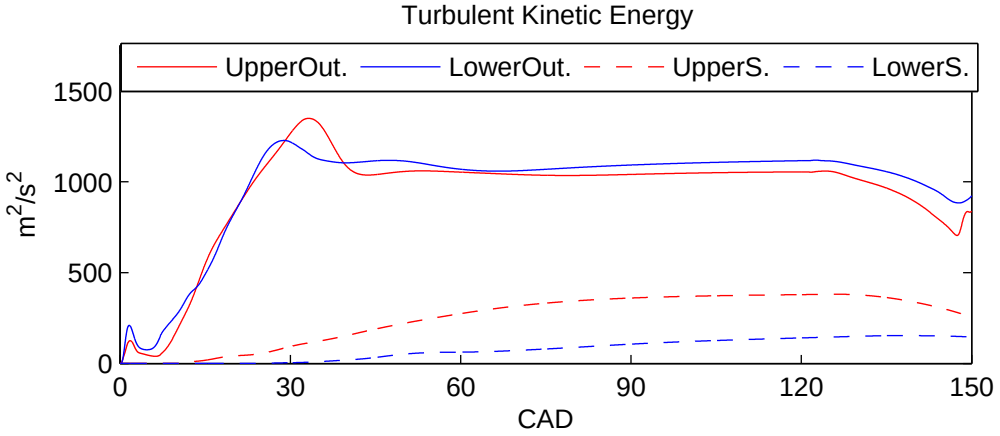

Figure 5.19: TKE - Inlets and Slices

5.3 Pressure Influence

The following sub-sections describes the impact of the pressure variations given for the different cases in Table 5.1. The results are justified by examination of the given hydrodynamic quantities which are presented in Appendix A and B.

5.3.1 Rail Pressure

The results given in Appendix A compares the benchmark case (Case A) against case R1 and R2. They two latter cases differ from the benchmark case by having 1800 and 600 bar rail pressure, respectively.

Change in rail pressure yields a change in mass flow. The mass flow does not scale proportionally with rail pressure though. Case R2 has a larger decrease in mass flow than R1 has increase, compared to case A. There is no significant change in the mass flow between the lower and upper injector hole as the rail pressure is altered. The fuel flow reaches the upper slice earlier when rail pressure is increased and later when it is decreased. Thus is rail pressure affecting the spray penetration velocity. The effect is more dominant when rail pressure is decreased.

The change of vapour fraction at the inlets is minor. However, the rail pressure affects the vapour fraction at the outlets significantly. Especially for case R2 where the fraction is nearly reduced by half compared to the benchmark case. For case R1 the vapour forms earlier and the fraction is somewhat elevated with a high peak towards the end of the injection.

Both the velocity at the inlets and the outlets scale almost proportionally with the pressure. The pressure at the inlets share this trend, but here the pressure difference between the two injector hole inlets increase with increasing rail pressure. The lower outlet pressure for Case R2 behaves radically different then for the other cases by maintaining an almost constant pressure throughout the injection.

5.3.2 In-Cylinder Pressure

Appendix B present results where the benchmark case is compared against case S1 and S2. The in-cylinder pressure is 120 bar for case S1 and 60 bar for case S2, whereas the in-cylinder pressure for the benchmark case is 90 bar. The rail pressure for all cases in this comparison is kept constant at 1200 bar.

The most predominant changes compared to the benchmark case are for the vapour volume fraction (Figure B.2) and the pressure (Figure B.4) at the outlets. Other hydrodynamic quantities are less affected by the variation in in-cylinder pressure due to a discrepancy, in the numerical model, which is thoroughly explained in Section 5.5.

5.4 Single Orifice Nozzle

A single orifice has been developed to serve as a comparison basis for the twin nozzle. Its grid is produced by the same methodology used for the twin nozzle. The grid, except for the injector hole and the spray box, corresponds to the one used for the twin nozzle. The grid's dimensions and cell distribution are given in Appendix C.1. The injector hole is placed at a position equivalent to the gap between the two injector holes in the twin nozzle. The single hole orifice has a diameter of 0.38mm. This dimension produces nearly the same injected fuel quantity as the twin nozzle. The injected quantity during the different stages are shown in Table 5.3.

	0-30 CAD	30-120 CAD	120-150 CAD	Total
Quantity injected [mg]	1.84	7.39	2.02	11.26

Table 5.3: Quantity injected - Conventional nozzle

The combined cross sectional area of the two twin nozzle injector holes, does not equal the cross sectional area of the injector hole in the singe orifice nozzle, but they still inject roughly the same fuel quantity. This is due to head loss, which essentially is pressure loss due to the friction that arises along the length of injector holes. Smaller pipe diameters and longer pipes yields an increase in head loss [9]. Some of the rail pressure is lost in order to overcome the losses.

The single orifice case is denoted SA and all conditions, other then the grid itself, are equal to the benchmark case. The areas of interest are still selected by the same approach as shown in Figure 5.2, only the there is no upper and lower denotations. The inlet and outlet of the single injector hole present in case SA is simply named "outlet" and "inlet". The general single orifice nozzle characteristics resemble the behaviour of the upper outlet in the twin nozzle. For instance, take the mass flow through the outlets depicted in Figure 5.20. For case SA it follows the trend of the upper outlet in case A.

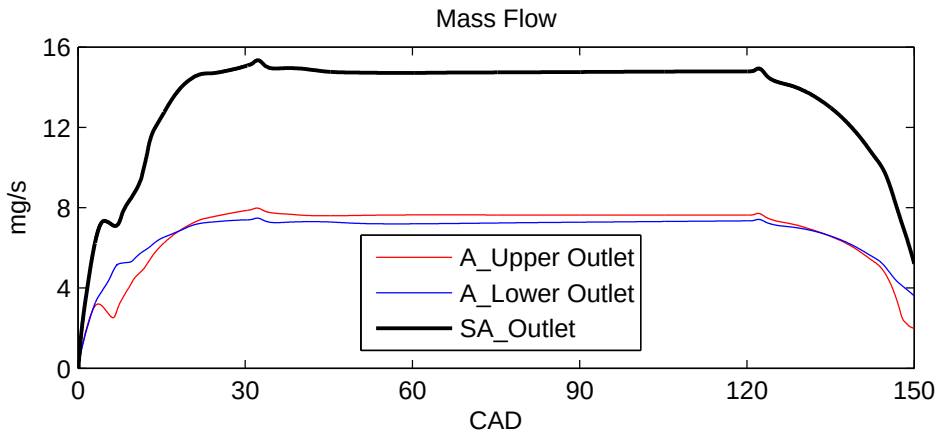

Figure 5.20: Mass flow comparison - Outlets

The mass flow through the upper and lower slice (Figure 5.21) implies a faster spray penetration. The initial slopes are steeper and they present them self at an earlier time step. The discrepancy (as discussed in Section 5.2.1) for the lower slice is even larger for the SA case. The vortices presented in Figure 5.9 are present in the single orifice case also. Their extent is larger, explaining the discrepancy increase.

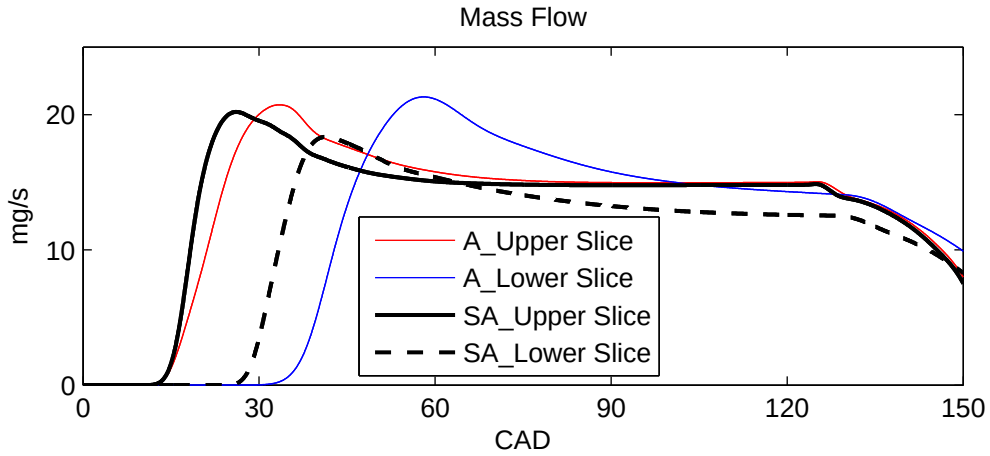

Figure 5.21: Mass flow comparison - Slices

Figure 5.22 portrays the vapour fraction at the inlets. The fraction for the single orifice nozzle is slightly less than for the lower inlet of the twin nozzle benchmark case. The initial spike is, as for the twin nozzle, due to cavitation on the needle seat that travels into the injector hole. However, the vapour fraction at the outlet is greater. Figure 5.23 shows that the larger injector hole diameter allows for more of the vapour formed at the sharp edged inlet to travel downstream to the outlet.

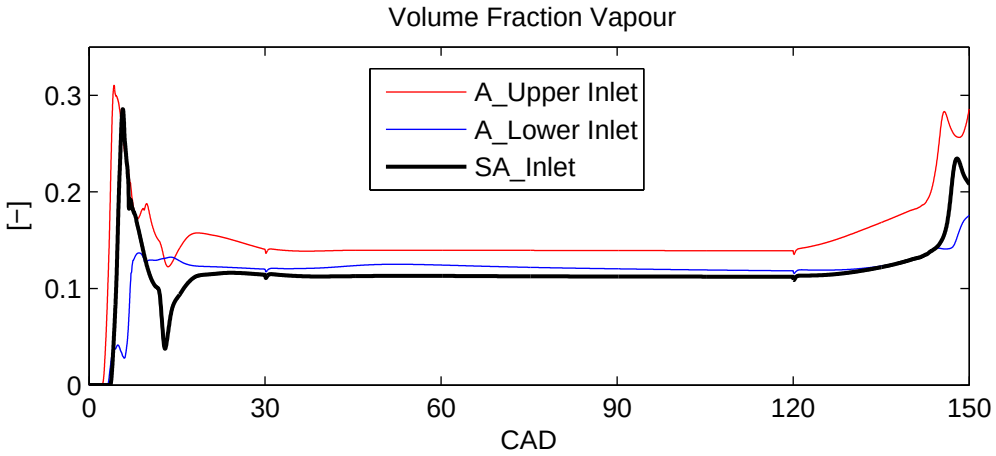

Figure 5.22: Vapour fraction comparison - Inlets

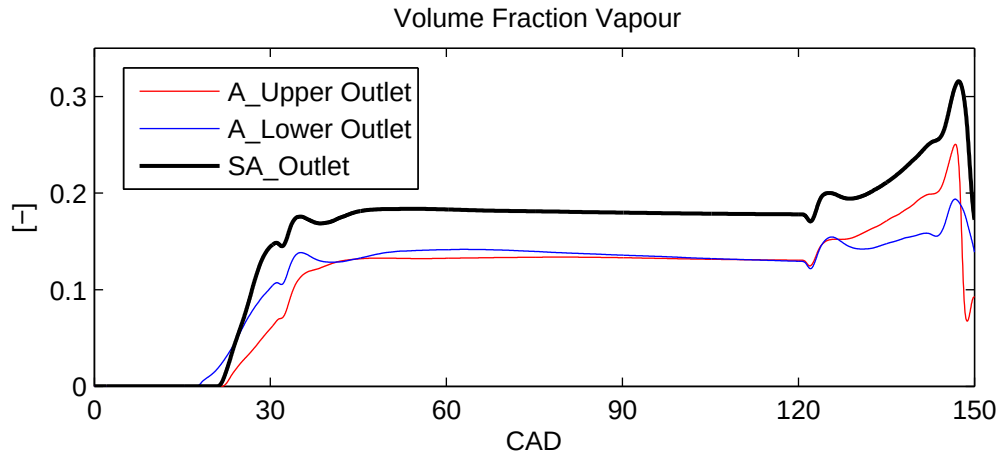

Figure 5.23: Vapour fraction comparison - Outlets

Velocity at the inlets and outlets is portrayed in Figure 5.24 and Figure 5.25. The inlet velocity for the two cases coincides. The outlet velocity though is much higher for the SA case and it must be in order to deliver the same amount of fuel through a smaller cross sectional area.

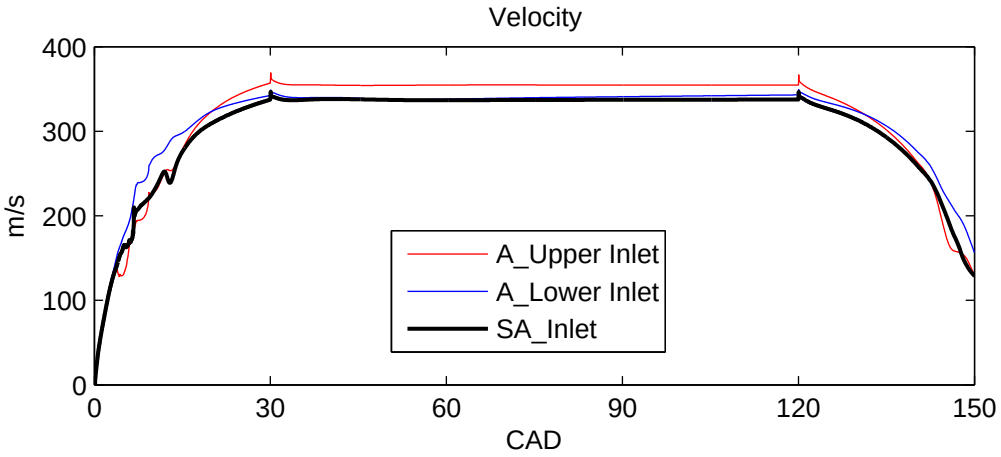

Figure 5.24: Velocity comparison - Inlets

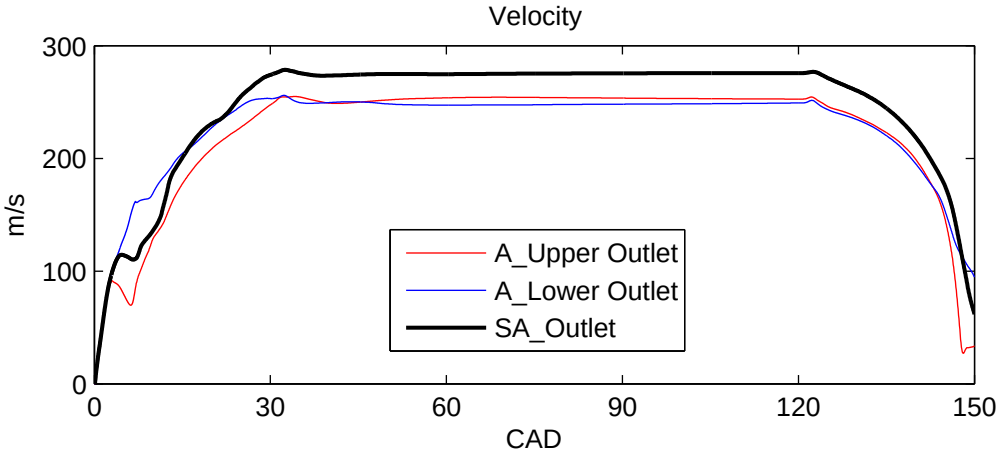

Figure 5.25: Velocity comparison - Outlets

Figure 5.26 shows that a vortex in the SAC volume is also present for the single orifice nozzle case. The vortex has a more circular shape then its twin nozzle equivalent. The streamlines travelling thorough the injector hole originates both from the vortex and from further up the nozzle. Whereas the streamlines for the lower injector hole in the twin nozzle case, originate only from the vortex, and the streamlines through upper injector hole only from further up the nozzle.

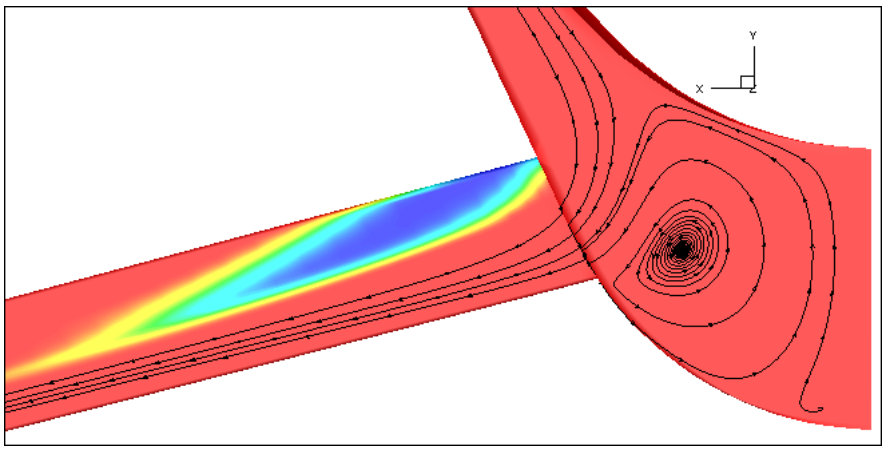

Figure 5.26: Streamlines - Case SA

The pressure at the inlets (Figure 5.27) for case SA is marginally different compared to the lower outlet of case A. The pressure at the outlet, depicted in figure 5.28, is due to the higher velocity, significantly lower.

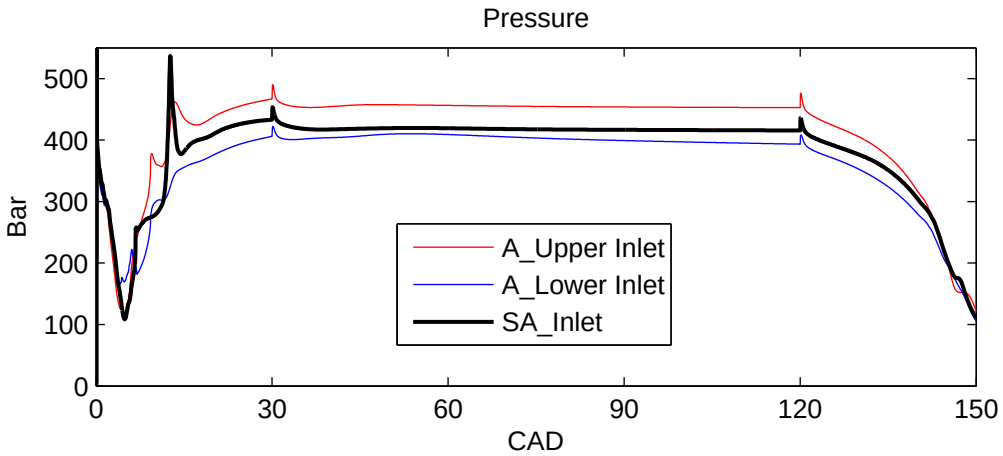

Figure 5.27: Pressure comparison - Inlets

The TKE for the outlets and the inlets is shown in Figure 5.29 and 5.30. The TKE for an injector hole with a larger diameter seems to experience less dissipation as the flow travels from inlet to outlet.

A 3D comparison of the fuel volume fraction for the single orifice nozzle and the twin nozzle is given in Appendix C.2. The 3D visualization shows greater penetration speed and smaller cone angle for the single orifice nozzle.

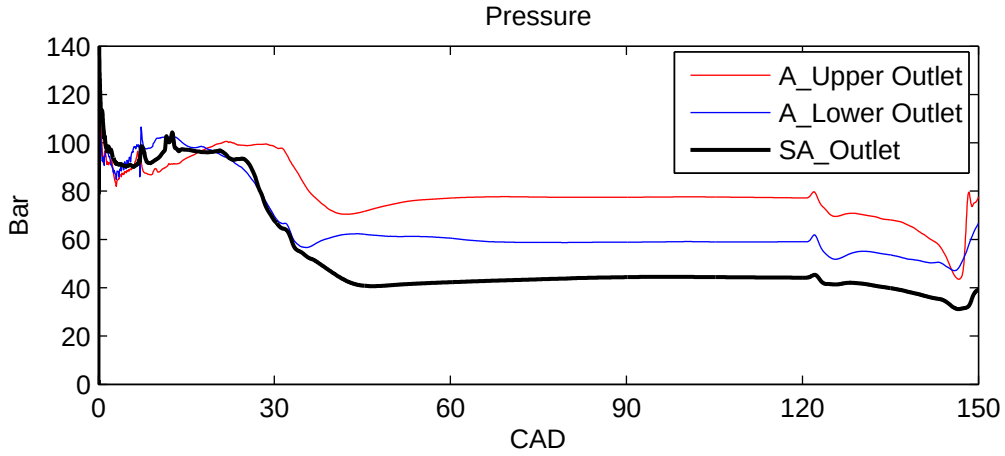

Figure 5.28: Pressure comparison - Outlets

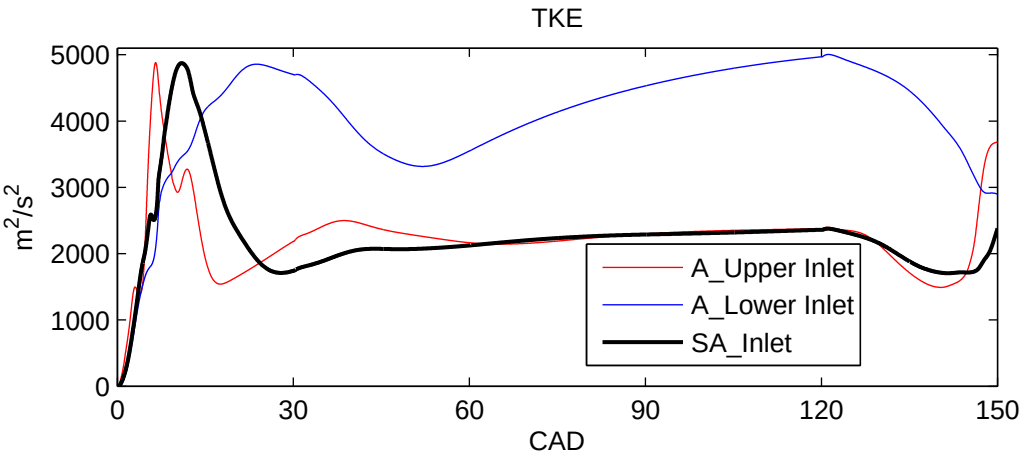

Figure 5.29: TKE comparison - Inlets

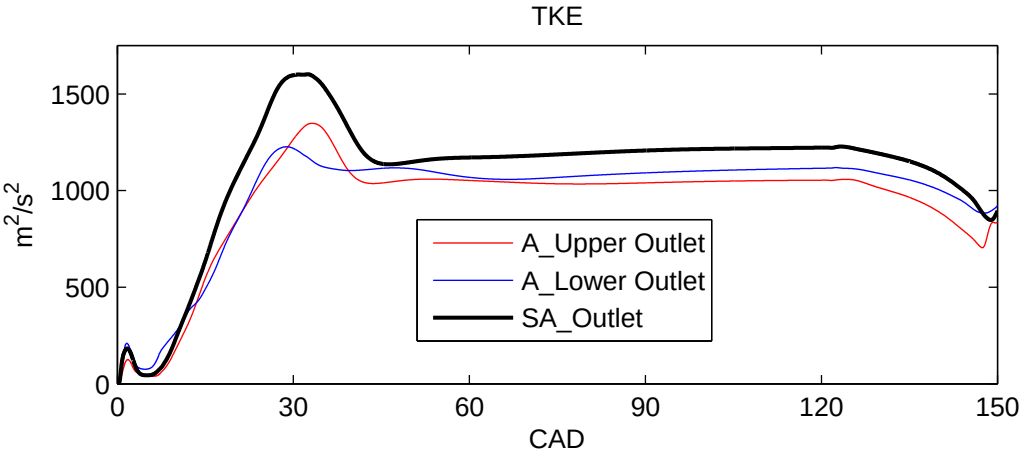

Figure 5.30: TKE comparison - Outlets

5.5 Closing Remarks

Injector calculations in FIRE are normally divided in two parts where the first part is what is done in the present study. During the simulation, data from the outlet selections, presented in Figure 5.2, is stored in a separate nozzle file. The data includes, but is not limited to, density, temperature, velocity components, volume fractions, KTE, turbulent dissipation rate nozzle direction vector etc. The concept is to use the data of a flow calculation inside a nozzle as start and boundary conditions for a spray calculation. There is then a direct coupling between the internal nozzle flow and the spray calculation, which is the second part of the injector calculation. The consequence is that the multiphase calculation of the internal nozzle flow pays less attention to the spray itself. Air is specified as the third phase and FIRE scales its density according to the inlet pressure (rail pressure). The air density in the spray box is therefore too high during the simulations. For case S1 and S2 the rail pressure was not changed and this explains why the measured hydrodynamic quantities did not change as the literature (Chapter 2) calls for. For case A,R1 and R2 the measured quantities for the slices depict the correct trend (as the rail pressure is changed), but not the correct numerical values. Measured quantities from the lower and upper selection slice were included in the study, but not emphasized. However, the results from the internal flow in the nozzle are not affected by the density discrepancy.

Chapter 6

Conclusion

Numerical multiphase simulations of L'Orange's twin nozzle have been performed using the high Reynolds number $k-\epsilon$ model implemented in the commercial software AVL FIRE. Nozzle behaviour has been investigated for various rail pressures and in-cylinder pressures. Twin nozzle performance was compared to a single orifice nozzle. The emphasis has been on the internal nozzle flow.

Before any conclusion is presented it is important to set forth that the model used deviates from the actual nozzle provided by L'Orange by not having rounded inlet edges. Rounding proved to be difficult to perform for a structured grid with AVL FIRE's internal meshing application. Secondly, the needle lift is somewhat unrealistic. In reality the needle will bounce when it hits its top and bottom position producing a more fluctuating needle lift profile.

Cavitation has a major effect on the internal twin nozzle flow. The vapour which is formed at sharp inlets travels all the way to the injector hole outlets, and reduces the effective cross sectional area which the fuel can flow through. This is especially true for the upper injector hole during the first part of the needle opening when there is cavitation at the needle seat. The mass flow and the velocity is higher for the upper injector hole than the lower. A vortex in the SAC volume seems to be the reason for this.

The mass flow and velocity scales with the rail pressure, but not proportional though. The effect is more pronounced when rail pressure is reduced. Rail pressure does not affect cavitation at the inlets, but at the outlets. Again are there bigger changes when the pressure is reduced. In-cylinder pressure affects internal nozzle flow mainly by change in pressure and cavitation at the outlets. The relative change is roughly the same whether the in-cylinder pressure is increased or decreased.

The single orifice nozzle diameter was chosen according to L'Orange's recommendation. L'Orange has experimentally established that a 0.27mm twin nozzle produces the same mass flow as a 0.38mm single orifice nozzle. The numerical model proposed in the present study, successfully reproduces equal mass flow for the two nozzle types, given equal pressure conditions.

With the current model it is hard to say exactly how a twin nozzle might outperform an ordinary nozzle. The TKE values at the outlet(s) are higher for the single orifice nozzle than the twin nozzle. The current model does not include a spray-break up model, so it is not possible to measure SMD values to quantify the success of the spray-break up more precisely.

However, the outlets in the twin nozzle have a smaller vapour fraction than the outlet in the single orifice nozzle. The presence of cavitation can reduce the effective cross sectional area and impair performance during full engine load when large quantities are injected. As the effective cross sectional area is larger for twin nozzles it might be more effective for injecting larger quantities even though its injector holes dimensions favour pilot injections.

The twin nozzle exhibits a slower spray velocity and wider cone angle than its single orifice equivalent. It is possible that engine manufacturers can take advantage of this by making shallower and wider piston bowls without have to worry about impinging.

Chapter 7

Recommendations for Further Work

For further work rounded inlet edges, and a more realistic needle lift profile should be implemented to model the actual operating conditions more precisely. Furthermore, a convergence study would be of interest to see if the grid resolution really is fine enough to catch all flow features. Unstructured grids provide more freedom in terms of mesh generation and should also be looked into.

Subsequent work could also compare the results obtained with other configurations e.g. conical injector holes, converging or parallel injector holes, various L/D ratios, different needle lift profiles.

To improve and extend to current work carrying out a spray calculation is highly recommended. Such calculations utilize the data stored in the nozzle file and provides accurate air densities. It also handles droplet heat-up, evaporation, condensation, primary and secondary break-ups with models specifically intended for spray simulation. This also gives a better foundation to investigate if the twin nozzle is able to facilitate adequate spray patterns independent of the injected fuel quantity.

The department is to receive a prototype of L'Orange's twin nozzle. This will allow for a validation of the current work and any future work based on this recommendation.

Bibliography

[1] W. A. Abdelghaffar, K. Karimi, and M. R. Heikal. *Fuel Spray Penetration in High Pressure Diesel Engines*. SAE International, 01 2007.

[2] M. Arai, M. Tabata, and H. Hiroyasu. *Disintegrating Process and Spray Characterisation of Fuel Jet Injected by a Diesel Nozzle*. SAE Technical, 1984.

[3] Osman Asi. *Failure of a diesel engine injector nozzle by cavitation damage*, volume 13. Engineering Failure Analysis, 2005.

[4] A. Bakker. Lecture 7 - meshing. http://www.bakker.org/dartmouth06/engs150/07-mesh.pdf, 2006. Lecture notes in course ENGS 150 at Dartmouth College.

[5] F. V. Bracco. *Modeling of Engine Sprays*, volume 93. SAE Technical, 1984.

[6] Cristopher Earls Brennen. *Cavitation and Bubble Dynamics*. Cambridge University Press, 2013.

[7] V. Caika, P.Sampl, R.Tatschl, and J. Krammer. *Coupled 1D-3D Simulation of Common Rail Injector Flow Using AVL HYDSIM and FIRE*. SAE Technical, 2009.

[8] C.Baumgarten. *Mixture Formation in Internal Combustion Engines*. Springer-Verlag Berlin Heidelberg, 1st edition, 2006.

[9] Yunus Cengel and John Cimbala. *Fluid Mechanics Fundamentals and Applications*. McGraw-Hill, 3rd edition edition, 2013.

[10] J.H. Ferziger and M. Peric. *Computational Methods for Fluid Dynamics*. Sprin, thrid edition edition, 2002.

[11] AVL FIRE. *Application Example: Diesel Injector*, 2013.

[12] AVL FIRE. *Eulerian Multiphase*, 2013.

[13] V. Ganesan. *Internal Combustion Engines*. Mechanical engineering. McGraw-Hill, 2012.

[14] Jian Gao, Yuhei Matsumoto, Makoto Namba, and Keiya Nishida. *Group-Hole Nozzle Effects on Mixture Formation and In-cylinder Combustion Processes in Direct-Injection Diesel Engines*. SAE Technical, 2007.

[15] Jian Gao, Yuhei Matsumuto, and Keiya Nishida. *Effects of Group-hole Nozzle Specifications on Fuel Atomization and Evaporation of Direct Injection Diesel Sprays*. SAE Technical, 2007.

[16] John B. Heywood. *Internal Combustion Engine Fundementals*. McGraw-Hill, 1988.

[17] H. Hiroyasu and M. Arai. *Structures of Fuel Sprays in Diesel Engines.* SAE Technical, 1990.

[18] IMO. Marpol regulation 14, annex vi. `http://www.imo.org/OurWork/Environment/PollutionPrevention/AirPollution/Pages/Default.aspx`, 2012.

[19] Kourosh Karimi. *Characterisation of Multiple-Injection Diesel Sprays at Elevated Pressures and Temperatures.* PhD thesis, School of Enginnering, University of Brighton, 2007.

[20] W. G. Lee and R. D. Reitz. *Comparison of Flow and Cavitation Processes in Conventional and Group-Hole Diesel Injector Nozzles using Numerical Simulations.* 11th Triennial International Annual Conference on Liquid Atomization and Spray Systems, 2009.

[21] S. Martinez-Martinez, F.A. Sanchez-Cruz, J.M. Riesco-Avila, A. Gallegos-Munoz, and S.M. Aceves. *Liquid penetration length in direct diesel fuel injection*, volume 28. Applied Thermal Engineering, 2008.

[22] A. Matsumoto, X. Xie, and M.-C. Lai. *Characterization of Diesel Common Rail Spray Behavior for Single- and Double-hole Nozzles.* SAE Technical, 2008.

[23] Gunter P. Merker, Christian Schwarz, and Rudiger Teichmann. *Combustion Engines Development.* Springer, 2012.

[24] N. Mitroglou, J. M. Nouri, Y. Yan, M. Gavaises, and C. Arcoumanis. *Spray Structure Generated by Multi-Hole Injectors for Gasoline Direct-Injection Engines.* SAE Technical, 2007.

[25] Klaus Mollenhauer and Helmut Tschoke. *Handbook of Diesel Engines.* Springer, 2010.

[26] Wolfgang V. Ohnesorge. *Die Bildung von Tropfen an Düsen und die Auflösung flüssiger Strahlen*, volume 16. ZAMM - Journal of Applied Mathematics and Mechanics / Zeitschrift für Angewandte Mathematik und Mechanik, 1936.

[27] Stavroula Patouna. *A CFD Study of Cavitation in Real Size Diesel Injectors.* PhD thesis, Universitat Politecnica De Valencia, 2013.

[28] Adam Pawlowski, Reinhold Kneer, Andreas M. Lippert, and Scott E. Parrish. *Investigation of the Interaction of Sprays from Clustered Orifices under Ambient Conditions Relevant for Diesel Engines*, volume 1. SAE Technical, 04 2008.

[29] Adam Pawlowski, Reinhold Kneer, Andreas M. Lippert, and Scott E. Parrish. *Investigation of the Interaction of Sprays from Clustered Orifices under Ambient Conditions Relevant for Diesel Engines.* SAE Technical, 2008.

[30] Reitz R.D. *Atomization and other Breakup Regimes of a Liquid Jet.* PhD thesis, Princton University, 1978.

[31] R.D Reitz and F.V. Bracco. *Mechanisms of Breakup of Round Liquid Jets*, volume 3. Enzyclopedia of Fluid Mechanics, 1986.

[32] H. Roth, E. Giannadakis, M. Gavaises, and C. Arcoumanis. *Effect of Multi-Injection Strategy on Cavitation Development in Diesel Injector Nozzle Holes.* SAE Technical, 2009.

[33] C. Schugger and U. Renz. *Experimental Iinvestigation of the Primary Breakup Zone of High Pressure Diesel Sprays from Multi-Orifice Nozzles.* 9th International conference on liquid atomization and spray system, 2003.

[34] Dennis L. Siebers. *Liquid-Phase Fuel Penetration in Diesel Sprays.* SAE Technical, 1998.

[35] T. Su, C. Chang, R. Reitz, and P. Farrell. *Effects of Injection Pressure and Nozzle Geometry on Spray SMD and D.I. Emissions.* SAE Technical, 1995.

[36] Hyun Kyu Suh and Chang Sik Lee. *Impact of Orifice Angle Configurations on the Droplet Atomization Enhancement of Diesel Fuel in a Group-Hole Nozzle*, volume 133. Journal of Engineering for Gas Turbines and Power, 2011.

[37] H.K. Versteeg and W. Malalasekara. *An Introduction to Computational Fluid Dynamics - The Finite Volume Method.* Pearson Prentice Hall, 2nd edition edition, 2007.

[38] A. Wierzba. *Deformation and Breakup of Liquid Drops in a Gas Stream at Nearly Critical Weber Numbers*, volume 9. Experiments in Fluids, 1993.

[39] Hyun Woo Won, Abhinav Sharma, Seung Eun Moon, Anyelo Vanegas, and Norbert Peters. *An Experimental Study of Cluster Nozzles for DI Diesel Engine.* SAE Technical, 2009.

[40] Doug Woodyard. *Pounder's Marine Diesel Engines and Gas Turbines.* Butterworth-Heinemann, Oxford, ninth edition edition, 2009.

[41] Zhi-Jun Wu, Zhi-Long LI, Wei-Di Huang, Hui-Feng Gong, Ya Gao, Jun Deng, and Zong-Jie Hu. *Comparisons of nozzle orifice processing methods using synchrotron X-ray micro-tomography.* Journal of Zhejiang University, 2011.

[42] Yuyin Zhang, Keiya Nishida, and Shinsuke Nomura. *Spray Characteristics of Group-hole Nozzle for D.I. Diesel Engine.* SAE Technical, 2003.

Appendix A

Rail Pressure

A.1 Mass Flow

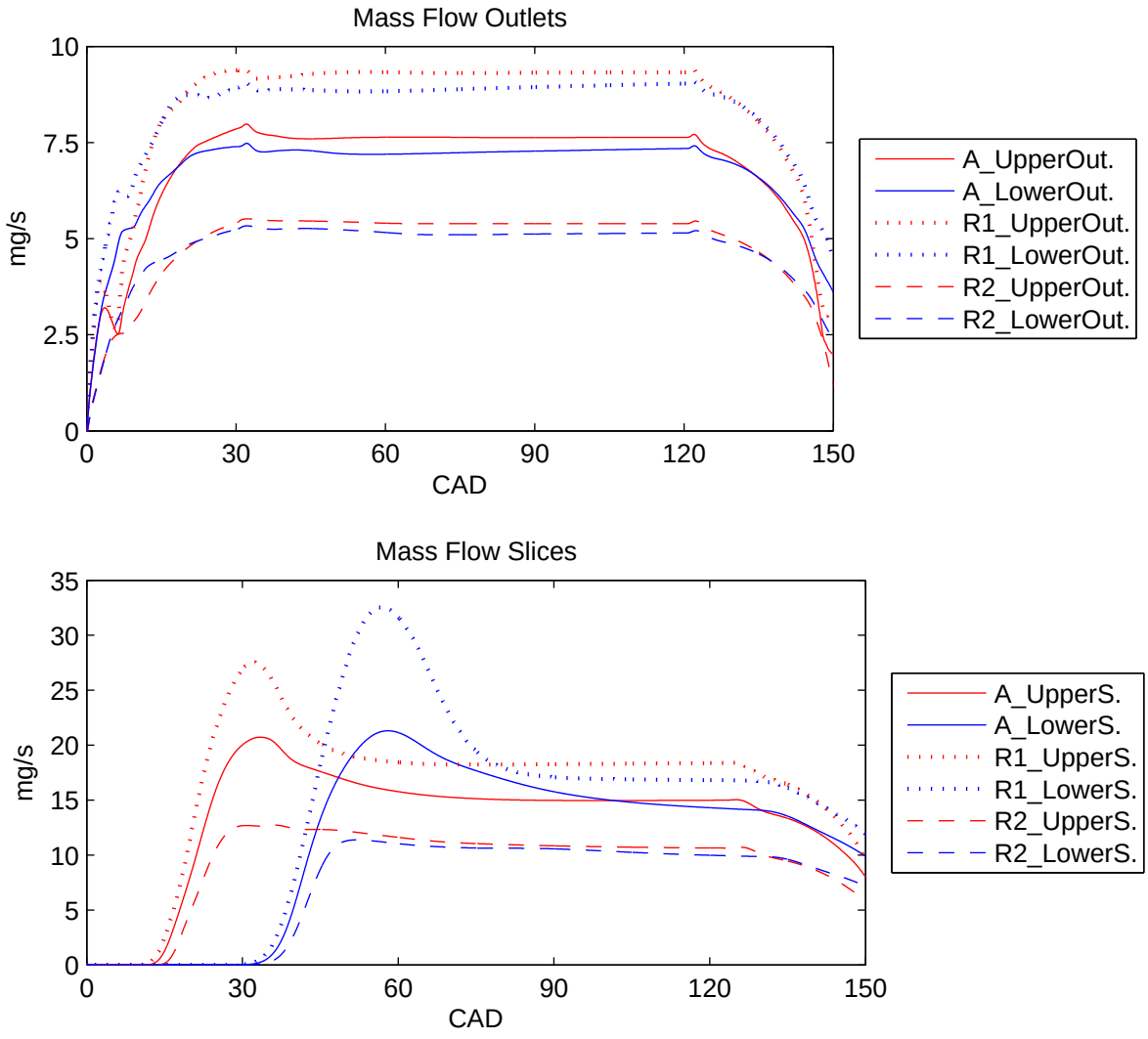

Figure A.1: Mass Flow - Inlets and Slice

A.2 Vapour Volume Fraction

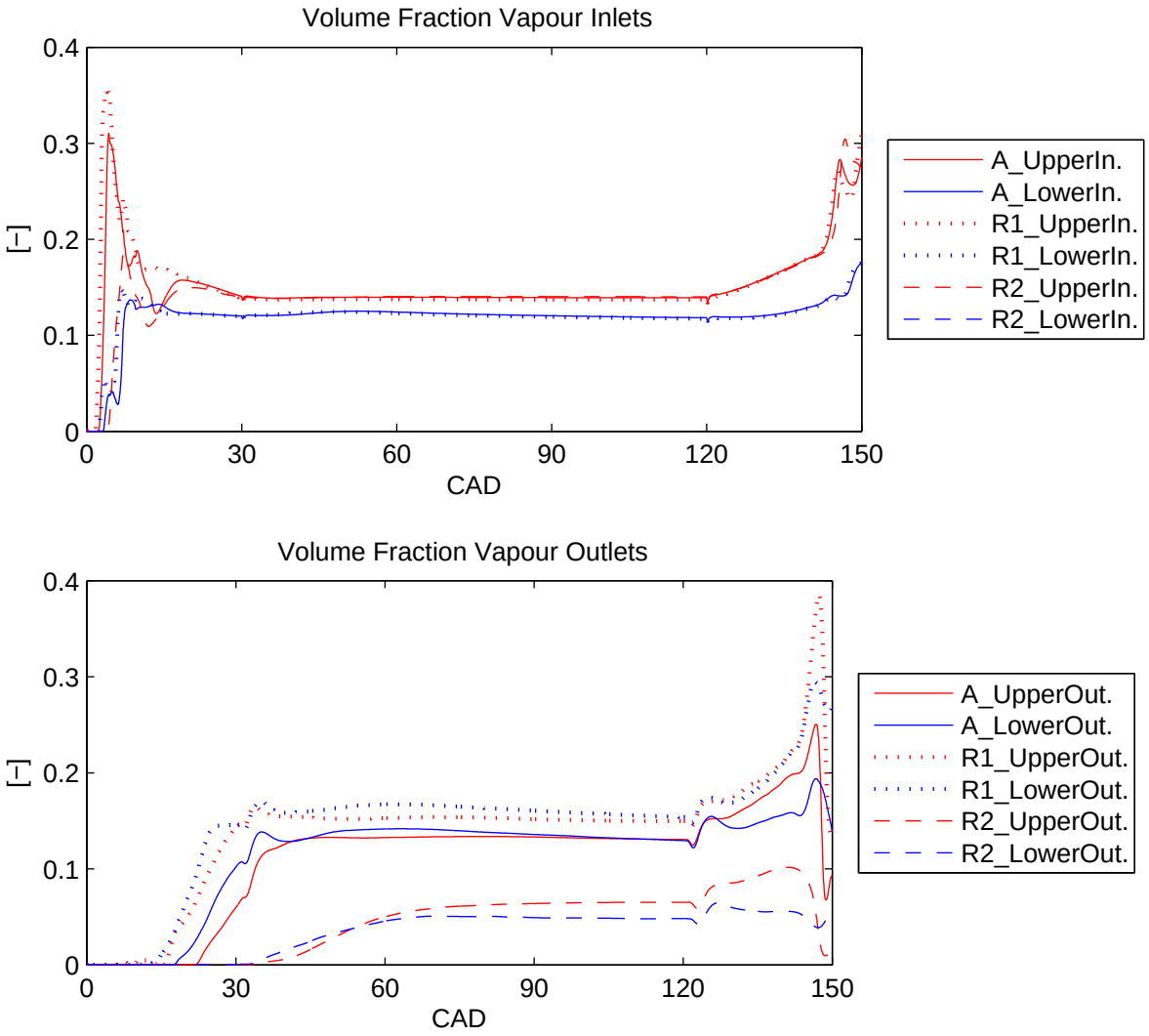

Figure A.2: Vapour Fraction - Inlets and Outlets

A.3 Velocity

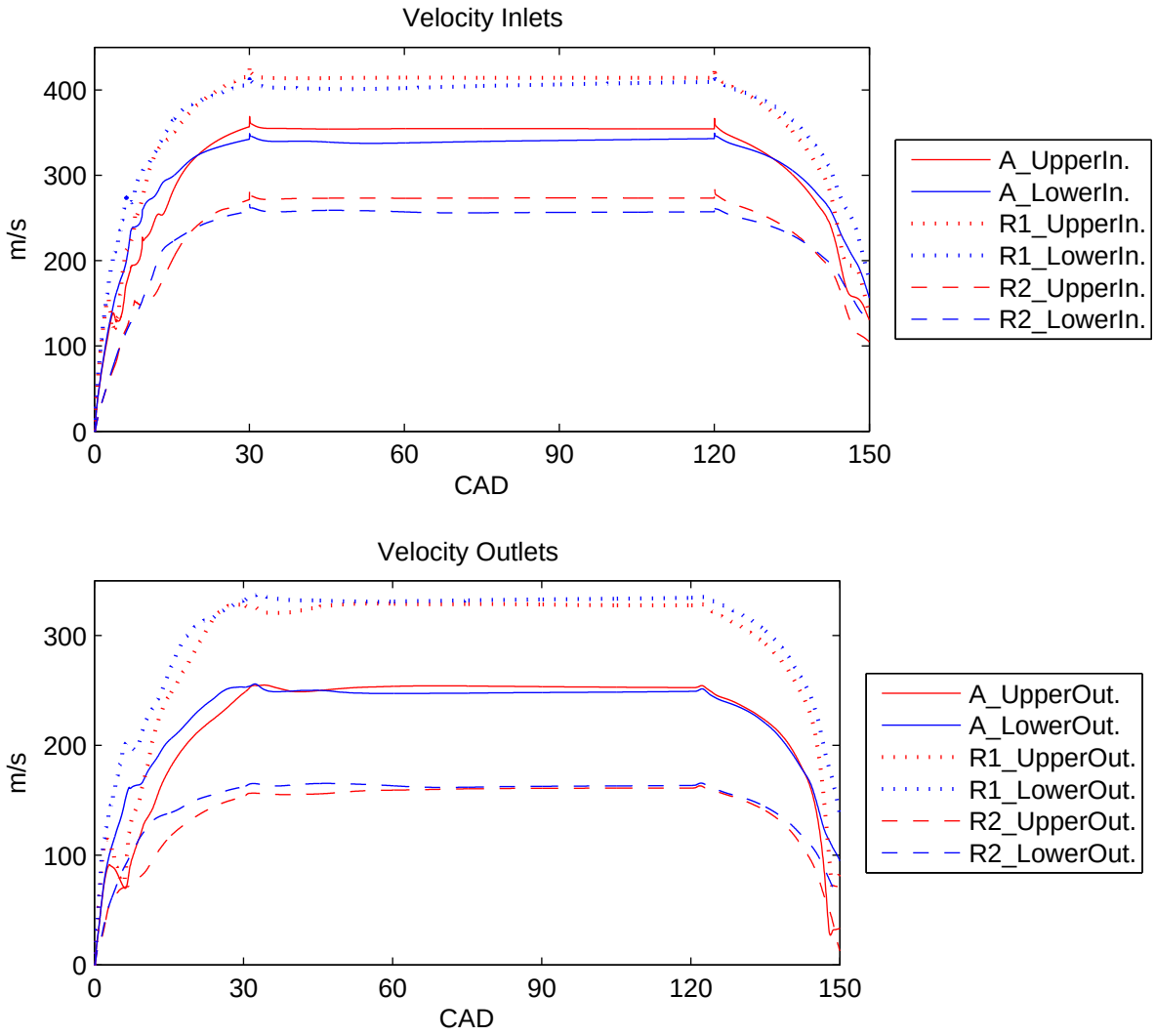

Figure A.3: Velocity - Inlets and Outlets

A.4 Pressure

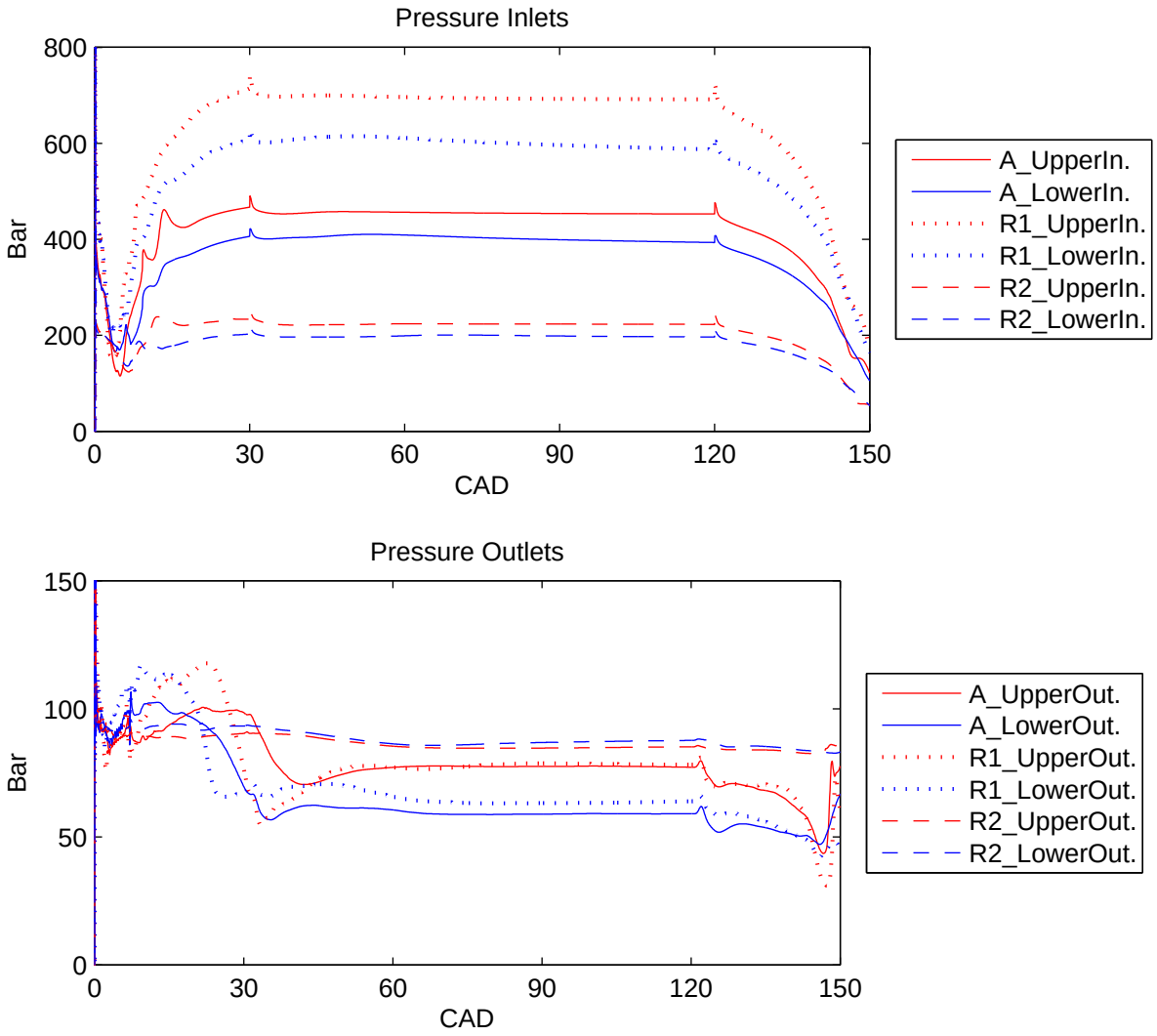

Figure A.4: Pressure - Inlets and Outlets

A.5 TKE

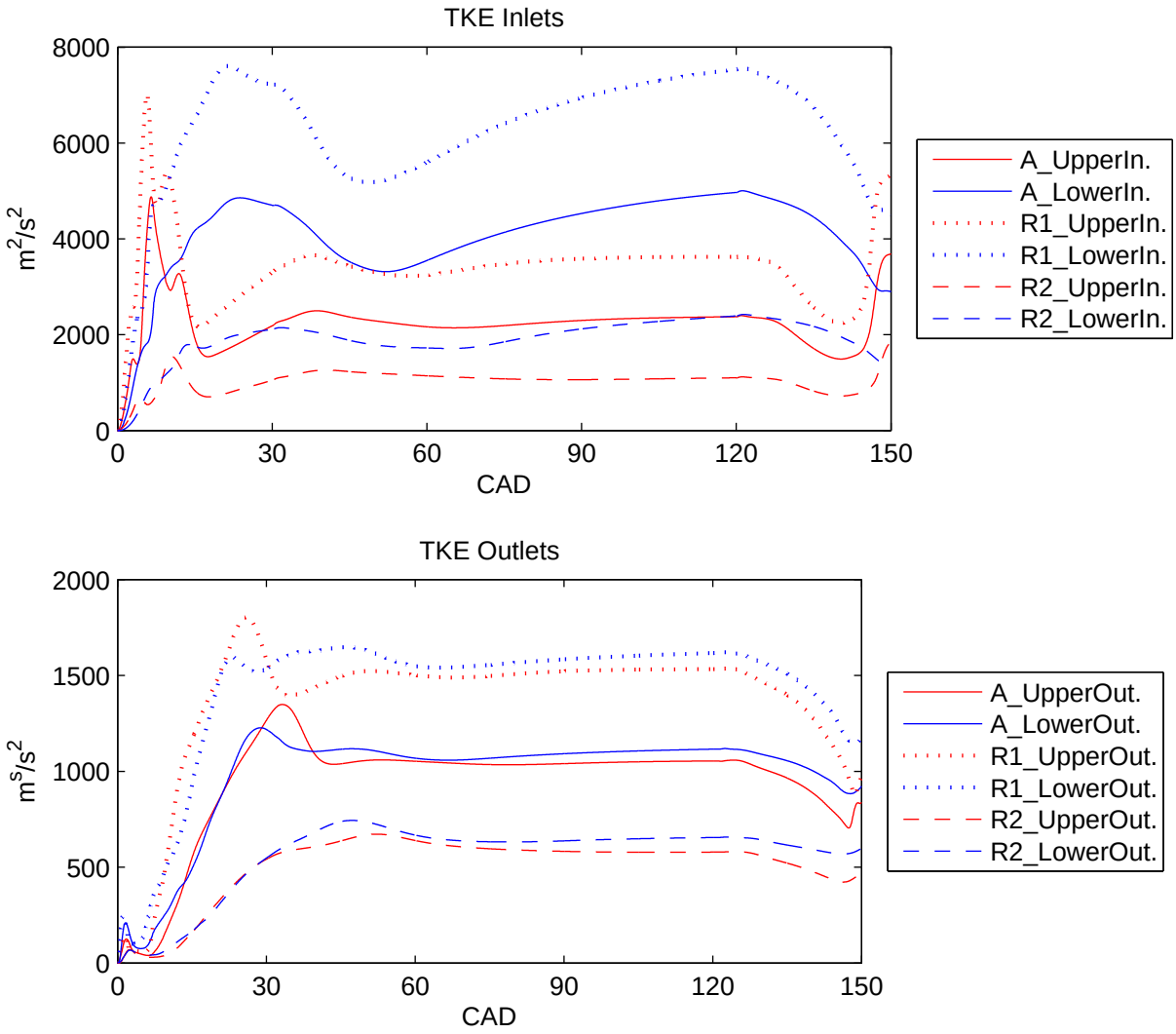

Figure A.5: TKE - Inlets and Outlets

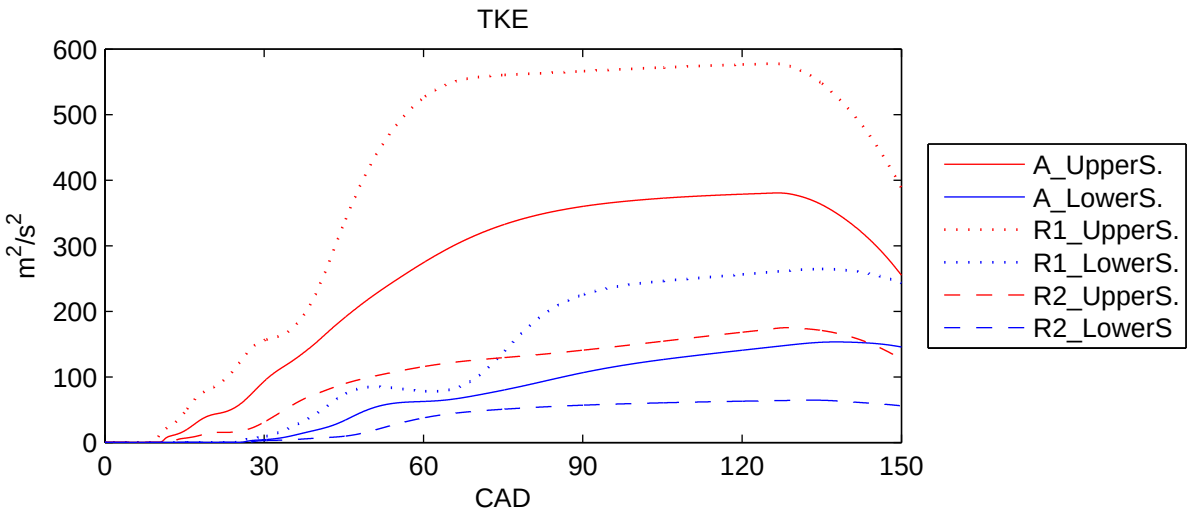

Figure A.6: TKE - Spray Box Slices

Appendix B

In-Cylinder Pressure

B.1 Mass Flow

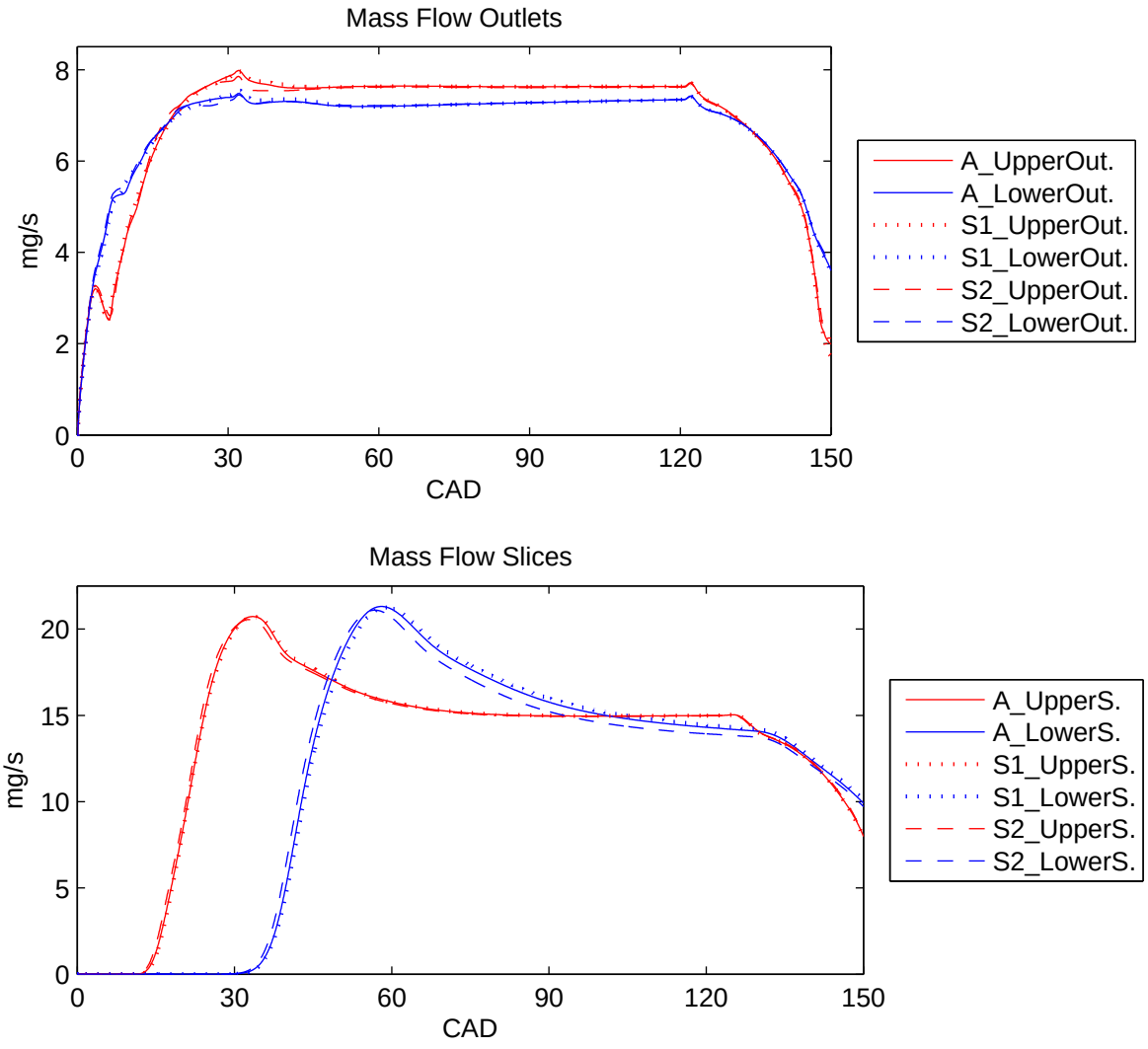

Figure B.1: Mass Flow - Inlets and Slices

B.2 Vapour Volume Fraction

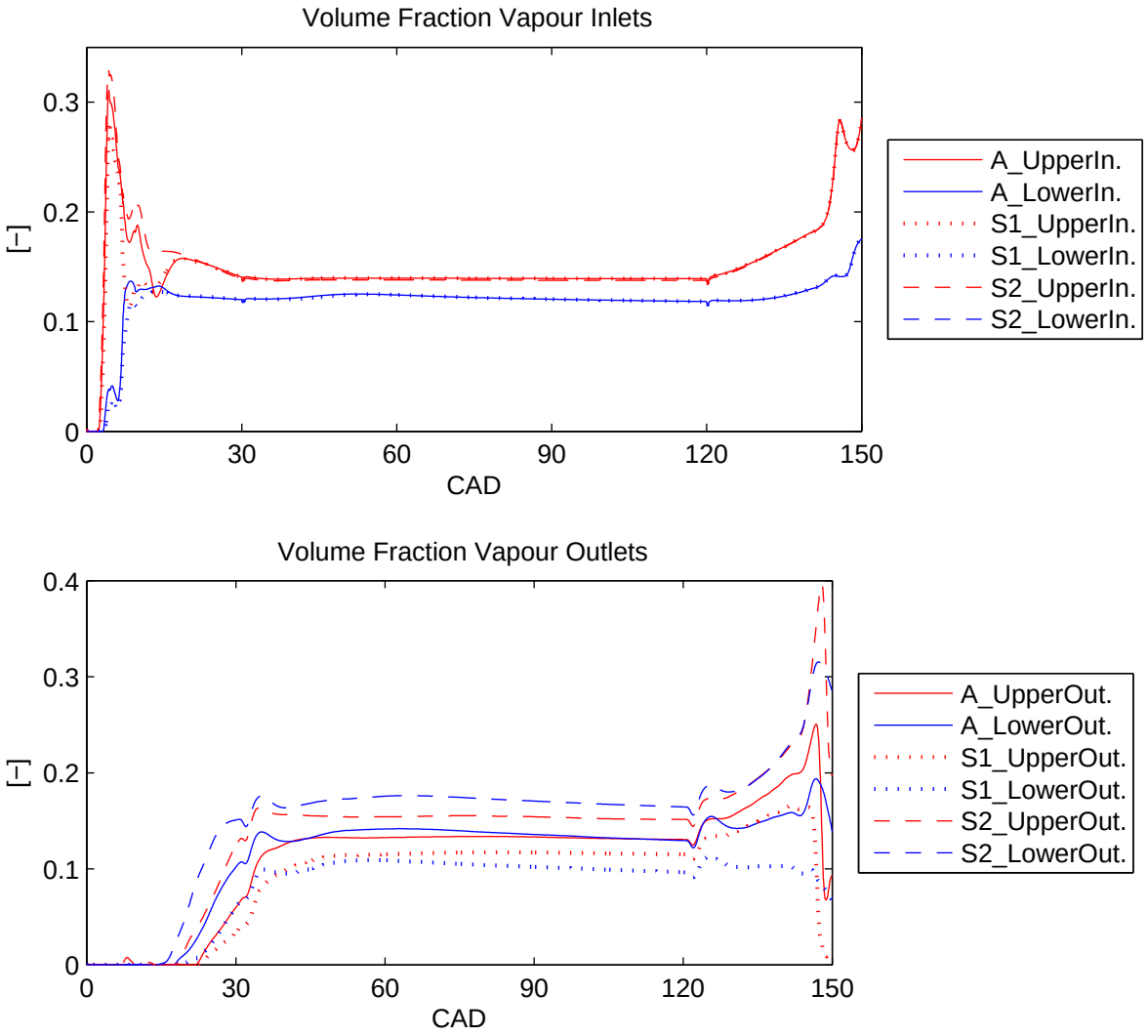

Figure B.2: Vapour Fraction - Inlets and Outlets

B.3 Velocity

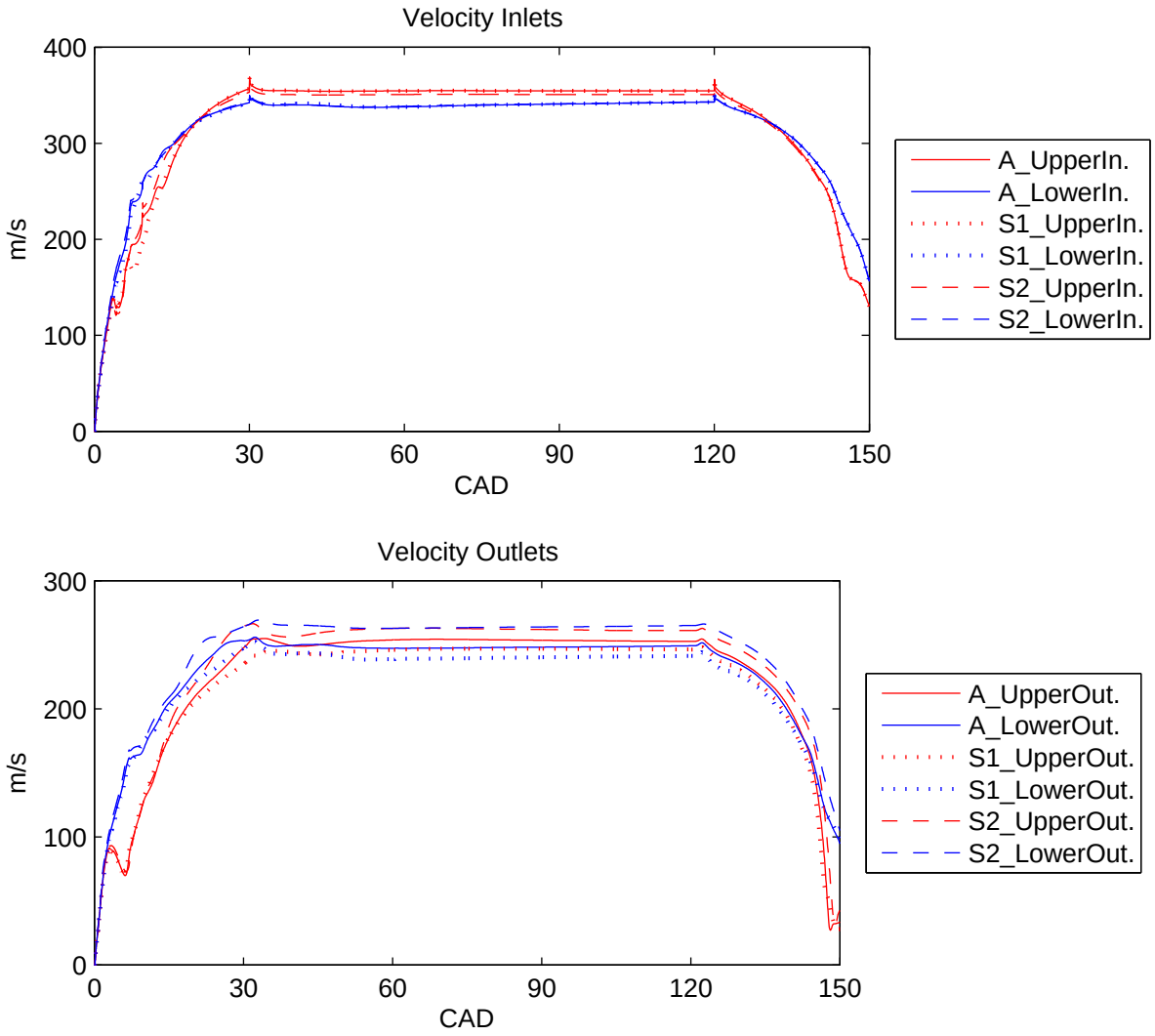

Figure B.3: Velocity - Inlets and Outlets

B.4 Pressure

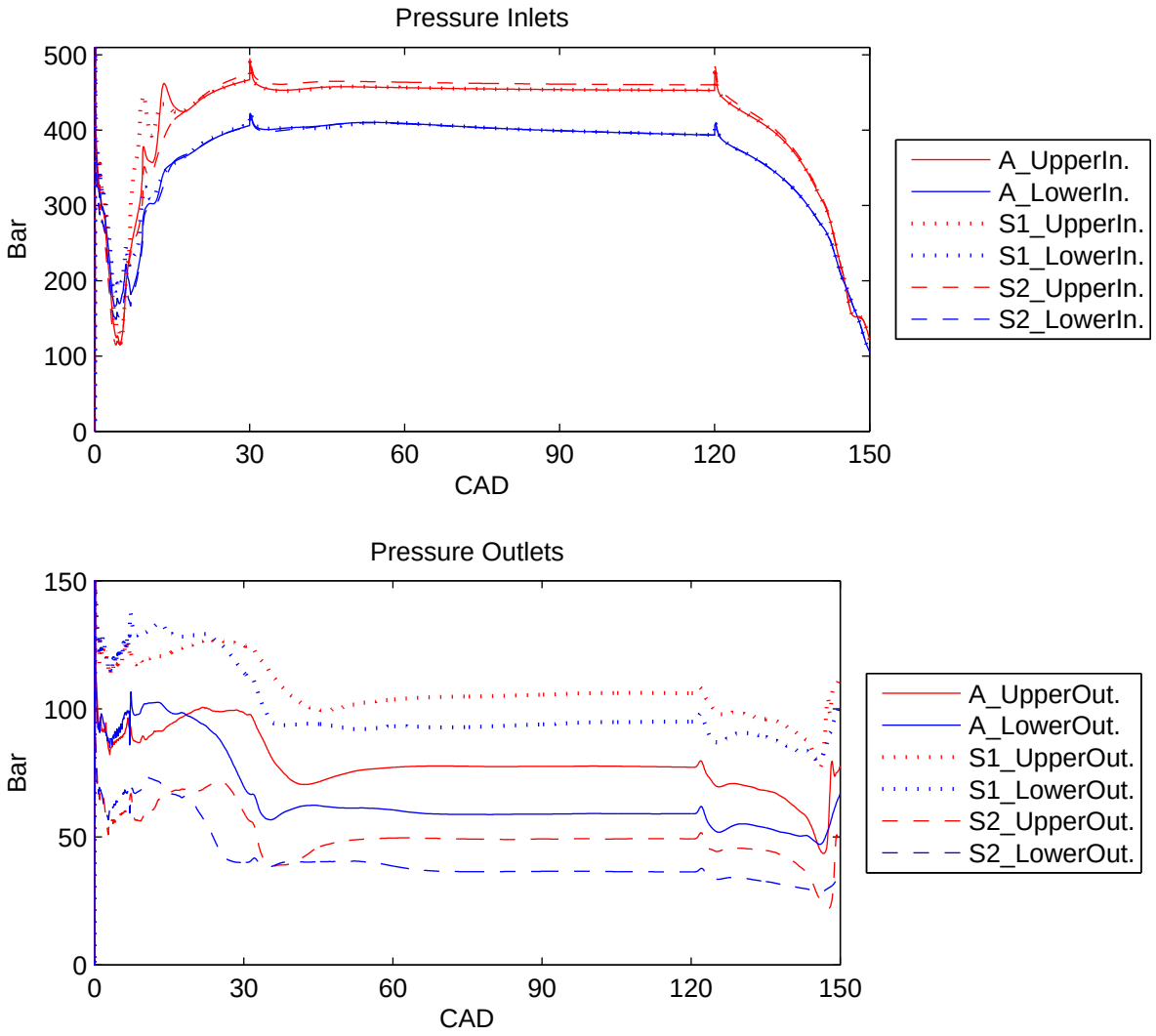

Figure B.4: Pressure - Inlets and Outlets

B.5 TKE

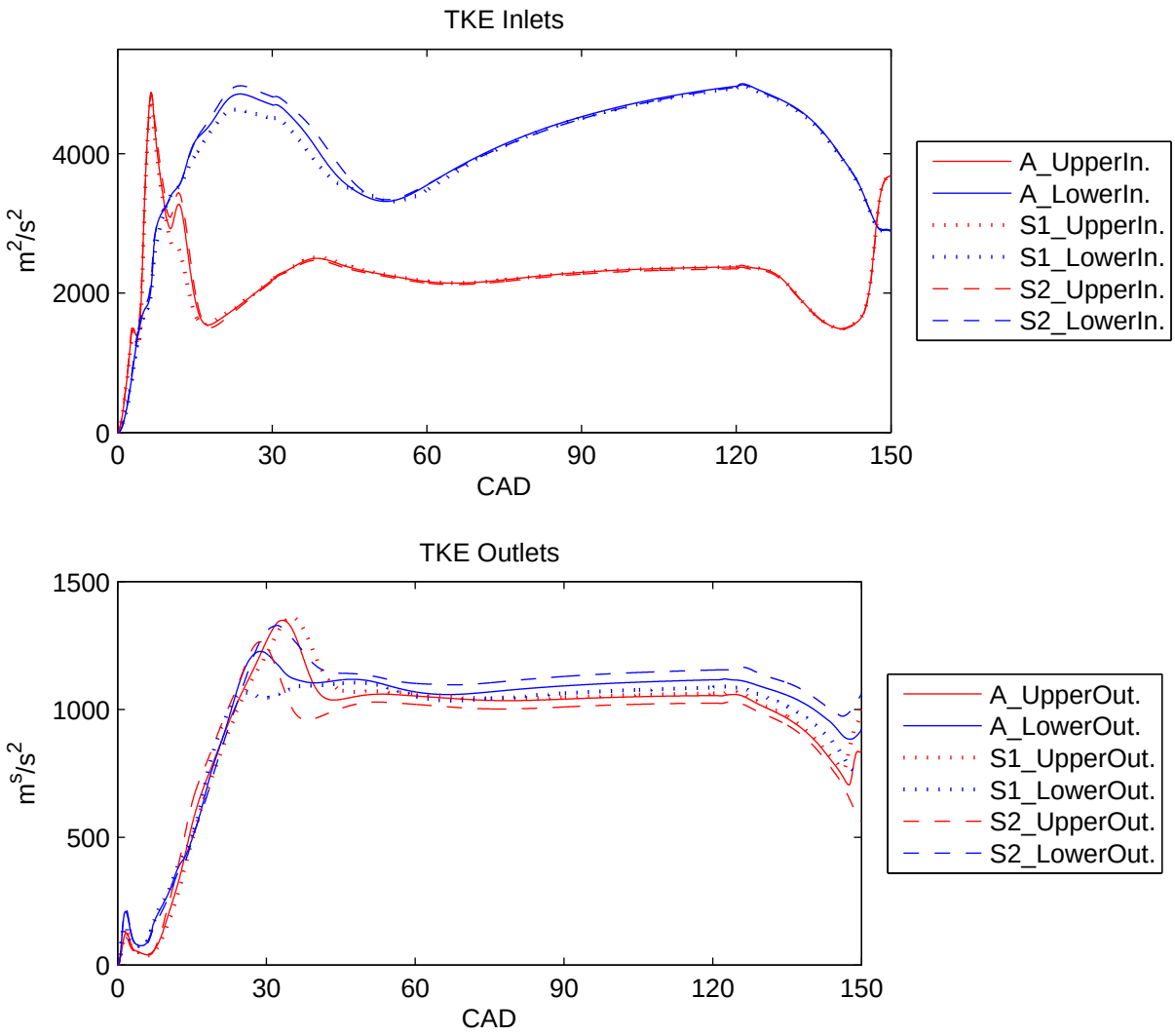

Figure B.5: TKE - Inlets and Outlets

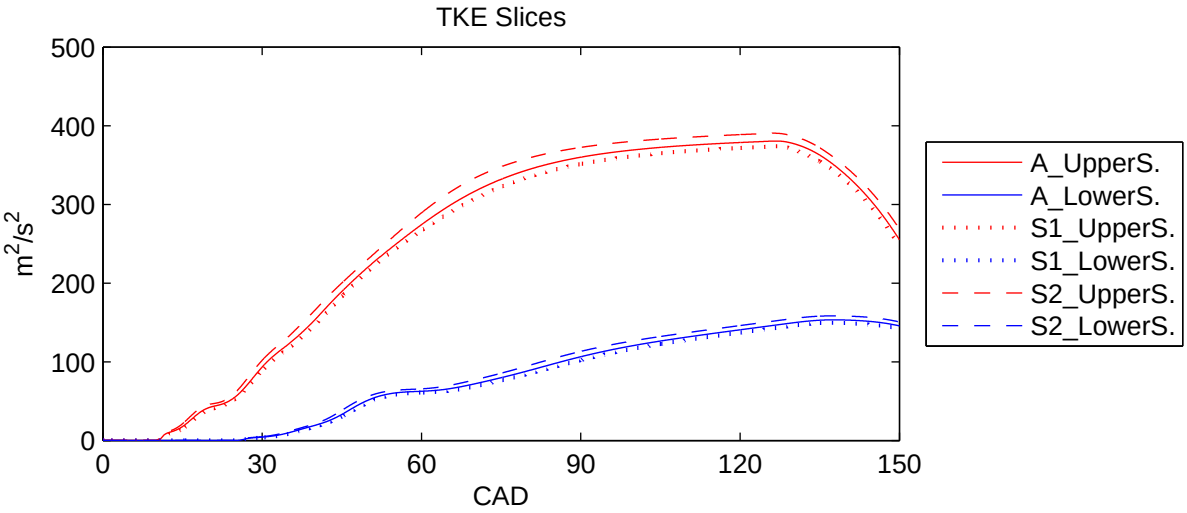

Figure B.6: TKE - Spray Box Slices

Appendix C

Single Orifice Nozzle

C.1 Dimensions

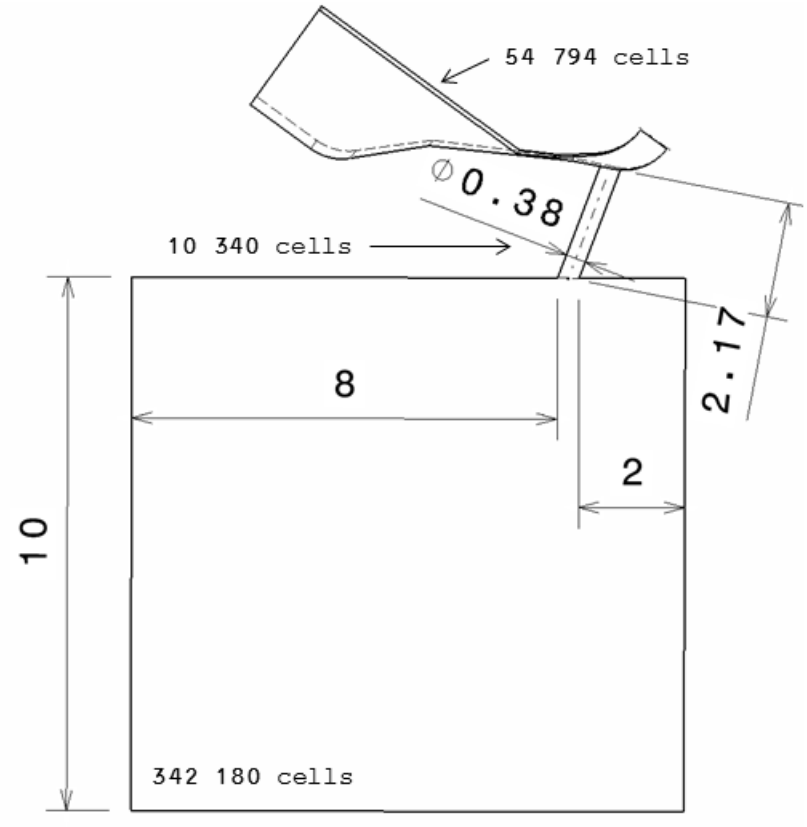

Figure C.1: Dimensions [mm] - Single orifice nozzle

C.2 3D Visualization

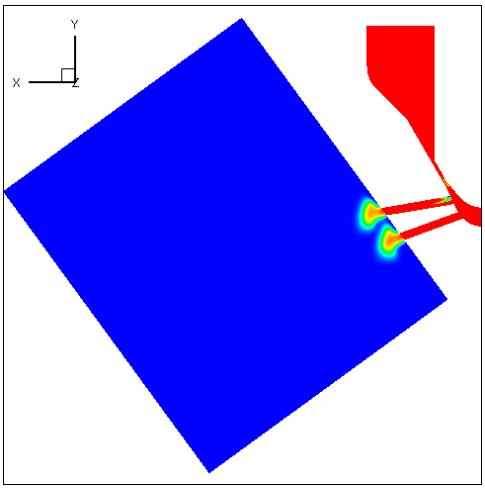

(a) 5 CAD

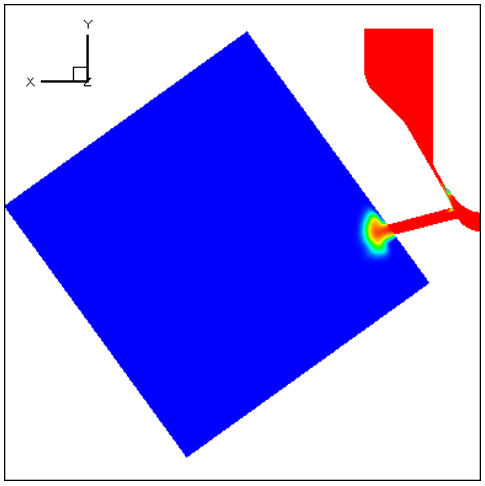

(b) 25 CAD

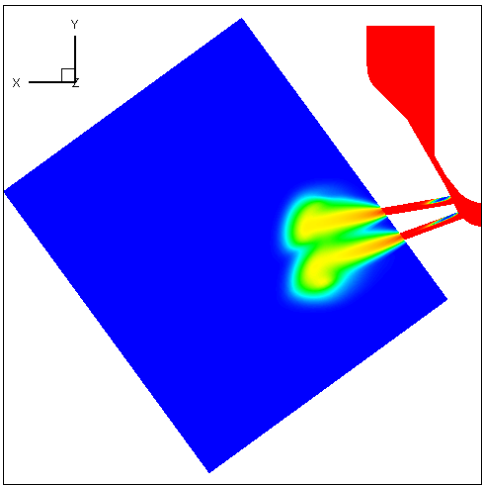

(c) 50 CAD

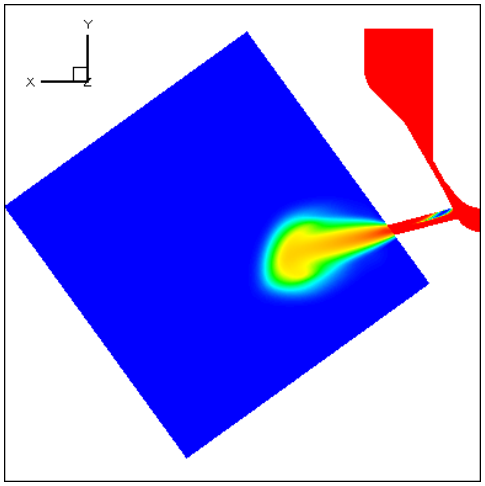

(d) 75 CAD

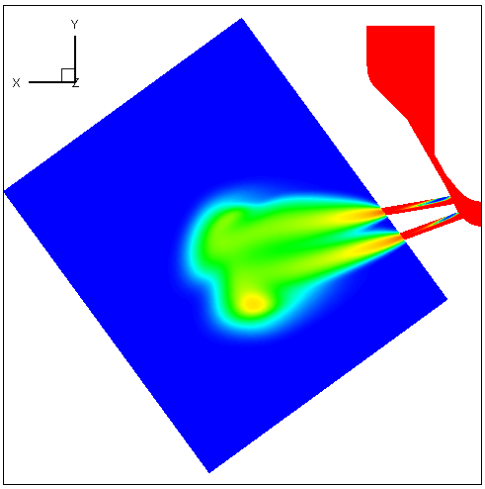

(e) 100 CAD

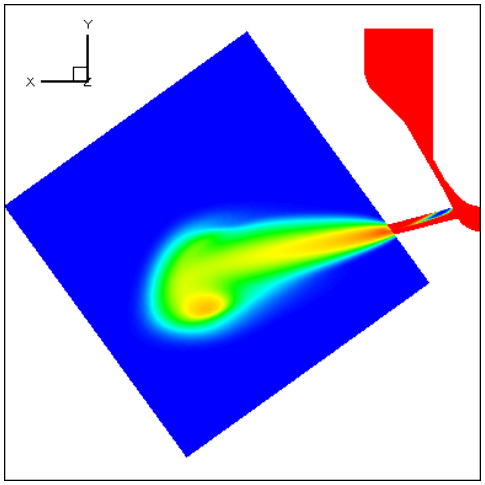

(f) 120 CAD

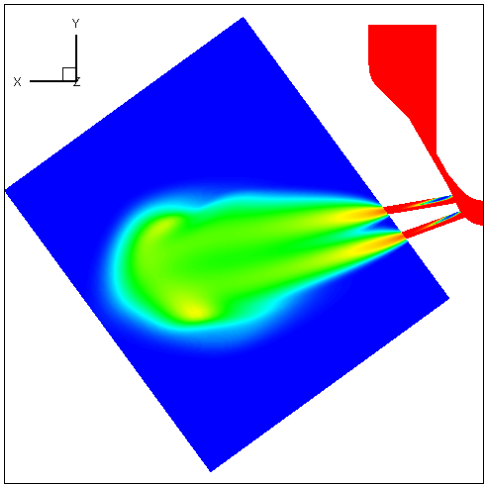

(g) 30 CAD

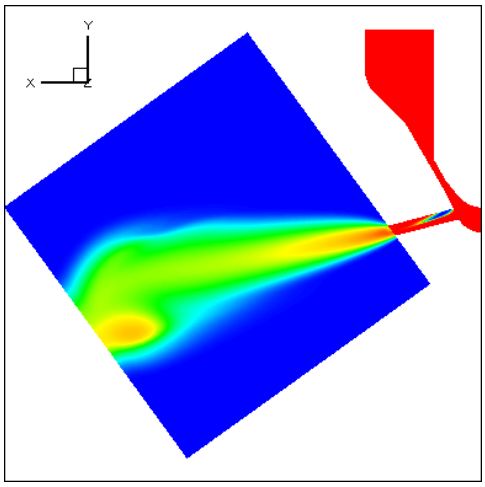

(h) 30 CAD

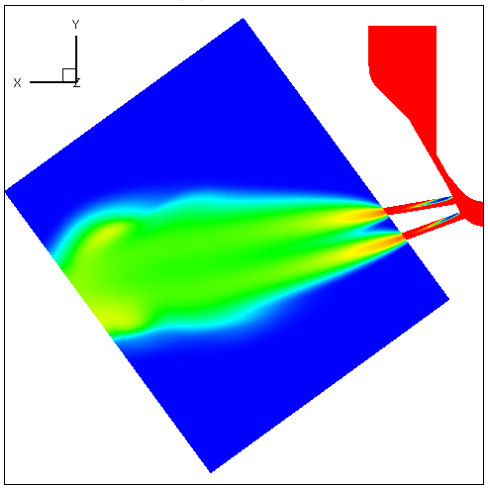

(i) 35 CAD

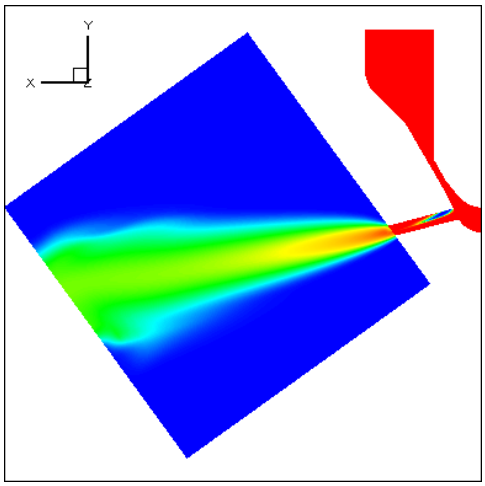

(j) 35 CAD

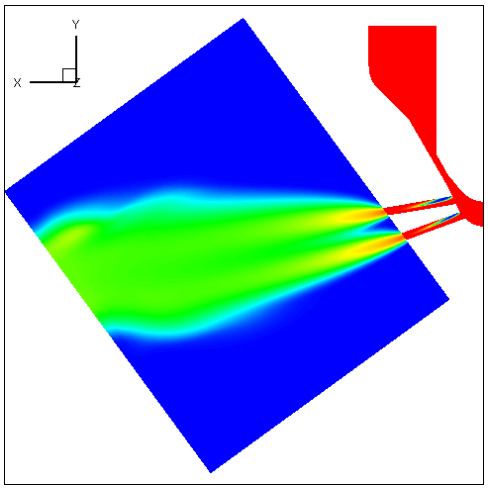

(k) 40 CAD

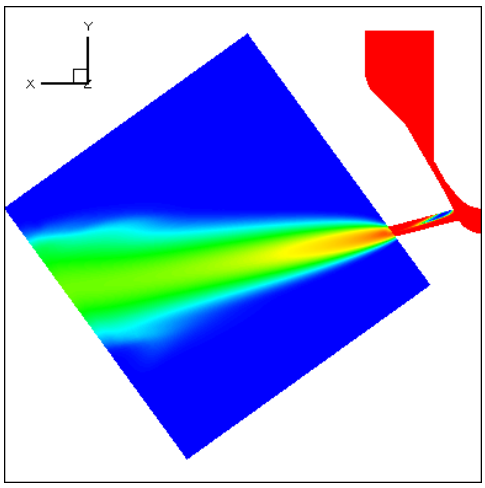

(l) 40 CAD

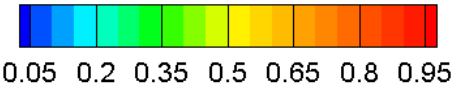

Figure C.2: Fuel phase fraction comparison